

SLAC-PUB 10620
August 2004
Revised
January 2005

High Power Klystrons: Theory and Practice at the Stanford Linear Accelerator Center *

Part I

George Caryotakis

Stanford Linear Accelerator Center 2575 Sand Hill Rd.
Menlo Park, CA 94025

Abstract

This is Part I of a two-part report on design and manufacturing methods used at SLAC to produce accelerator klystrons. Chapter 1 begins with the history and applications for klystrons, in both of which Stanford University was extensively involved. The remaining chapters review the theory of klystron operation, derive the principal formulae used in their design, and discuss the assumptions that they involve. These formulae are subsequently used in small-signal calculations of the frequency response of a particular klystron, whose performance is also simulated by two different computer codes. The results of calculations and simulations are compared to the actual performance of the klystron.

*Work supported by Department of Energy under contract number DE-AC02-76SF00515

**HIGH-POWER KLYSTRONS:
THEORY AND PRACTICE
AT THE STANFORD LINEAR ACCELERATOR CENTER**

George Caryotakis

PART I

Theory and Design

- 1. Klystron Historical Background, Applications, and the State-of-the-Art**
- 2. Ballistic (Kinematic) Theory**
- 3. Space-charge Wave Theory**
- 4. Gain-Bandwidth Calculations. Large Signal Codes and a Working Example.**
- 5. Advanced Klystron Configurations**

Appendix I: The Mathcad Small-Signal Code (A. Jensen, C. Wilsen)

Appendix II: The AJ-Disk 1D Code (A. Jensen)

Appendix III: The MAGIC 2D and 3D Codes (L. Ludeking, D. Smithe)

Appendix IV: R/Q, Coupling coefficient and beam-loading simulations, cavity stability. (G. Scheitrum, A. Jensen)

Appendix V: Relativistic corrections

FOREWORD

Klystrons are the *sine qua non* of particle accelerators. Since its dedication in 1962, the Stanford Linear Accelerator Center has elected to maintain its own klystron engineering and manufacturing facilities. This decision was certainly related to the fact that the 1950 Stanford Mark III electron accelerator employed the first megawatt-level klystrons in the world. Both that accelerator and its 21 klystron amplifiers were built at the University's Microwave Laboratory.

The SLAC Klystron Department, dedicated to the design and production of increasingly more powerful microwave sources, has developed specialized techniques to achieve these purposes. This knowledge should be permanently documented. Consequently, we have attempted to include in this document the theoretical foundations, the calculations and simulation tools, and the manufacturing processes employed at the Department to produce unique high-power klystrons. It is hoped that this material will help a new generation of SLAC engineers to design even more advanced klystrons for future particle accelerators, which are certain to challenge the state-of-the-art for microwave sources, once again.

This is Part 1 of a 2-part report. Most of the topics covered were presented in a series of lectures given at SLAC in the winter and spring of 2004, and still available on the Web in streaming video. The material in Part 1 will also appear as a chapter on Klystrons in a forthcoming book on Vacuum Electronics published by Wiley and edited by Robert Barker of the Air Force Office of Scientific Research.

Special thanks are due to several SLAC engineers who contributed to the collection of klystron topics, particularly in Part 2 of this report, which will appear later this year: Bob Phillips, who wrote a chapter on guns and beam transport, Daryl Sprehn, the project engineer for the family of SLAC PPM NLC klystrons, Erik Jongewaard, the designer of the B-Factory klystron used in the various code examples in Part 1, and Saul Gold, whose subject will be testing procedures and high-voltage modulators. The contributions of Craig Wilsen, an L3 klystron engineer, and Aaron Jensen, a Stanford graduate student, are gratefully acknowledged. Both worked on the Mathcad and "Japandisk" codes used in the Appendices. In particular, Aaron rewrote Japandisk in C++ and made it considerably more flexible and friendly.

Glenn Scheitrum and I had many discussions on technical substance and on the vagaries of Microsoft software. We both wish to thank Kate McMillen, who patiently did battle with both Word and Math Type and retained her sanity through dozens of editing iterations.

A CD is attached and can be used to run the Mathcad and MAGIC codes.

Chapter 1.

Klystron Historical Background, Applications, and the State-of-the-Art

The klystron was invented to overcome the transit-time effects which set the operational limits in triodes and tetrodes. Klystrons are the most efficient of linear beam tubes and are capable of the highest peak and average powers. They are useful over an extremely broad frequency range, from low UHF (200 MHz) to W-band (100 GHz). The gain of multi-cavity klystrons can be very high. Gains of 60 dB, or even higher, and efficiencies of 70 per cent are not unusual.

Maximum peak power in klystrons is limited by RF breakdown, which is a function of the pulse duration. At 1-2 microsecond pulse lengths, 75-MW has been attained at X-band¹ and over 150 MW at S-band.² Average power is a function of body cooling, since klystron collectors can be made arbitrarily large. At X-Band, a CW power of 1-MW has been attained.³

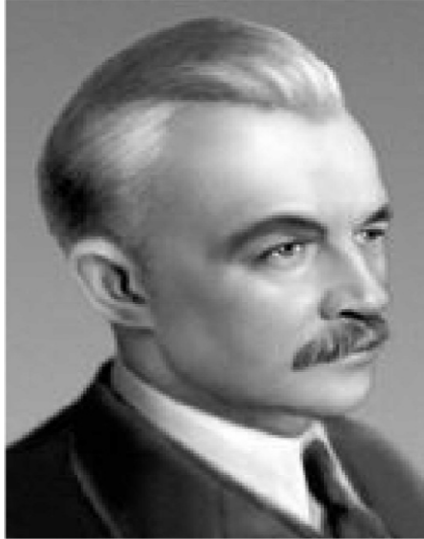
On the minus side, klystrons are narrow-band devices, compared with traveling-wave tubes (TWTs, see Chap. 4). For many radar applications and for all electronic countermeasures (against radar), only TWTs are suitable. Klystrons are useful for some communication applications, since limited klystron broad-banding is always possible. A wide bandwidth in a klystron requires low beam impedance (i.e. - high perveance, and/or high power). At very high powers, or high frequencies, lower perveance beams are used for better electron optics. In those circumstances, a 1% bandwidth for CW klystrons may be difficult. At a few megawatts pulsed, at S-band, 10% bandwidth is possible.

Low-power klystrons, particularly reflex oscillators, lost the battle to solid-state replacements in radar and communication equipment some time ago. However, millimeter-wave klystron amplifiers, producing several tens of watts of average power are not likely to be replaced by solid-state devices, which cannot produce competitive powers at these frequencies.

It is instructive to follow the progress of klystrons and their applications in the 20th century. The triode was invented in 1906 by DeForest, although arc-based Morse-code transmitters were still in use as late as 1912. Wireless was available in WWI, but the superheterodyne receiver was not invented until 1918 (Armstrong).⁴ By 1930 it was clear that higher frequencies were desirable and that transit-time limitations would prevent triodes and tetrodes from providing adequate power for new applications. The search for new RF sources began.

Prior to WW II the total available RF spectrum was about 100 MHz. (approximately 10 TV channels). Today, RF sources exist to take advantage of a spectrum 1000 times wider. Klystrons are now in use, or in development, over that entire spectrum. This is not the case with any other microwave power source.

The invention of radar sparked interest in microwaves and gave birth to the cavity magnetron, which made possible airborne radar and helped the Allies win WW II. Only low-power, mostly "reflex" klystrons were used in WWII. High-power klystrons owe their initial development to particle accelerators, for which the first megawatt klystron was designed and built at Stanford. Radar led to electronic countermeasures (ECM) and TWTs. Magnetic fusion required millimeter wavelengths and caused gyrotrons to be invented in Russia.



D. A. Rozhansky

Fig. 1 D. A. Rozhansky

The invention of the klystron was the work of several people, the first of whom was D. A. Rozhansky, a Professor of Physics at the Leningrad Polytechnic Institute. He proposed a method of producing e-beams of “varying density” in 1932. As far as we know, Rozhansky did not construct any apparatus to test his theory, nor did he publish. However, he worked with a very bright young physicist at his Institute, Agnessa Arsenjeva, who later became Mrs. Oskar Heil. The Russians consider Rozhansky, along with the Heils, the inventors of velocity modulation.

Oskar Heil studied at Goettingen University and probably met Arsenjeva there. They were married in Leningrad in 1934. The same year, Heil applied for an Austrian Patent on “A Procedure and Apparatus for Producing Short Waves.” Subsequently Heil and Arsenjeva both studied with Rutherford at the Cavendish Laboratory in Cambridge, England. In 1935, while Arsenjeva was recuperating from illness in the Italian Alps, they published the classic paper on velocity modulation and electron bunching.⁵



Fig. 2 Oskar and Agnessa Heil

Arsenjeva returned to Russia and Heil went to work at Standard Telephone and Cables (STC) in England. STC developed a line of Heil tubes, called “Coaxial-line Oscillators,” as shown in (Fig. 3).⁶ The operation of the Heil tube was based on a short beam traversing a coaxial line at right angles, with a transit time designed to launch the coaxial mode to a load.

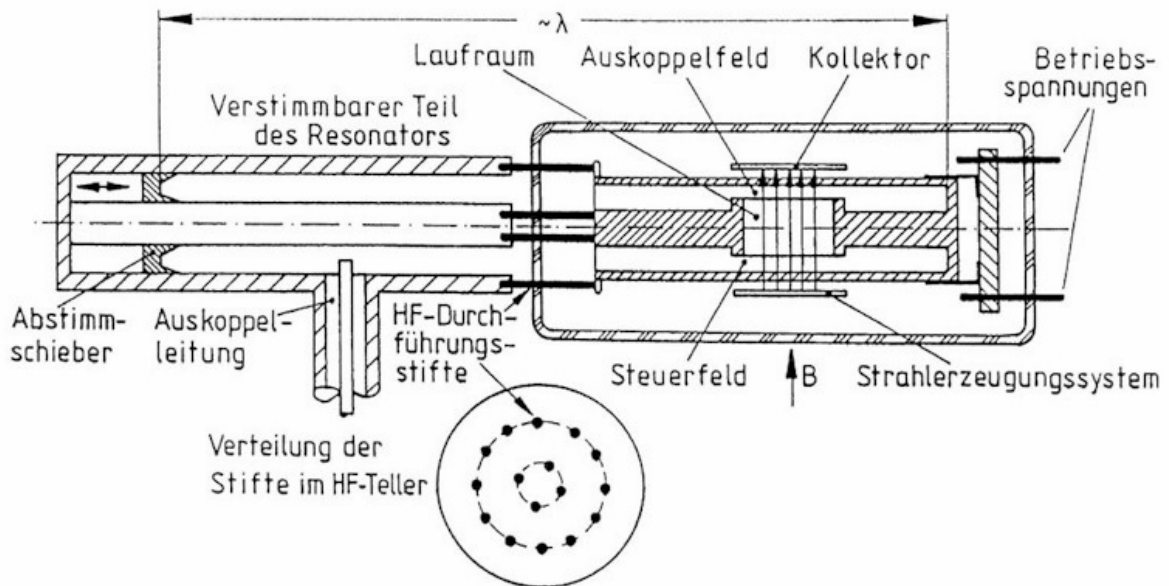


Fig. 3 The Heil velocity modulation tube

Heil left STC the day before England went to war and continued his work at Standard Lorentz in Berlin. His tubes were used in WWII. After the war he was brought to the U.S. by the military and worked at Wright Patterson AFB before being hired by Eimac and moving to California. He died in 1994. Agnessa Heil never left Russia again and died in St. Petersburg in 1991.

During the pre-WWII period, W. W. Hansen, an Associate Professor of Physics at Stanford University, was investigating “a scheme for producing high-voltage electrons,” for use in X-ray spectroscopy. In the process, he invented the microwave cavity (i.e.- a resonator that did not depend on inductors and capacitors to store energy), which made it possible to develop high voltages at high frequencies, with low losses. He also developed the theory necessary to treat resonators as circuit elements, and derived the first analytical expressions for the eigenvalues in cavities of various shapes. His resonators were named “rumbatrons,” presumably because of the back-and-forth travel of electromagnetic waves inside them. The invention of the klystron would not have been possible without Hansen’s rumbatrons. His original UHF resonant cavity survives and is shown in (Fig. 4). Hansen published a paper titled “A Type of Electrical Resonator” in the Journal of Applied Physics in 1937. His experimental cavity resonated at 380 MHz and had a Q_0 of 50,000.⁷

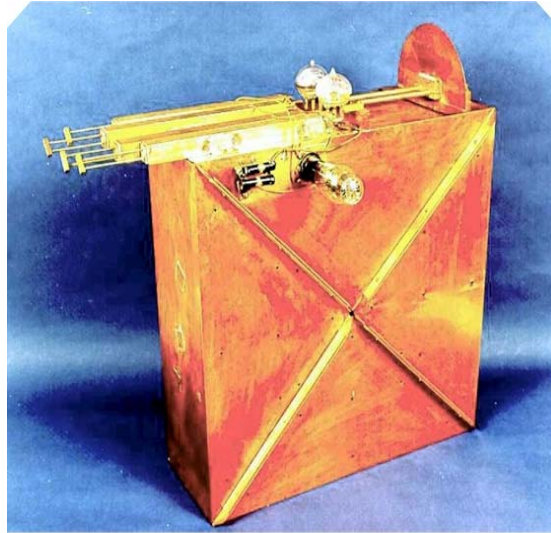


Fig. 4 The Hansen "Electrical Resonator"

Working with Bill Hansen as Research Associates at the Stanford Physics Department, were the Varian brothers, Russell, a physicist, and Sigurd, a former "barnstormer" and Pan-American Airlines pilot. "Sig" Varian believed that high-frequency transmitters could be used aboard airplanes to make "blind" (instruments-only) landings possible. The missing component was a source of high-frequency power. Hansen and the Varians investigated a number of ideas for a microwave source. They were apparently not aware of the Heils' 1935 paper on velocity modulation. Russ Varian conceived of it qualitatively, and on June 15, 1937, applied for a patent.

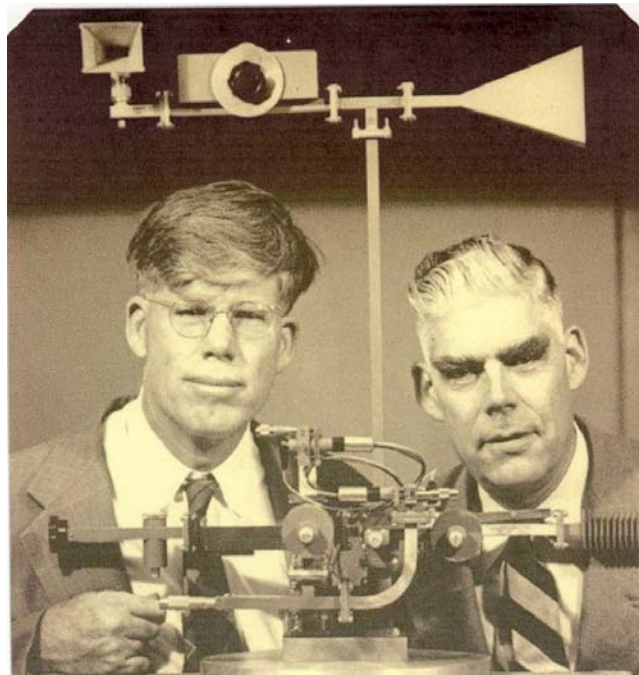


Fig. 5 Russell and Sigurd Varian

On July 21, 1937, Russ Varian entered in his journal the sketch of a two-cavity oscillator, and the following month he and his brother built one. The use of the resonant cavities invented by Hansen made the Varian patent much more useful than the 1934 Heil patent. With help from the Stanford Classics Department, the device was named “klystron” after the old Greek verb (κλύζω), for waves washing on the seashore.

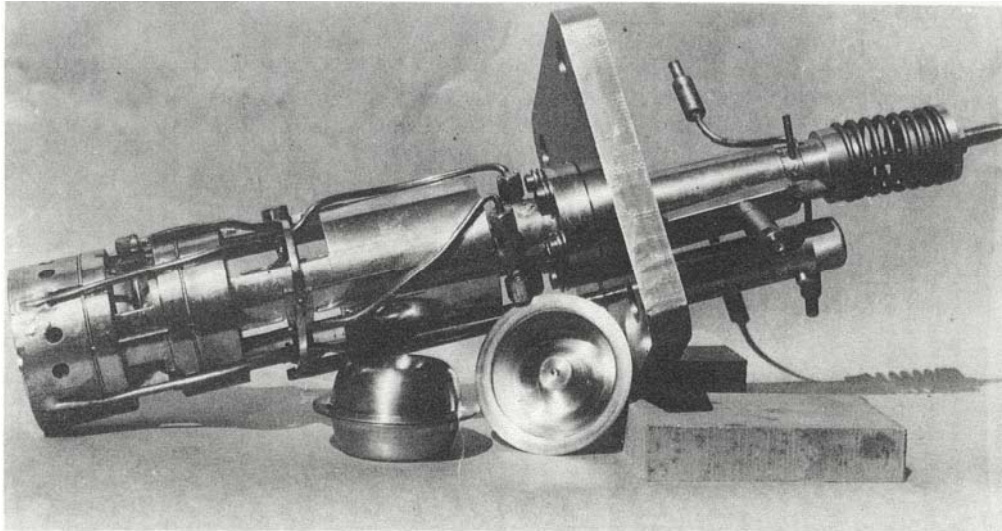


Fig. 6 The Stanford “Model A” klystron

Both Varian brothers died in the 60’s. Varian Associates, the company they founded, sold its tube business to an investment concern in 1996. It was renamed “Communications and Power Industries,” or CPI. The former Varian Associates is now three independent companies, the largest of which manufactures medical accelerators for cancer therapy. CPI was sold to another investment concern in 2003.

Work on klystrons became very intensive during WWII. Radar was independently invented in Germany and Britain before the war, and was initially implemented at UHF frequencies using triodes as sources. In 1940 the development of the magnetron by Randall and Boot in Britain provided a powerful microwave source suitable for airborne high-frequency radar transmitters. The same year, (and before Pearl Harbor) a visit by British scientists to America launched an extraordinary collaboration between Britain and the US, which resulted in magnetrons and klystrons being manufactured for the war effort in Western Electric, Sperry, and other American factories. The reflex version of the klystron, perfected at Sperry and in British laboratories, served as the local oscillator in super heterodyne radar receivers. Together, the magnetron and the reflex klystron made possible airborne S-band radar, a major factor in securing air superiority for the RAF. “Power” klystrons did not exist during the war. The primary reason was lack of adequate beam optics. Klystron amplifiers were mostly of the 2-cavity type, usually without focusing magnets, often with gridded gaps. Beam transmission below 50% was common. In these circumstances one could not expect average power above a few watts, and that made klystrons unsuitable for transmitter use. In early 1944, Ed Ginzton, then at Sperry, visited Britain to exchange information on Doppler radar and “to become acquainted with the development of velocity-modulated tubes in England.” He was very impressed with an EMI two-resonator, external-cavity klystron, the CV (Common Valve) 150. His description of this tubes performance is very interesting. He writes:⁸

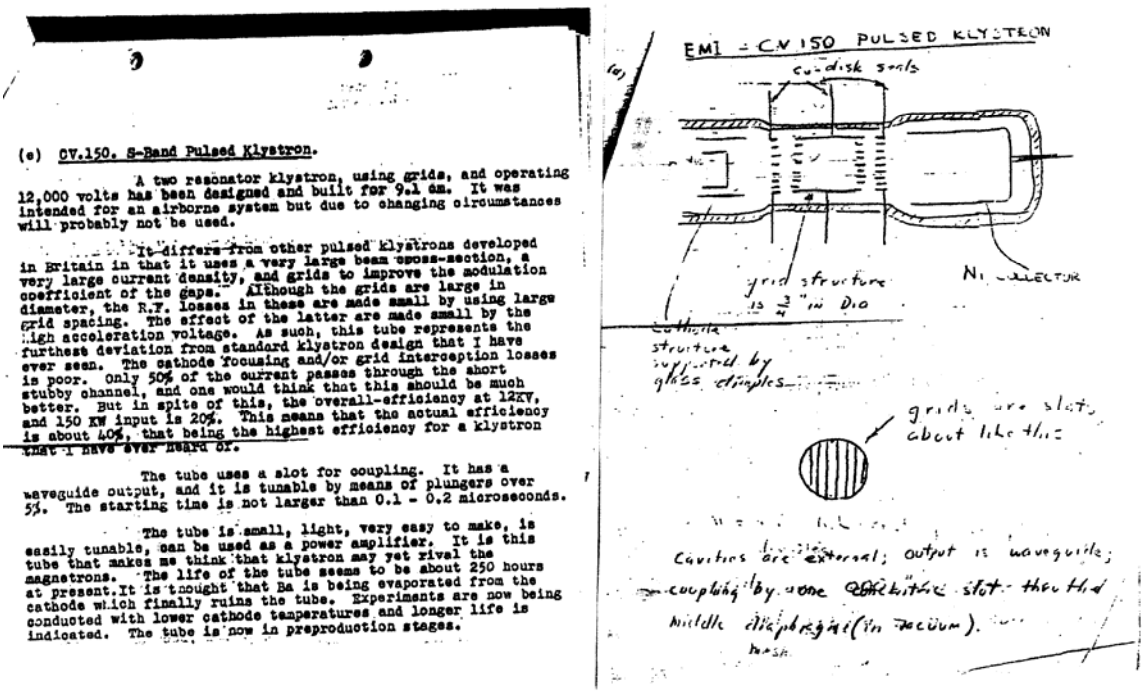


Fig. 7 A page from the Ginzton Diary

“...I saw a klystron of a remarkably simple design which produced 20,000 watts of power, well beyond any klystron made in the United States at that time. The fact that it was so simple and so beautiful impressed me enormously, and led me to develop a still bigger tube a few years later. A two resonator klystron, using grids, and operating 12,000 volts has been designed and built for 9.1 cm. It was intended for an airborne system but due to changing circumstances will probably not be used. It differs from other pulsed klystrons developed in Britain in that it uses a very large beam cross-section, a very large current density and grids to improve the modulation coefficient of the gaps. Although the grids are large in diameter, the RF losses in these are made small by using large grid spacing. The effect of the latter are made small by the high acceleration voltage. As such, this tube represents the furthest deviation from standard klystron design that I have ever seen. The cathode focusing and/or grid interception losses are poor. Only 50% of the current passes through the short, stubby channel and one would think that this should be much better. But in spite of this, the overall-efficiency at 12kV, and 150 kW input is 20%. This means that the actual efficiency is about 40%, that being the highest efficiency for a klystron that I have ever heard of. The tube uses a slot for coupling. It has a waveguide output, and it is tunable by means of plungers over 5%. The starting time is not larger than 0.1 – 0.2 microseconds. The tube is small, light, very easy to make, is easily tunable, and can be used as a power amplifier. It is this tube that makes me think that the klystron may yet rival the magnetrons. The life of the tube seems to be about 250 hours at present. It is thought that Ba is being evaporated from the cathode which finally ruins the tube. Experiments are now being conducted with lower cathode temperatures and longer life is indicated. The tube is now in preproduction stages...”

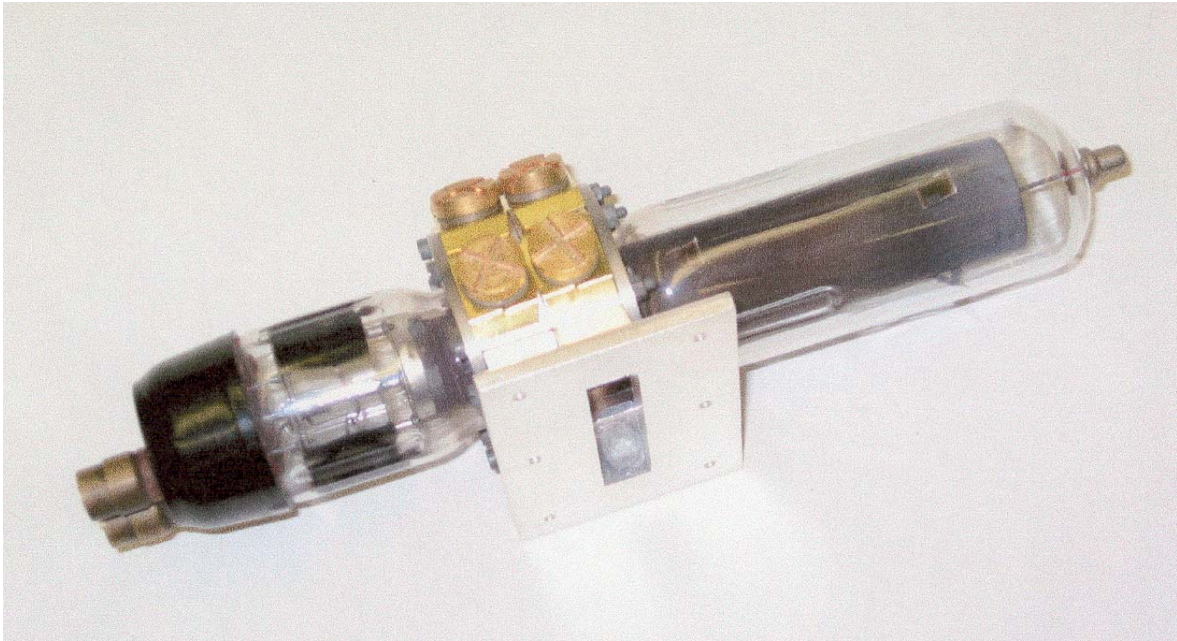


Fig. 8 The EMI CV-150 Klystron

Ginzton did succeed in building a much bigger tube a few years later. Along with Hansen and Marvin Chodorow, he returned to Stanford University after the war, and began work on an S-band accelerator. It was based on a newly invented disk-loaded waveguide slow-wave structure, which was much lighter and more compact than existing lower frequency accelerators.⁹

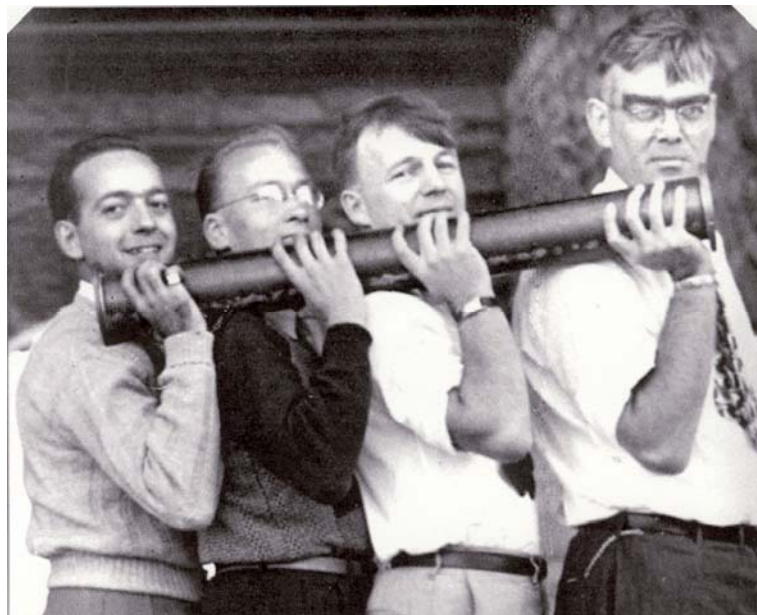


Fig. 9 Hansen and students with the first coupled-cavity electron accelerator

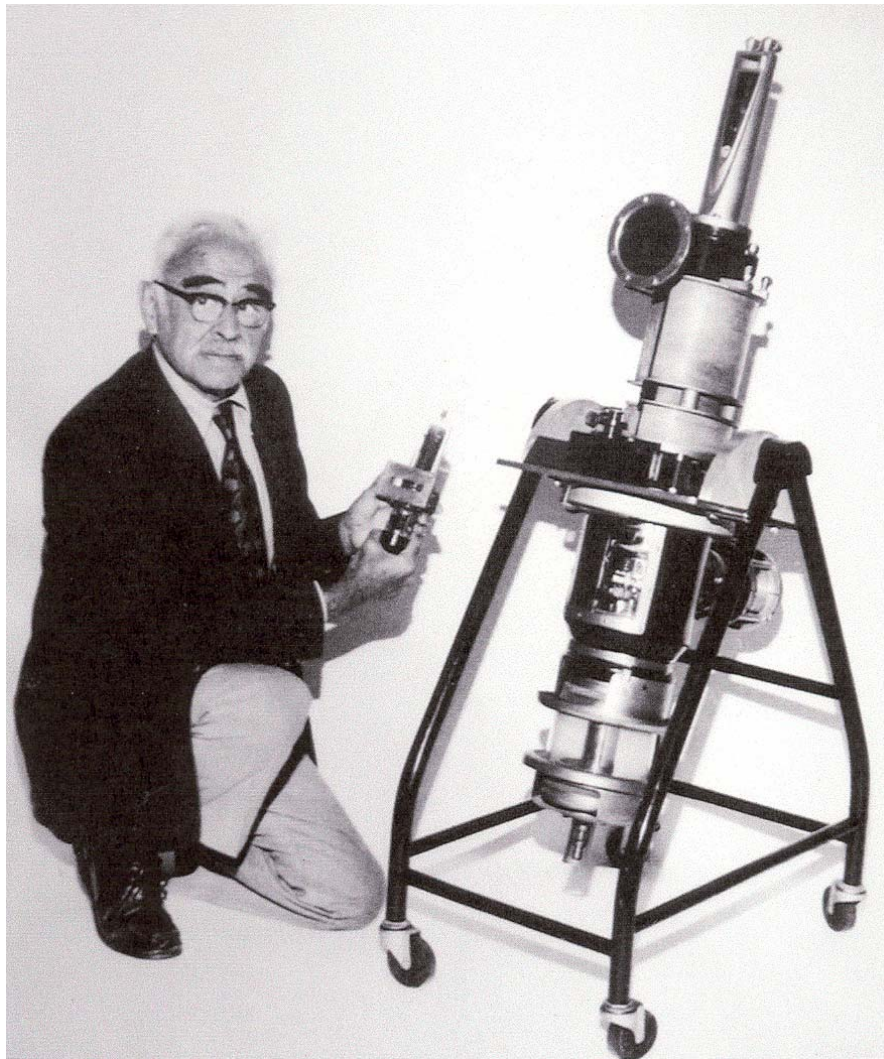


Fig. 10 Marvin Chodorow comparing the CV-150 to the Mark III klystron

As would be the case with many others to follow, this first microwave linear accelerator required a power level many times higher than the klystron state-of-the-art (CV-150). Improvements in electron beam optics, made possible by J. R. Pierce's work at Bell Labs, were essential to this endeavor. Other components also had to be designed for the first time, such as high-voltage modulators and insulators. In 1948, the Stanford klystron for the S-Band Mark III electron accelerator, with its three cavities and wound-on beam-focusing electromagnet, eventually reached a power output of 30 MW with 1-microsecond pulses. It was the first multi-megawatt microwave source of any kind. In the next 50 years, there would be many more advances, but none as impressive or as widely imitated. Klystrons could now be designed to power transmitters for radar, UHF television, and space communications.

The velocity modulation principle, which made klystrons possible, was explained by Russell Varian as follows,¹⁰ (in a book written by his wife, Dorothy): “Just picture a steady stream of cars from San Francisco to Palo Alto; if the cars left San Francisco at equal increments and at the same velocity, then even in Palo Alto they would be evenly spaced and you would call this a direct flow of cars. But suppose somehow the speed of some cars, as they left San Francisco, was increased a bit and others retarded. Then, with time, the fast cars would tend to catch up with the slow ones and they would bunch into groups. Thus, if the velocity of the cars was sufficiently different or the time long enough, the steady stream of cars would be broken and, under ideal conditions, would arrive in Palo Alto in clearly defined groups. In the same way an electron tube can be built in which the control of the e-beam is produced by the principle of bunching, rather than the direct control of a grid in a triode...”

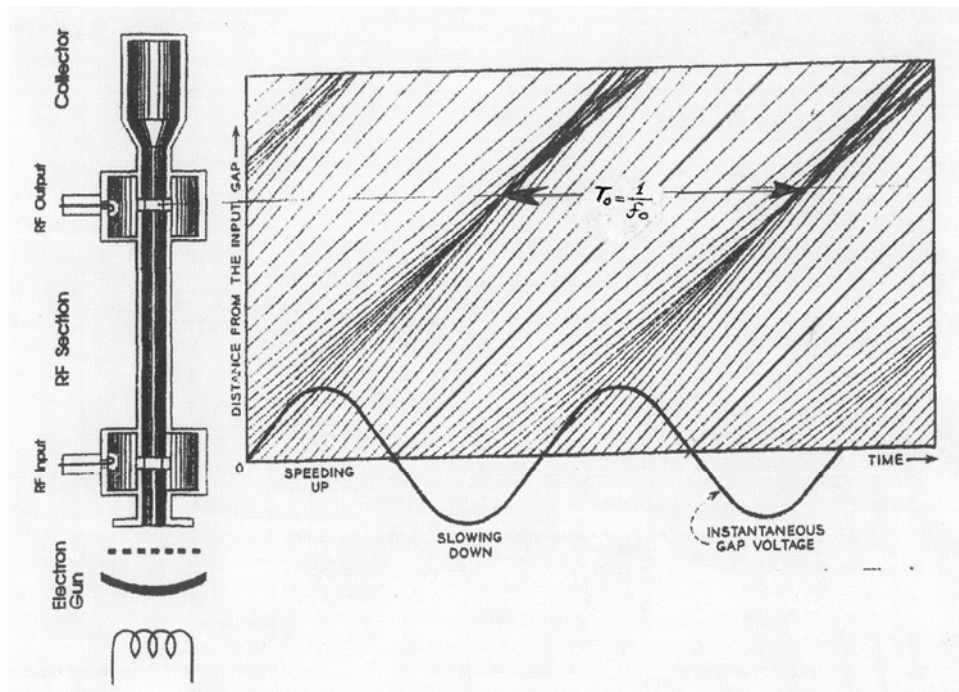
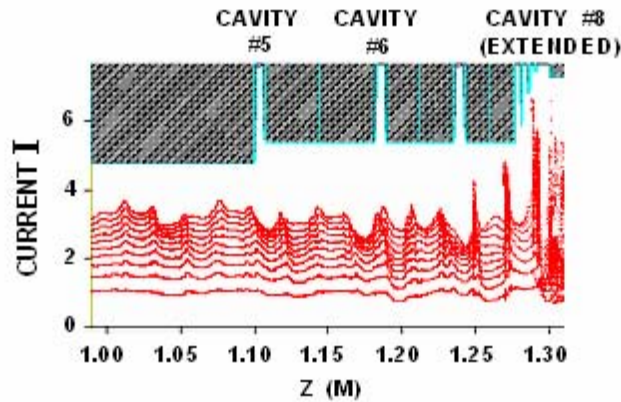


Fig. 11 The Applegate diagram

This is illustrated by the “Applegate” above, showing electrons from an electron gun traversing a gap in the first cavity, and having their velocity modulated by the voltage across that gap.¹¹ As a result, they arrive in bunches at the second, or output cavity. Bunches form around the electrons crossing the first gap when the sinusoidal voltage there crosses from negative to positive (from decelerating to accelerating). Bunches arrive at the second cavity with a period T_0 , which corresponds to the period of the sinusoidal power input to the first cavity. The bunching action shown in the Applegate diagram is entirely ballistic (or kinematic), i.e. the charge of the electrons does not come into play as their trajectories come very close and actually cross. In an average klystron, space charge will modify these trajectories and the interaction between cavities and beam will be better described by “space-charge wave theory,” which treats space charge as an elastic medium and describes electron motion in terms of waves.



MAGIC SIMULATION (OUTPUT SECTION OF 8-CAVITY PPM KLYSTRON)

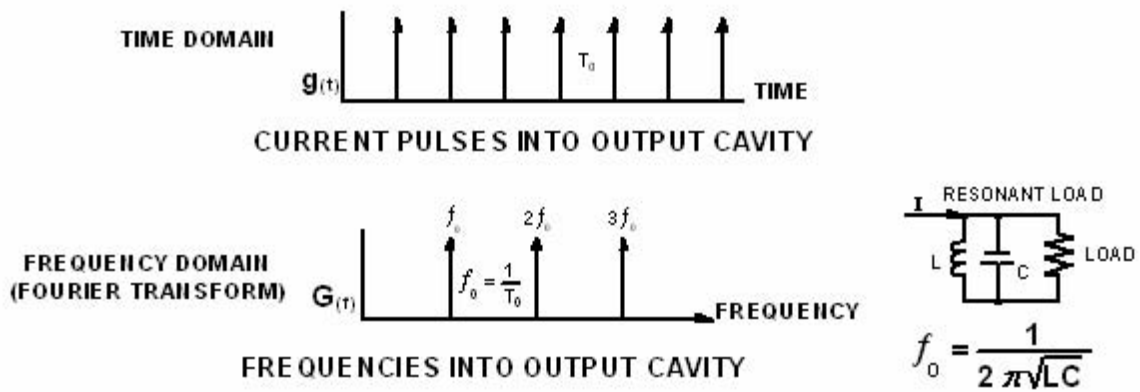


Fig. 12 Bunching and harmonic generation in a klystron

Figure 12 shows a MAGIC simulation of the build-up of RF current in a PPM klystron (See Ch. 5). Bunches form gradually, but get quite pronounced as they approach the output cavity. At that point they are much like mathematical “unit impulses.” If they are idealized that way, they would be a train of pulses represented by the function $g(t)$ below, spaced by T_0 seconds, where T_0 is the inverse of the frequency of operation for the klystron. That train of pulses has a frequency content given by its Fourier transform, represented by $G(f)$. It consists of the fundamental and all its harmonics. The resonant circuit of the output cavity selects just the fundamental (if it is tuned there) and power at that frequency is fed to the load.

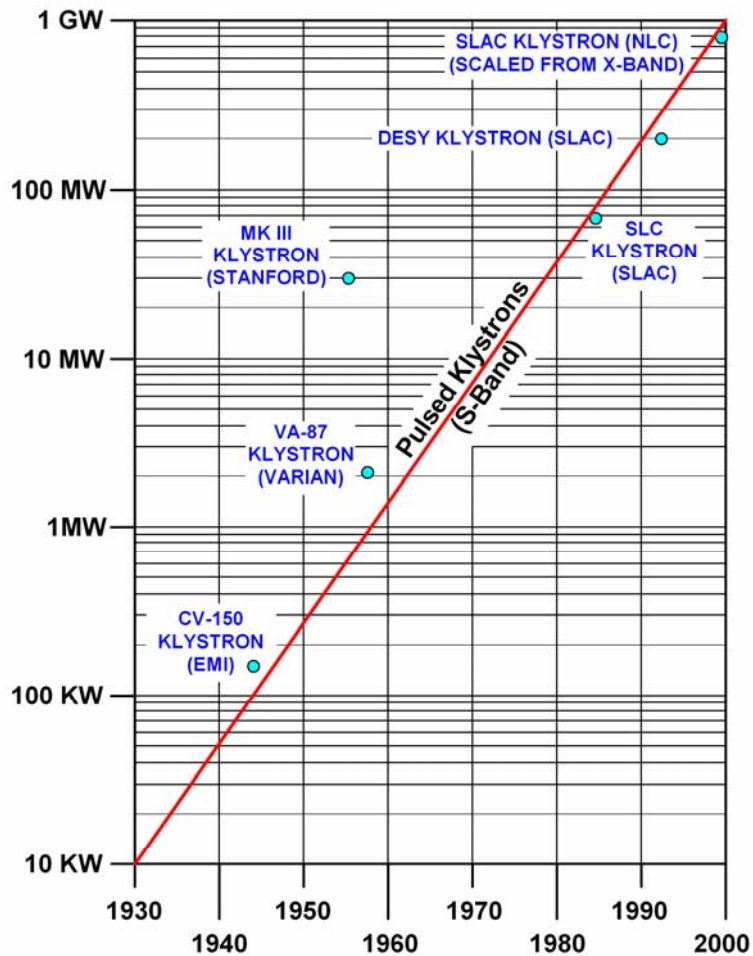


Fig. 13 Progress in the development of pulsed klystrons

Figure 13 illustrates the progress in klystron power in the 60 years since WWII. The trend line for S-band pulsed CW klystrons cannot be expected to go through all the points represented by actual tubes, but nevertheless shows a definite pattern, where output power increases 10-fold every 14 years. Notice how far ahead of its time was the Stanford MK III klystron. The scaling used to put on the chart an X-band pulsed klystron recently developed at SLAC follows the Pf^2 law, which does not strictly apply to pulse tubes since it relates frequency to the surfaces available for cooling, rather than to the surface gradient. That SLAC klystron produces 75 MW at 11.4 GHz, with 1.6 microsecond pulses.¹² It shows on the graph as $16 \times 75 = 1200$ Megawatts (plotted as 1 GW).

Consider now some applications illustrating how the power available from klystrons has made possible systems for which klystrons were usually specifically designed. In almost every case, except the first one (a radar which has been replaced by an active phased array), klystrons remain the only practical sources for these systems, some of which have been in existence for decades.

Radar: As a result of plans laid in the late 1950's, three huge radar stations, each with a range of 3,000 miles, were built to give the US early warning of possible Soviet trans-polar nuclear missile attacks. This was known as the Ballistic Missile Early Warning System or BMEWS. Only one of those radars, at Clear, Alaska, was built on American soil. The others were sited at Thule in Greenland and on Fylingdales Moor in Yorkshire, England. The original FPS50 'billboard' radars and the FPS49 parabolic radars were replaced in the early 1990's by solid-state phased-array systems which have much the same range but are far less susceptible to jamming.

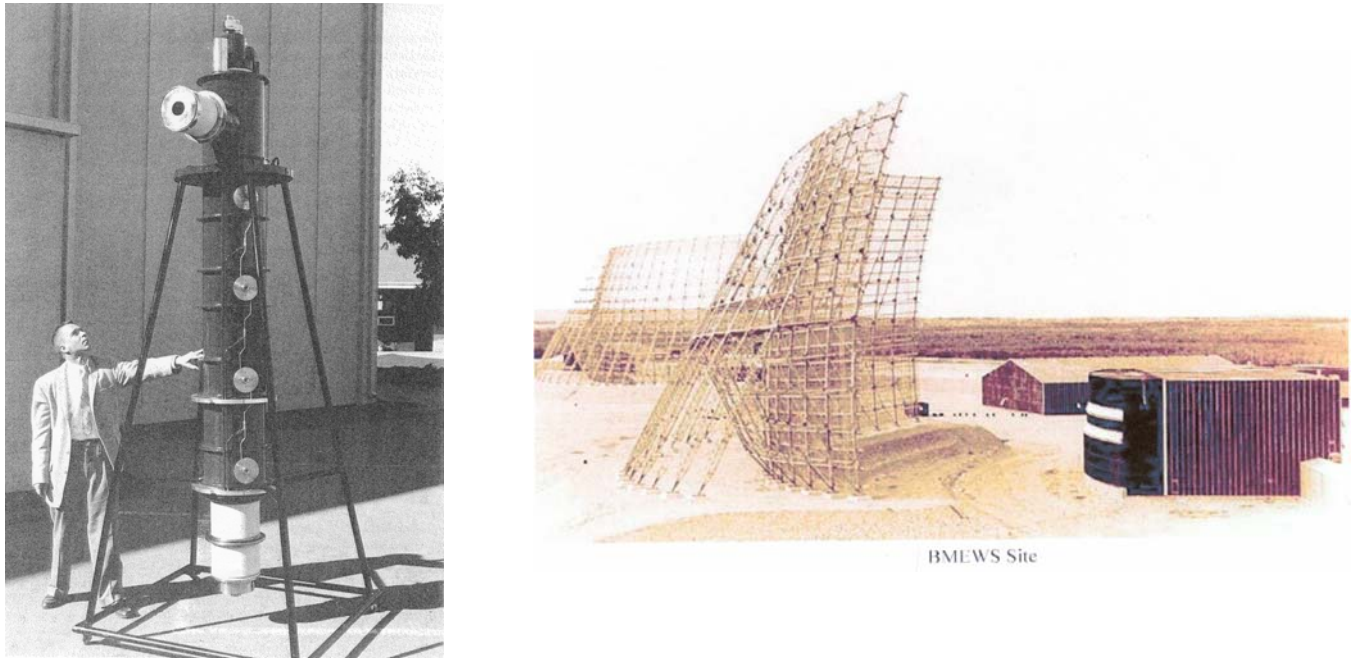


Fig. 14 The VA-812 and the BMEWS system

The first BMEWS klystrons were made by Eimac in the late 50's and replaced the tetrodes that were initially designed into the system. The Eimac klystrons (X626s) were external cavity tubes and did exhibit some ceramic charging problems, which led to a contract to Varian for a large quantity of the integral cavity klystrons (VA812s). In the end, Litton ended up with most of that business, which was considerable. Integral cavity klystrons were specified when Litton won the contract. Those tubes all had modulating anodes and were operated in floating-deck long-pulse modulators. The BMEWS klystrons operated at 150 kV and produced 1.25-MW peak and 75-MW average power at approximately 450 MHz. At that average power, those klystrons were the most powerful ever produced. The term "superpower" was coined to describe them. The fact that they have been replaced in the BMEWS function by transistors in a phased array configuration illustrates the trend of solid-state incursions in microwave transmitters wherever power or frequency is low, or if parabolic antennas can be replaced by phased arrays.

UHF television was one of the early klystron applications. The bandwidth required is relatively small, the power too high for transistors to be practical, and the most important requirement is high power at high efficiency. The original klystrons were Eimac external cavity tubes, at about 30-kW output, mostly in GE transmitters. Subsequently, Varian, working with RCA, introduced a line of integral cavity tubes. Two interesting high-efficiency devices, based on the original klystrons, resulted from an eventual Eimac-Varian collaboration. One was the

“Klystrode,” invented at Eimac, (or the IOT when it was re-invented at EEV), in which a gridded gun is part of the input cavity circuit and the beam current is a function of the RF drive, as it is in a tetrode. Another was an external cavity klystron equipped with a multi-stage depressed collector (MSDC). The MSDC klystron had an output power of 60 kW, 46 dB gain, and a 70% “peak synch” efficiency. The efficiency for the klystrode is defined differently: Its average efficiency over a normal TV spectrum is 35 % higher than its peak synch efficiency. The gain for the klystrode is lower, 22 dB, but the peak synch power is 80 kW.

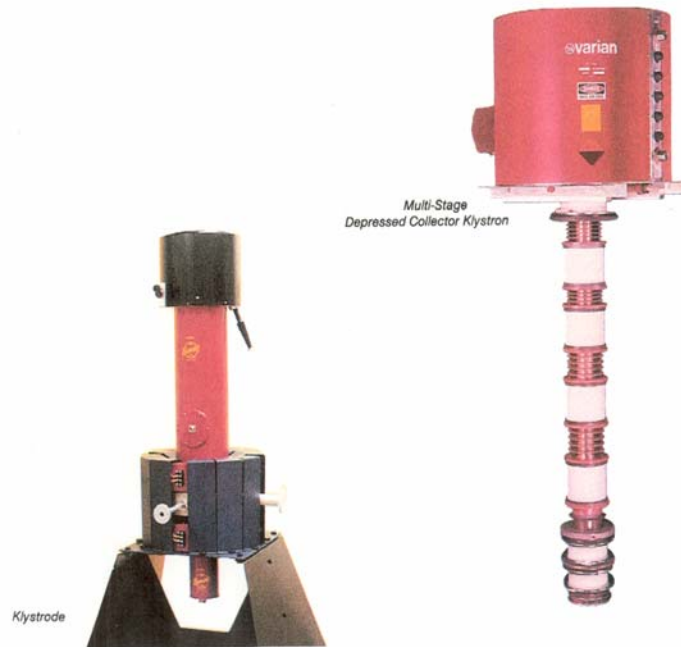


Fig. 15 UHF-TV klystrons: An integral cavity “Klystrode,” and an external cavity MSDC klystron

Medicine is a major and socially important klystron application. Shown in (Fig.16) is a Varian Clinical Accelerator or “Clinac.”¹³ In this hospital equipment an S-band standing-wave accelerator allows the generation of high output, stable X-ray modes at widely separated energies, providing a full range of treatment capability. The accelerator is located inside a rotating gantry and is driven by a 5-MW pulsed klystron. There are more than 4,000 medical accelerators in operation around the world. Most are powered with magnetrons but higher energy modern machines require klystrons. In societies with health-care services comparable to the US or western Europe, the average person has a one in eight chance of being treated on a linear accelerator in his or her lifetime.

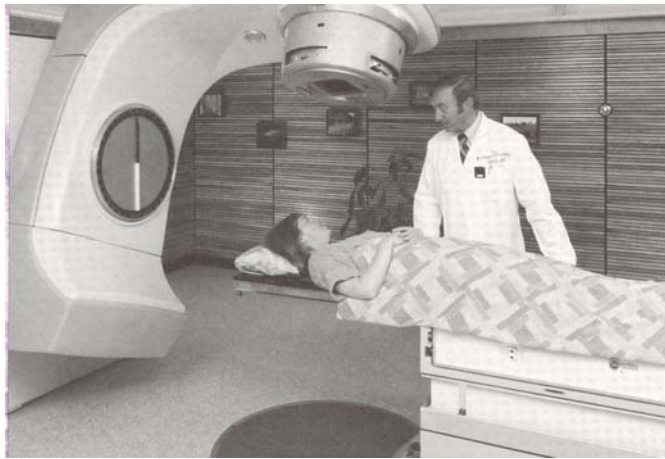


Fig. 16 A Varian “Clinac”

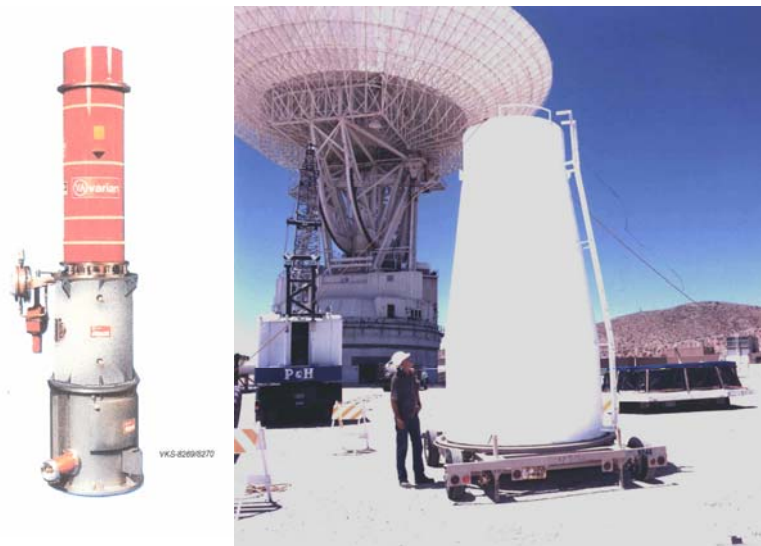


Fig. 17 The DSN 220 ft. antenna, the Varian 500-kW CW S-band klystron, and the module at the antenna center that houses several klystrons

Communications. The NASA Deep Space Network (DSN) is an international network of antennas that supports interplanetary spacecraft missions and radio and radar astronomy observations for the exploration of the solar system and the universe. The network also supports selected Earth-orbiting missions. The DSN currently consists of three deep-space communications facilities placed approximately 120 degrees apart around the world: at Goldstone, in California's Mojave Desert; near Madrid, Spain; and near Canberra, Australia. This strategic placement permits constant observation of spacecraft as the Earth rotates, and helps to make the DSN the largest and most sensitive scientific telecommunications system in the world.

At each facility, 220-ft antennas are powered by a 500-kW, CW S-band klystron and two 150-kW, X-band klystrons, operated in parallel. There is also another 25-kW X-band klystron. S-band is used for communications with orbiting spacecraft. The high-power X-band tubes are used in a radar mode. The 25-kW klystron is actually the tube recently used to send commands to the Mars orbiter and Spirit.

All the above klystrons, except for their exceptionally high power, are more or less conventional. They were designed about 30 years ago, as were the systems they power.

It is now instructive to consider five specific examples, which represent the current state-of-the-art for very high-power klystrons.

The first is the Varian 3030A, an experimental X-band klystron, which in 1969 produced a CW output of 1030 kW.^{14,3}

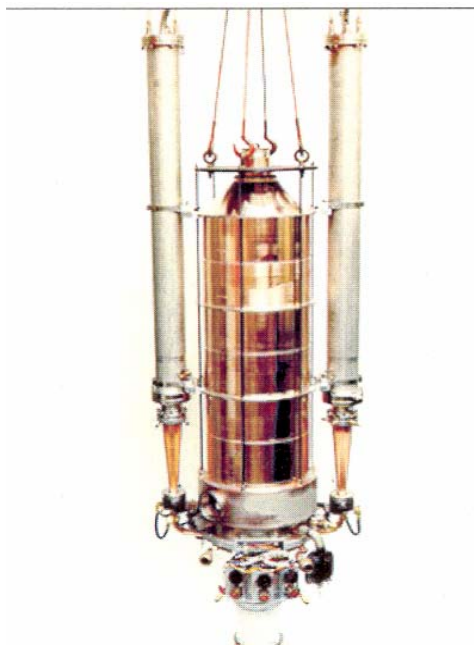


Fig. 18 The Varian X-Band 1-MW CW klystron

This tube (Fig. 18) is about 80% collector, illustrating the point that klystrons are not nearly as limited in their average power by frequency, as are crossed-field tubes. They just require large collectors. Nevertheless, ohmic losses in the output cavity do limit the output at X-Band. Also, the surface available for cooling a single cavity is not sufficient to handle the I^2R losses associated with the output power desired. A circuit efficiency of 99%, associated with a desired output of 1-MW CW would require that 10 kilowatts watts of power dissipation be

removed from the klystron's output cavity to prevent it from overheating and drifting in frequency. Such a cavity would have the approximate surface of a matchbox.

A solution to that problem was an extended interaction output cavity¹⁵ (i.e. - a larger, essentially overmoded cavity, designed to be “synchronous” with the beam for the mode chosen). Such a cavity has not only a larger surface from which to remove the heat, but also a higher R/Q, which leads to a lower Q_{ext} and a higher circuit efficiency. This concept, was originally demonstrated by Tore Wessel-Berg at Stanford. Wessel-Berg's objective was a wider bandwidth. He also contributed to the design of the X-3030.

The 3030 development project was a product of the Cold War. Its 35-year power record would probably have been exceeded by now, had the interest in “Superpower” klystrons remained as high as it was in the 50's and 60's. Today, scientific high-energy particle accelerators are setting the pace in the development of very high-power klystrons. The “Next Linear Collider” (NLC)¹⁶ is being designed, initially, as a 500-GeV collider and ultimately a 1-TeV e+e- machine. Its full length will be approximately 30 kilometers (18 miles). Current design for the 500-GeV version calls for as many as 4000 X-band klystrons, each delivering 75 MW, with 1.6 microsecond pulses and an average power of 14.4 kW.¹⁷ Those 11.4-GHz klystrons operate at 500 kV, with a perveance of about 0.7×10^{-6} . Beam confinement is by Periodic Permanent Magnet (PPM) focusing because, given the number of klystrons, the NLC power budget does not permit the use of electromagnets (Fig. 19).



Fig. 19 The SLAC 11.4 GHz, 75-MW PPM klystron

Figure 20 shows the SLAC 15-ft long B-factory klystron (BFK).¹⁸ It operates at 90 kV, with a microperveance of 1 and produces 1.25-MW CW. It has seven cavities which are tuned capacitively by moving a flexible cavity wall and changing the gap length. Overall efficiency is 60%, gain 50 dB and the nominal bandwidth is 10 MHz. The collector is capable of dissipating full beam power. The klystron is operated horizontally. The BFK design was a joint undertaking between SLAC and Varian. In Chapter 4, the experimental gain response of the BFK of the klystron will be compared to analytical calculations, as well as to 1-D and 2-D simulation codes.



Fig. 20 The SLAC 1.25 MW CW B-Factory klystron

Finally, (Fig. 21a) shows the TESLA Linear Collider multiple-beam klystron (MBK), TH1801, produced by Thales Electron Devices (Formerly *Thomson Tubes Electroniques*). Seven beams (one of which is centered), each of microperveance 0.5 are launched into independent drift tubes but common cavities. After their energy is extracted at the output, they are directed to a common collector. The MBK design was adopted because of the extraordinary power and efficiency requirements of the TESLA Superconducting Linear Collider. The tube frequency is 1300 MHz, the peak power output 10 MW, the average power 150 kW and the efficiency “goal” 70%. The operating voltage is 110kV. The pulse duration is 1.5 milliseconds and the PRF 10 Hz. The long pulse places severe thermal requirements (which are exacerbated by an elevated voltage) and the high efficiency calls for low perveance. The MBK design addresses both issues. Thales has reported an efficiency of 65%.



Fig. 21a The Thales MBK



Fig. 21b The CPI MBK.

Shown in (Fig. 21b) is the CPI VKL-8301, which was built for TESLA to the same specification.¹⁹ It is also an MBK, but its design is fundamentally different and is based more on life cycle cost than on initial price. It employs six beams, on a larger “bolt circle” than the French tube, and without a center beam. This arrangement (which employs individual intermediate cavities) makes possible larger cathodes and lower cathode current densities. Hence the life of the VKL-8301 can be expected to be longer than the TH1801.

Chapter 2.

Kinematic Theory of Velocity Modulation

2.1 Introduction

This section and the next will present the principal formulae used in the design of klystron amplifiers. The analytical small-signal Mathcad code (Appendix I) contains such formulae and is used for the preliminary design of a new klystron. The theory below is included because it is necessary for the proper treatment of coupling coefficients and beam loading in complex cavities. This is important, particularly at millimeter wave frequencies or very high peak powers, where extended interaction cavities may be necessary.

The AJ-Disk 1-D simulation code (Appendix II) uses a combination of analytical formulae and electron dynamics and is used for a quick assessment of the power and efficiency of the new klystron design. Finally, the 2-D and 3-D MAGIC codes (Appendix III) simulate klystron performance using first principles (electron dynamics and Maxwell's equations). Simulation codes contain no small-signal approximations and are increasingly more accurate as they proceed from 1-D to 2-D to 3-D. In the process, they also become more time-consuming. They are described in the Appendices, where they are used to treat a working klystron example, with its actual performance compared to the results from three different codes. This is useful information, since klystron design in the 21st century is being carried out almost entirely on computers (i.e. - with little or no "cold-testing" or "beam testing").

The kinematic (no space charge) analysis below follows several authors who published books on klystrons shortly after WW II. The velocity modulation (or "bunching") two-cavity theory below is the only large signal analytical treatment of klystrons in this chapter. It leads to the Bessel function coefficients of the current harmonics and a calculation of two-cavity amplifier efficiency. The subsequent derivation of the coupling coefficient and the presentation of the beam-loading formulae are based on small signal approximations, which are valid for all but the final cavities of a multi-cavity klystron. Neither treatment takes space charge into account. That is done in Chapter 3. All derivations in this and the next section are non-relativistic.

2.2 Two-Cavity "Bunching" Theory

Consider a klystron consisting of two cavities, a "buncher" and a "catcher," both gridded, as shown in (Fig. 22). Let a beam of electrons, which has been accelerated by a potential V_0 to a velocity u_0 , traverse the first pair of grids, where it is acted upon by an RF voltage $V_1 \sin \omega t$, reduced by a "coupling coefficient" M . The latter modifies the voltage across the grids due to the finite transit time, resulting in a lower effective voltage modulating the e-beam. Expressions for the coupling coefficient M (always less than 1) will be derived later.

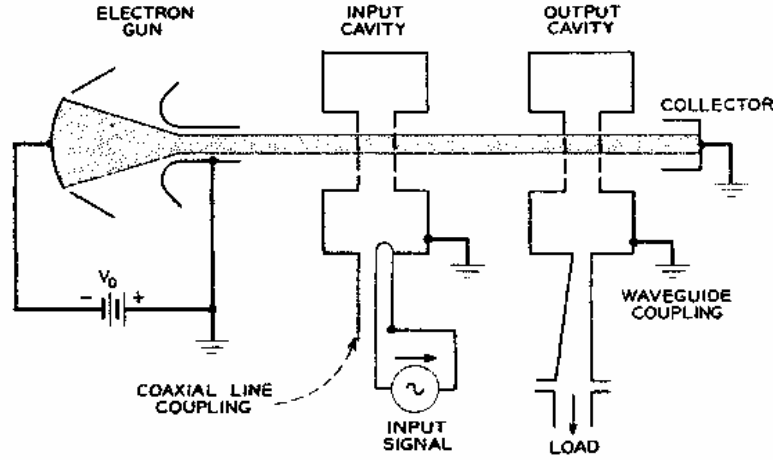


Fig. 22 A two-cavity klystron (this figure, and a number of others that follow are from Reference 11)

The electrons in the beam enter the gridded gap with energy

$$\frac{1}{2}mu_0^2 = eV_0 \quad (1)$$

where the e is the electron charge. The electron energy is modified by the RF field at the gap and the following relationship can be written for the exit velocity u :

$$\frac{1}{2}mu^2 - \frac{1}{2}mu_0^2 = eMV_1 \sin \omega t \quad (2)$$

From the above it follows that

$$u = u_0 \sqrt{1 + \frac{MV_1}{V_0} \sin \omega t} \quad (3)$$

If one assumes that $V_1 \ll V_0$ (which is a good assumption for the first cavity of a two-cavity klystron), then

$$u \cong u_0 \left(1 + \frac{MV_1}{2V_0} \sin \omega t \right) \quad (4)$$

Consider first the case for which the first interaction gap is very narrow, such that the finite transit time of the entering electrons can be neglected. (Later, the activity within both interaction gaps will be discussed.) The electrons then enter, and leave the first gap at time t_1 , then drift for a distance l , and arrive at the center of the second gap at time t_2 . Then (invoking again the small-signal assumption $V_1/V_0 \ll 1$)

$$t_2 = t_1 + \frac{l}{u} = t_1 + \frac{l}{u_0 \left(1 + \frac{MV_1}{2V_0} \sin \omega t_1\right)} \approx t_1 + \frac{l}{u_0} - \frac{lMV_1}{2u_0V_0} \sin \omega t_1 \quad (5)$$

or, in terms of phase $\omega t_2 = \omega t_1 + \theta_0 - X \sin \omega t_1$ (6)

where, $\theta_0 = \omega l/u_0$, and the dimensionless quantity $X = MV_1\theta_0/2V_0$ is called the ‘‘bunching parameter.’’ When $X > 1$, ωt_2 is a multivalued function of ωt_1 , and there is electron overtaking.

The quantity of charge leaving the buncher in the time interval t_1 to $t_1 + dt_1$ is $I_o dt_1$, at $t_1 = 0$, where I_o is the beam DC current entering the buncher. This charge, after drifting, enters the catcher in the interval t_2 to $t_2 + dt_2$. If I_t (total current, DC and RF) is the current transported by the beam to the entrance to the catcher, then through conservation of charge,

$$I_o dt_1 = I_t dt_2 \quad (7)$$

Differentiating Eq. (6) yields

$$\frac{dt_2}{dt_1} = 1 - X \cos \omega t_1 \quad (8)$$

which can be combined with Eq. (7) to give

$$I_t = \frac{I_o}{(1 - X \cos \omega t_1)} \quad (9)$$

For $X = 1$, the current at the catcher becomes infinite (Fig. 23), since the finite charge transported from the buncher at $t_1 = 0$ arrives at the catcher in a zero time interval ($dt_2/dt_1=0$). To calculate I_t , one must then sum the absolute values of all current contributions to I_t from time segments t_{11} , t_{12} , etc, at the buncher as follows,

$$I_t = I_o \left[\frac{1}{|1 - X \cos \omega t_{11}|} + \frac{1}{|1 - X \cos \omega t_{12}|} + \dots \right] \quad (10)$$

The current waveforms at the catcher are shown in (Fig. 24). Note that at the lower values of X they are almost sinusoidal, but they become rich in harmonics at $X = 1$ and above.

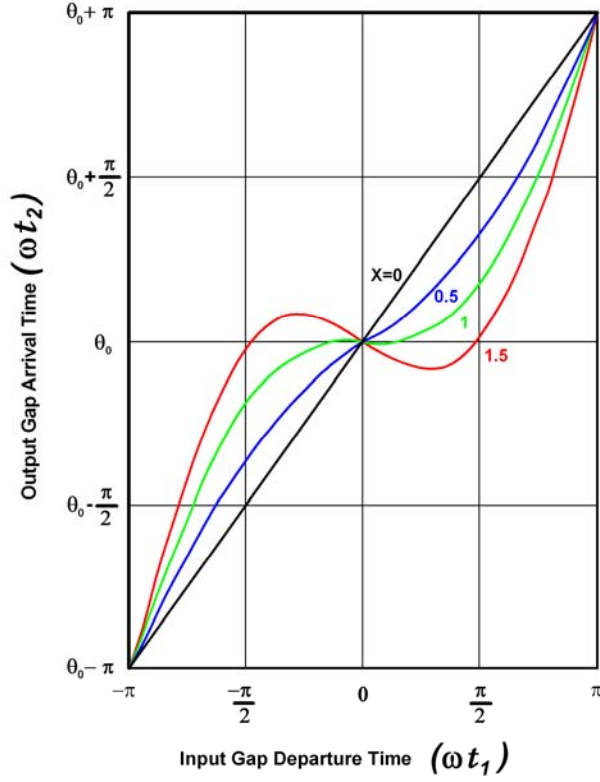


Fig. 23 Electron vs. arrival departure phase in a two-cavity klystron, as a function of the bunching parameter X . (Ref. 11)

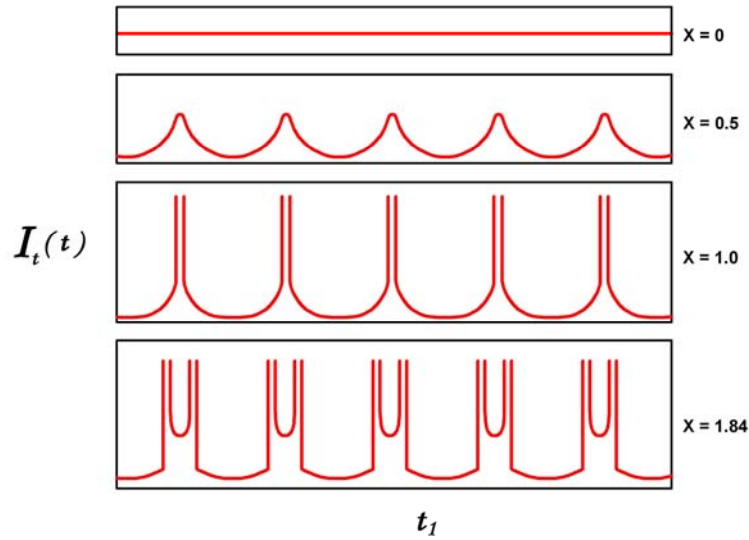


Fig. 24 Bunching waveforms as a function of X (Ref. 11)

Since I_t is clearly a periodic function of ωt_2 , it can be expanded in a Fourier series, as follows,

$$I_t = I_o + \sum_1^{\infty} [a_n \cos n(\omega t_2 - \theta_0) + b_n \sin n(\omega t_2 - \theta_0)] \quad (11)$$

with coefficients given by

$$a_n = 1/\pi \int_{\theta_0 - \pi}^{\theta_0 + \pi} I_t \cos n(\omega t_2 - \theta_0) d(\omega t_2) \quad (12)$$

and

$$b_n = 1/\pi \int_{\theta_0 - \pi}^{\theta_0 + \pi} I_t \sin n(\omega t_2 - \theta_0) d(\omega t_2) \quad (13)$$

Substituting Eq. (6) and Eq. (7) into (12) and (13) above, these become

$$a_n = \frac{I_0}{\pi} \int_{-\pi}^{\pi} \cos n(\omega t_1 - X \sin \omega t_1) d(\omega t_1) \quad (14)$$

and

$$b_n = \frac{I_0}{\pi} \int_{-\pi}^{\pi} \sin n(\omega t_1 - X \sin \omega t_1) d(\omega t_1) \quad (15)$$

Note that b_n is identically equal to zero, since the integrand is an odd function of ωt_1 . It turns out that the expression Eq. (14) for the a_n coefficients is also a representation of the Bessel functions of the first kind and n th order as in

$$a_n = 2I_0 J_n(nX) \quad (16)$$

Therefore, the catcher RF current I_t can be written as the following series

$$I_t = I_0 + 2I_0 \sum_1^{\infty} J_n(nX) \cos n(\omega t_1 - \theta_0) \quad (17)$$

The $n = 1$ harmonic (the fundamental) is simply

$$I_1 = 2I_0 J_1(X) \cos(\omega t - \theta_0) = \text{Re} \left[2I_0 J_1(X) e^{j(\omega t - \theta_0)} \right] \quad (18)$$

When $X < 1$, the series in Eq. (17) converges for all values of t_2 . For $X = 1$, and $X > 1$, there are discontinuities at various t_2 values as was shown in (Fig. 24) (which would disappear if space charge were taken into account). The harmonic amplitudes correspond to the peaks of the Bessel functions (Fig 25). If the current I_t were a series of δ -functions (as in the example in Fig. 12), then all harmonics would be equal. In this case, they are almost equal.

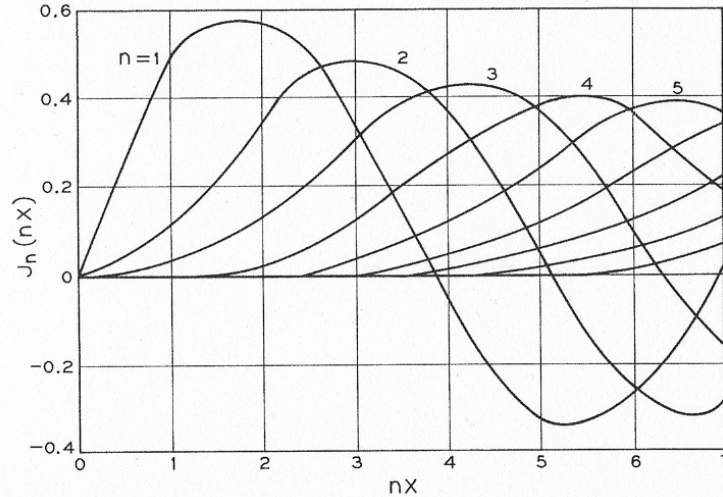


Fig. 25 The first 5 Bessel functions of the first kind. (Ref. 11)

One can now calculate the output power from the fundamental ($n = 1$), using Eq. (18) and the maximum value of $J_1(X)$, which is 0.582 and occurs at $X = 1.84$. The output power is the product of the RF current I_1 and the maximum voltage that can be developed across the output gap without reflecting electrons, which is the beam voltage V_0 . Both are peak values, so

$$P_{out} = \frac{1.16I_0}{\sqrt{2}} \times \frac{V_0}{\sqrt{2}} = 0.58I_0V_0 = 0.58P_{in} \quad (19)$$

Consequently, for the two-cavity klystron, without space charge and with sinusoidal voltage modulation, the maximum efficiency is 58%. The above derivation is completely valid, even when there is electron overtaking. The small-signal approximation, used to formulate the expressions used in launching the velocity-modulated beam into the drift space is not employed beyond the buncher in arriving at the above result.

However, as will be seen in the following sections, the effects of space charge and a number of other issues force a much lower efficiency in the two-cavity klystron case. On the other hand, it has been shown by simulation and experiment in multiple cavity klystrons that the use of a 2nd harmonic cavity, or multiple cavities properly arranged, can produce I_1/I_0 ratios as high as 1.8. In one case, a multi-cavity experimental klystron efficiency of 74% has been a result of such optimum bunching,²⁰ which incidentally relies on space-charge forces, as discussed in the next section.

The velocity modulation kinematic treatment above was first published (in the US) by D. L. Webster,²¹ a collaborator of Hansen and the Varians at Stanford. His 1939 *Journal of Applied Physics* article included, in addition to the “bunching” theory, a brief theory of “debunching”

(i.e. - an accounting of the effects of space charge on the velocity modulation process). Eugene Feenberg, a member of the wartime Sperry Gyroscope “Tube Development Laboratory,” developed the Webster theory into a considerably more detailed mathematical treatise, which included the addition of a third cavity to the original two-cavity klystron, and the first formulae for coupling coefficients and beam-loading in gridded and ungridded klystron cavity gaps. The Feenberg “Notes on Velocity Modulation”²² are not easy reading and were never published.

2.3 Small-Signal Analysis for the Coupling Coefficient

The Feenberg theory and most of the books on klystrons published in the 1940’s and the early 1950’s developed formulae for the design of klystrons that included the assumption that $u_0 \ll c$. However, with the previously mentioned original Ginzton/Chodorow megawatt Stanford klystron, relativistic beams have become rather commonplace in radar and accelerator klystrons and relativistic corrections are necessary in the design. The derivations that follow are not relativistic, but the table in Appendix V provides correction factors for all pertinent klystron parameters and variables.

The objective is to define a coupling coefficient \underline{M} and to derive expressions for it under different assumptions for the geometry of the interaction gap and the beam. A strong magnetic confining field is assumed, with no radial electron motion allowed. Initially, the calculation will consider electron motion only on-axis. Subsequently, M will be averaged over the assumed cylindrical beam.

The coupling coefficient M is probably the most important parameter used in the design of a klystron because the klystron gain is a function of M^{2n} (where n is the number of cavities), and because it is very sensitive to the beam diameter, which is never known precisely. Hence, discrepancies in the calculated or simulated gain of a klystron can usually be traced to inaccuracies in the evaluation of the coupling coefficient.

We begin with the equation of motion of an electron in a gridded gap field $E(z)$ defined as

$$E_z(z, t) = E_m f(z) e^{j\omega t} \quad (20)$$

Where $f(z)$ is a “field shape factor,” and the quantity E_m is related to the rf voltage V_1 across the gap by the equation

$$V_1 = \int_0^d E_z(z, t) dz = \int_0^d E_m f(z) e^{j\omega t} dz \quad (21)$$

A parameter, α (for small-signal $\alpha \ll 1$), will be used to define the depth of modulation in relation to the DC beam voltage

$$\alpha = V_1 / V_0 \quad (22)$$

Now, the acceleration of electrons entering the gap field is given by

$$\frac{d^2 z}{dt^2} = \frac{e}{m} E(z, t) = \frac{e}{m} E_m f(z) e^{j\omega t} \quad (23)$$

We multiply both sides of Eq. (23) by $2dz$ to obtain the square of the derivative of the velocity u

$$2 \frac{dz}{dt} \frac{d^2z}{dt^2} dt = \frac{d}{dt} \left(\frac{dz}{dt} \right)^2 dt = 2E_m \frac{e}{m} f(z) e^{j\omega t} dz \quad (24)$$

If the field in the gap is small, ($\alpha \ll 1$) the electron position at time t would be approximately

$$u_0 t \approx z + \alpha h(z) \quad (25)$$

We introduce $\beta_e = \frac{\omega}{u_0}$, “the beam propagation factor.” Multiplying both sides of Eq. (25) by β_e , we obtain, approximately

$$\omega t = \beta_e z \quad (26)$$

Replacing ωt by $\beta_e z$ and integrating Eq. (24)

$$\frac{mu^2}{2} - \frac{mu_0^2}{2} = eE_m \int_0^d f(z) e^{j\beta_e z} dz \quad (27)$$

where u the velocity of the electrons exiting the gap and u_0 the velocity corresponding to the beam voltage V_0 . Thus, the change in electron kinetic energy as it traverses the gap is effected through an “effective voltage”

$$V_{eff} = E_m \int_0^d f(z) e^{j\beta_e z} dz = \int_0^d E_z(z, t) e^{j\beta_e z} dz \quad (28)$$

We form a ratio of the effective voltage to the integral of the applied field and define the ratio as the coupling coefficient M

$$M(\beta_e) = \frac{\int_0^d E_z(z) e^{j\beta_e z} dz}{\int_0^d E_z(z) dz} \quad (29)$$

The coupling coefficient is seen to be a dimensionless quantity, dependent only on the field shape factor. If the field is constant, as it is across a gridded gap, the integral in the denominator is trivial.

Equation (29) can be generalized by extending the integration over the entire z -axis. It can then be applied to a gridless gap, such as that in (Fig. 26). A more general expression for the coupling coefficient is then

$$M(\beta_e) = \frac{\int_{-\infty}^{\infty} E_z(z) e^{j\beta_e z} dz}{\int_{-\infty}^{\infty} E_z(z) dz} = \frac{V_{eff}}{V_1} \quad (30)$$

In words, M is equal to the “convolution” of the axial electric field $E(z)$ with the exponential $e^{j\beta_e z}$, divided by the voltage V_1 (integral of the field) across the gap.

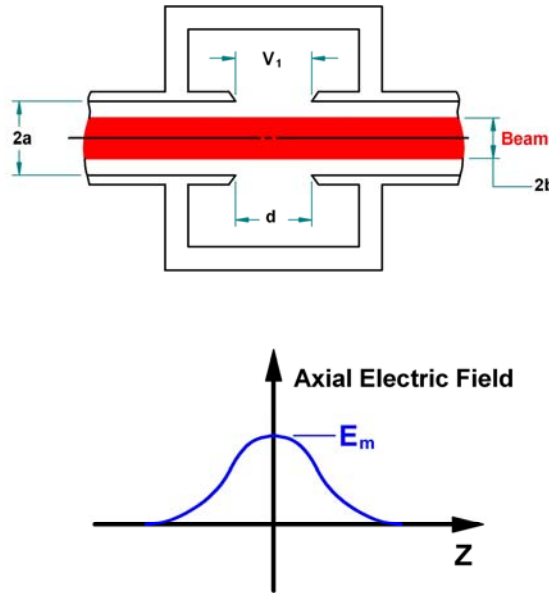


Fig. 26 A gridless klystron cavity and the electric field at the axis

Note also, that if the field $E_z(z)$ is a piecewise-continuous function of z , it can be written in terms of the inverse Fourier integral

$$g(\beta_e) = \frac{1}{2\pi} \int_{-\infty}^{\infty} E_z(z) e^{j\beta_e z} dz \quad (31)$$

which means that M can be also written in terms of the Fourier transform of the electric field

$$M(\beta_e) = \frac{2\pi}{V_1} g(\beta_e) \quad (32)$$

$$M(a, \beta_e) = \frac{1}{V_1} \int_{-\frac{d}{2}}^{\frac{d}{2}} E_z(a, z) e^{j\beta_e z} dz = \frac{1}{V_1} \int_{-\frac{d}{2}}^{\frac{d}{2}} \frac{1}{\pi d/2} \frac{V_1}{\sqrt{1 - \left(\frac{z}{d/2}\right)^2}} e^{j\beta_e z} dz \quad (38)$$

With a good table of integrals, one obtains the most commonly used coupling coefficient for gridless gaps at $r = a$, namely

$$M(a, \beta_e) = J_0\left(\frac{\beta_e d}{2}\right) \quad (39)$$

With this as the boundary condition, we shall now calculate M anywhere in the gap and average it over the beam.

In the absence of space charge and for a field varying sinusoidally with time in a vacuum, Maxwell's equations reduce to the wave equation

$$\nabla_{r,z}^2 E_z = \frac{1}{c^2} \frac{\partial^2 E_z}{\partial t^2} \quad (40)$$

where c is the velocity of light. Since

$$\frac{\partial^2 E_z}{\partial t^2} = -\omega^2 E_z \quad (41)$$

one obtains

$$\nabla_{r,z}^2 E_z = -k^2 E_z \quad (42)$$

where $k = \omega/c$. If the variation with z is as $e^{j\beta z}$, then

$$\nabla_r^2 E_z = (\beta^2 - k^2) E_z \quad (43)$$

Since, unlike in a closed waveguide, the axial electric field cannot be zero on axis at the center of the gap, the solution to Eq.(43) has the form $I_0(\gamma r)$, with

$$\gamma^2 = \beta^2 - k^2$$

And $\beta > k$. Since the axial field is completely specified at the surface $r = a$, it can be described by the Fourier integral

$$E_z(r, z) = \int_{-\infty}^{\infty} \frac{I_0(\gamma r)}{I_0(\gamma a)} g(\beta) e^{-j\beta z} d\beta \quad (44)$$

At $r = a$

$$E_z(a, z) = \int_{-\infty}^{\infty} g(\beta) e^{-j\beta z} d\beta \quad (45)$$

and

$$g(\beta) = \frac{1}{2\pi} \int_{-\infty}^{\infty} E_z(a, z) e^{j\beta z} dz \quad (46)$$

Let us now find the effective potential (integral of the field) experienced by an electron traveling with the beam velocity u_0 at a radius r along a line parallel to the axis. Using Eq. (30) and Eq. (44)

$$V_{eff} = \int_0^d E_z e^{j\beta_e z} dz = \int_{-\infty}^{\infty} \int_{-\infty}^{\infty} \frac{I_0(\gamma r)}{I_0(\gamma a)} g(\beta) e^{j(\beta_e - \beta)z} d\beta dz \quad (47)$$

We now use the following identity

$$\int_{-\infty}^{\infty} e^{j(\beta_e - \beta)z} dz \equiv 2\pi \delta(\beta_e - \beta) \quad (48)$$

where the “delta function” $\delta(\beta_e - \beta)$ has the property that, when multiplied by another function of β , and integrated over β from minus to plus infinity, it returns that function evaluated at β_e . Consequently, using Eq. (48) with Eq. (47) yields

$$V_{eff} = \int_{-\infty}^{\infty} dz \int_{-\infty}^{\infty} \frac{I_0(\gamma r)}{I_0(\gamma a)} g(\beta) e^{j(\beta_e - \beta)z} d\beta = 2\pi \int_{-\infty}^{\infty} \frac{I_0(\gamma r)}{I_0(\gamma a)} g(\beta) \delta(\beta_e - \beta) d\beta$$

and

$$2\pi \int_{-\infty}^{\infty} \frac{I_0(\gamma r)}{I_0(\gamma a)} g(\beta) \delta(\beta_e - \beta) d\beta = 2\pi \frac{I_0(\gamma_e r)}{I_0(\gamma_e a)} g(\beta_e) \quad (49)$$

Then

$$V_{eff}(r, \beta_e) = 2\pi g(\beta_e) \frac{I_0(\gamma_e r)}{I_0(\gamma_e a)}$$

and

$$M(r, \beta_e) = \frac{V_{eff}(\beta_e)}{V_1} = 2\pi \frac{1}{V_1} g(\beta_e) \frac{I_0(\gamma_e r)}{I_0(\gamma_e a)} \quad (50)$$

where

$$\gamma_e^2 = \beta_e^2 - k^2 \quad (51)$$

For simplicity, drop the “e” subscript from γ from this point on, with the understanding that γ will always be represented by Eq. (51) and will always be real, where klystrons (or TWTs) are concerned. On the other hand, it is conventional in most textbooks to keep the subscript “e” in $\beta_e = \omega/u_0$. Now, at $r = a$, Eq. (50) becomes

$$M(a, \beta_e) = 2\pi \frac{1}{V_1} g(\beta_e) \quad (52)$$

Comparing with Eq. (39), we conclude that

$$2\pi \frac{1}{V_1} g(\beta_e) = J_0\left(\frac{\beta_e d}{2}\right) \quad (53)$$

Hence, the general expression for the coupling coefficient anywhere in the gap is, from Eq. (50)

$$M(r, \beta_e) = \frac{V_{eff}(\beta_e)}{V_1} = 2\pi \frac{1}{V_1} g(\beta_e) \frac{I_0(\gamma r)}{I_0(\gamma a)} = J_0\left(\frac{\beta_e d}{2}\right) \frac{I_0(\gamma r)}{I_0(\gamma a)} \quad (54)$$

It is now appropriate to average the coupling coefficient over the beam. Note, however that, as long as there is a strong magnetic field and laminar beam flow, we should be averaging not M but M^2 , since M^2 is what appears in the expression for the voltage gain between two cavities (the coupling coefficient for coupling voltage from circuit to beam is the same as that for coupling current from beam to circuit). Therefore, assuming drift tubes and filling factors to be the same for the two cavities, we can form an expression for the averaged square of the coupling coefficient as follows:

$$\overline{M^2} = \frac{2\pi \int_0^b M^2(r, \beta_e) r dr}{\pi b^2} = J_0^2\left(\frac{\beta_e d}{2}\right) \times \frac{2}{b^2 I_0^2(\gamma a)} \int_0^b r I_0^2(\gamma r) dr \quad (55)$$

From a table of integrals

$$\int_0^b r I_0^2(\gamma r) dr = \frac{b^2}{2} [I_0^2(\gamma b) - I_1^2(\gamma b)] \quad (56)$$

We denote by M_a the coupling coefficient at $r = a$, and by \overline{M} the averaging factor in the equation below, we can choose to write

$$M_a = J_0(\beta_e d / 2) \quad (57)$$

$$\bar{M} = \frac{\sqrt{I_0^2(\gamma b) - I_1^2(\gamma b)}}{I_0(\gamma a)} \quad (58)$$

$$M = J_0(\beta_e d / 2) \frac{\sqrt{I_0^2(\gamma b) - I_1^2(\gamma b)}}{I_0(\gamma a)} \quad (59)$$

We shall use this expression for the coupling coefficient of a single cavity.

Instead of obtaining the equation above analytically, one could simulate the electric field by one of several codes, calculate M_a numerically, and multiply the result with the calculated \bar{M} . Some typical klystron parameters are $\beta_e d = 1$ radian, $\gamma a = 1$ radian and $b/a = 0.6$. For such values, one obtains $M_a = 0.765$, $\bar{M} = 0.69$ and $M = 0.53$. For comparison, the “gridded” coupling coefficient of Eq. (34) would yield: $M = 0.959$. Obviously Eq. (34) is quite useless for gridless gaps. On the other hand, for a much lower γa (the BFK has $\gamma a = 0.594$, $b/a = 0.65$ and $\beta_e d = 0.987$), we obtain $M = 0.885$ ($M_a = 0.974$, $\bar{M} = 0.935$, and $\sin(\beta_e d / 2) / \beta_e d / 2 = 0.96$). This is much closer, but it would still seriously overstate the gain of a multicavity klystron.

2.4 Beam-Loading

To conclude this section, one needs to provide a formula for the beam-loading conductance, G_b . The early large-signal bunching theory of Webster required the assumption of closely spaced gridded gaps. This is unacceptable for high-power klystrons, (because of grid interception), as well as for the “extended interaction” cavities discussed later, where the electric field is far from constant across the gap. Fremlin, Gent et al,²⁴ were probably the first to present a detailed analysis of beam-loading in 1946. At the time, klystrons were mostly two-cavity or reflex oscillators, and the calculation of start-oscillation current was critical to their design.

The original analysis was Gent’s, simplified by Branch in a 1960 paper.²⁵ It is important to define the coupling coefficient, M , as a function of the electric field, as we have done. The calculation of the related beam-loading parameter G_b , proceeds along similar lines, but the derivation is rather cumbersome and will not be reproduced here. The result can be stated as follows

$$\frac{G_b}{G_0} = -\frac{\beta_e}{4} \frac{\partial |M|^2}{\partial \beta_e} \quad (60)$$

Equation (60) is quite general and applies to all gap shapes, as well as to the “extended” or “sheet beam” cavities that will be discussed later. Its meaning is that the ratio of the beam loading conductance G_b to the beam conductance $G_0 = (I_0/V_0)$ is entirely determined by the coupling coefficient M and its variation with the dc beam voltage. Beam-loading formulae using space-charge theory will be restated later, and it will be shown that the kinematic treatment leading to Eq. (60), and an analysis based on space-charge theory arrive at the same important result, for small signals.

The next section, on space-charge waves, will also show that the magnitude of the coupling coefficient M in extended cavities is optimized by synchronizing the phase velocity (of the forward wave) in an extended cavity, to the beam velocity.

Using Eq. (34) with (60), along with a little differential calculus, will verify the beam loading formula for plane gridded gaps.

$$\frac{G_b}{G_0} = \frac{1}{2} \frac{\sin \beta_e d / 2}{\beta_e d / 2} \left\{ \frac{\sin \beta_e d / 2}{\beta_e d / 2} - \cos \beta_e d / 2 \right\} \quad (61)$$

If, in the same way, Eq. (54) for M for a gridless cylindrical geometry is squared, differentiated with β_e according to Eq. (60), and averaged over the beam to obtain G_b/G_0 , a very complicated expression for beam loading results. It is used in the Mathcad small-signal code (in Appendix I) since it is a closed expression and does not require a simulation of the field, and assumes the same gap geometry as Eq. (59) does. It takes the form,

$$G_b / G_0 = \left[\frac{\beta_e d}{4} J_1 \left(\frac{\beta_e d}{2} \right) J_0 \left(\frac{\beta_e d}{2} \right) \bar{M}^2 + \frac{1}{2} J_0^2 \left(\frac{\beta_e d}{2} \right) \left\{ \gamma a \frac{I_1(\gamma a)}{I_0(\gamma a)} \bar{M}^2 - \frac{I_1^2(\gamma b)}{I_0^2(\gamma a)} \right\} \right] \quad (62)$$

where \bar{M} is given by Eq (58).

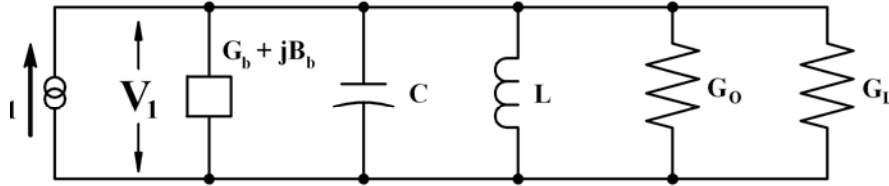


Fig. 27 Equivalent circuit for a klystron output cavity

A klystron cavity equivalent circuit, including the beam loading conductance (and susceptance) is shown in (Fig. 27). Calculation of the susceptance is even more onerous than the conductance calculation. A formula for a gridless gap is provided by Feenberg²⁶ but only for the beam filling the drift tube, and an infinitesimal gap.

Figure (28) shows both beam conductance and susceptance for a gridded gap to indicate the general relation of these quantities to the gap width. Note that G_b/G_0 becomes negative when the transit angle exceeds 2π , while the susceptance becomes inductive after π . In the gridless case, G_b/G_0 turns negative at about $\beta_e d > 4.6$ radians.

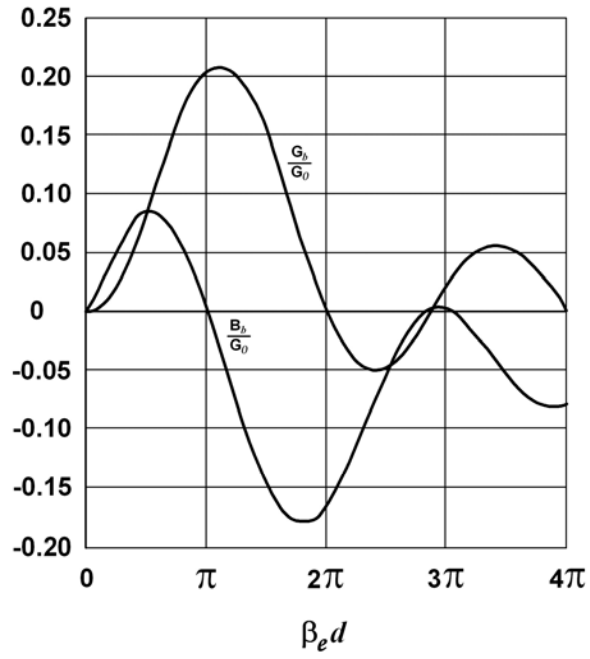


Fig. 28 Normalized beam loading conductance and susceptance for a gridded gap, as a function of transit angle

Chapter 3.

Space-charge Theory

3.1 Introduction

In kinematic theory, which was the earliest mathematical treatment describing beam interaction with microwave fields, the fields due to the beam's space charge were ignored and calculations were based only on the effects of the fields in the interaction gap. Energy between cavities was transmitted through ballistic electron motion. Kinematic theory does not provide the tools necessary for a satisfactory analysis of multicavity klystrons. For this, a small-signal space-charge wave theory is necessary.

This section develops the space-charge wave formulation and employs it to derive expressions that are useful in calculating the gain and bandwidth of multicavity klystrons, and of linear beam tubes, in general. It also derives an equation for beam loading that is consistent with Eq. (59), but is cast in a form that is both more informative, and useful for computer calculations. The theory below follows Chodorow,²⁷ Zitelli,²⁸ and Wessel-Berg.²⁹ Derivations are abbreviated. The objective, as in Chapter 2, is to expose the student or engineer to the origins of design equations and highlight the assumptions that are involved in their derivation. These equations will be subsequently used in an example of actual klystron designs.

The initial basic assumptions are:

- No electron motion or current is assumed to exist along any dimension, other than the z-dimension. This requires the presence of a strong magnetic field, which is usually the case with modern klystrons.
- The analysis assumes small-signal RF variables. Products of RF quantities will be neglected.
- This will be a non-relativistic analysis. Relativistic correction formulae are provided in Appendix V.

All electrical quantities will be written as sums of the DC and AC terms, the AC term being small compared to the DC term (as per the definition of "small-signal"). Cross products of AC terms will be neglected. The unit system is MKS throughout this section.

Equations (63) below provide the equations for total velocity, current density and charge density, respectively, DC terms are denoted by the subscript $\underline{0}$. The AC terms u , i and ρ will be functions of the coordinates transverse to the electron motion (x and y in Cartesian coordinates) and the z -dependence is exponential, indicating a traveling wave.

$$\begin{aligned}u_t &= u_0 + ue^{j(\omega t - \gamma z)} \\i_t &= i_0 + ie^{j(\omega t - \gamma z)} \\\rho_t &= \rho_0 + \rho e^{j(\omega t - \gamma z)}\end{aligned}\tag{63}$$

Note that in Chapter 2, the symbol used for the total current was I_t , and for the RF current I_1 . These were not necessarily small-signal currents. Here, only lower-case letters will be used, except for voltage. Naturally, i_0 is identical to I_0 .

3.2 Fundamental Space-Charge Wave Analysis

Expressions for space-charge waves will be derived from three general equations: a) the wave equation for the electric field (derived from Maxwell's equations), b) the continuity of charge and c) the force equation. Equations, initially in Cartesian and finally in cylindrical coordinates, will be derived for the quantities above and manipulated to find expressions for the wave motion of current between klystron cavities. This is expressed by the factor $e^{j(\alpha x - \gamma z)}$, representing a traveling wave with a propagation constant γ , the value of which will be determined. It is intuitively obvious that γ will be a function of the space charge, the voltage, the frequency and the geometry of the drift tube. Furthermore, one should be able to derive an expression for the rf current imparted to the beam through velocity modulation by a cavity gap voltage V_1 , with the small-signal condition $V_1 \ll V_0$, and with space charge taken into account.

The effect of the space charge is to act as an elastic medium between the concentrations of electrons (bunches) which form as a result of velocity modulation. The result is the formation of waves of charge similar to those formed in spring-weight systems. In the early days of klystrons, the RF current calculated as in Eq. (18) was reduced by a "debunching factor"³⁰ $\sin(hz)/hz$, where z is measured from the center of the cavity gap (with the V_1 modulating voltage) where the current was calculated, and $h/2\pi$ was designated as the "wave number." In the derivations which follow, h will be replaced by its modern equivalent the plasma frequency

ω_p ($\omega_p = \sqrt{\frac{e \rho_0}{m \epsilon_0}}$), a function of the charge density ρ . It will be further modified by a reduction

factor \underline{R} , which will take into account the effect of the drift tube walls in reducing the effects of the space charge between bunches (hence increasing the rf current which was reduced by the "debunching factor").

The large-signal expression for the fundamental current in a beam which has been modulated by a klystron cavity was given by the first line of Eq. (18) in terms of the "bunching parameter," $X = \frac{MV_1 \theta_0}{2V_0}$. The series representing the Bessel function in that equation reduces as follows, for $X \ll 1$

$$J_1(X) \approx \frac{X}{2} = \frac{MV_1 \theta_0}{4V_0} \quad (64)$$

Hence, the magnitude of small-signal current, reduced by the "debunching factor," would then be, empirically

$$|i_1| = \frac{I_0 M \theta_0}{2V_0} \frac{\sin(\beta_p l)}{\beta_p l} V_1 \quad (65)$$

The mathematics that follows will now derive the above formula and show that β_p must be modified by the presence of a drift tube.

The electric field in the drift tube is

$$\vec{E} = \vec{E}(x, y) e^{j(\alpha x - \gamma z)} \quad (66)$$

where, as discussed previously, γ is the unknown propagation constant. The starting point is the inhomogeneous wave equation (i.e., a differential equation containing “sources,” involving the charge and the current to the right of the equal sign). It is this equation that governs the operation of every electron device:

$$\nabla^2 \bar{E} - \frac{1}{c^2} \frac{\partial^2 \bar{E}}{\partial t^2} = \frac{1}{\epsilon_0} \bar{\nabla} \rho + \mu_0 \frac{\partial \bar{i}}{\partial t} \quad (67)$$

where c is the velocity of light, ϵ_0 and μ_0 the permittivity and permeability of free space, and $k = \omega/c$ is the wave number in free space. It is only necessary to work with the z-components of the vectors E , i , and ∇ , since the other components can all be derived from E_z . One then has (initially in Cartesian coordinates, and omitting the subscript z for the current and velocity, since no motion is allowed, except in the z-direction).

$$\nabla_{\perp}^2 E_z - (\gamma^2 - k^2) E_z = \frac{1}{\epsilon_0} \nabla_z \rho + j\omega\mu_0 i \quad (68)$$

where

$$\begin{aligned} \nabla_z \rho &= \frac{\partial \rho}{\partial z} \\ \nabla_{\perp}^2 E_z &= \frac{\partial^2 E_z}{\partial x^2} + \frac{\partial^2 E_z}{\partial y^2} \end{aligned} \quad (69)$$

The objective in what follows is to eliminate ρ and i from Eq. (67) and to obtain an equation in E_z alone. The equation of continuity is

$$\frac{\partial i}{\partial z} + \frac{\partial \rho}{\partial t} = 0 \quad (70)$$

which can be written, using Eq. (63), as

$$-j\gamma i + j\omega\rho = 0 \quad (71)$$

Products of rf current and rf charge may be neglected. This yields

$$i_t = (\rho_0 + \rho)(u_0 + u) \approx i_0 + \rho_0 u + \rho u_0 \quad (72)$$

and

$$i = \rho_0 u + \rho u_0 \quad (73)$$

Neglecting the term $u \times B$ (which is negligible, except for relativistic velocities), the force equation is

$$\eta E_z = \frac{du}{dt} \quad (74)$$

where η is defined as e/m . The total velocity derivative with time in the equation above should not be confused with the partial derivative used to observe the behavior of the beam at a fixed point. The total derivative of $u(z,t)$ is equal to the sum of changes, both with time and distance, or

$$\frac{du}{dt} = \frac{\partial u}{\partial t} + \frac{\partial u}{\partial z} \frac{dz}{dt} = \frac{\partial u}{\partial t} + u_0 \frac{\partial u}{\partial z} \quad (75)$$

Hence

$$\eta E_z = \frac{\partial u}{\partial t} + u_0 \frac{\partial u}{\partial z} = j(\omega - u_0 \gamma) u \quad (76)$$

In order to eliminate ρ and i from Eq. (68) and reduce it to a homogeneous form, two more relationships are required. From Eq. (71) and Eq. (73), we can obtain $\underline{\rho}$ and \underline{i} in terms of \underline{u} and then use Eq. (74) to relate them to \underline{E}_z

$$\rho = \frac{\gamma \rho_0}{\omega - u_0 \gamma} u \quad (77)$$

and

$$i = \frac{\omega}{\gamma} \rho = \frac{\omega \rho_0}{\omega - u_0 \gamma} u \quad (78)$$

Replacing \underline{u} , using Eq. (76) in both equations above, one obtains

$$\rho = \frac{\eta \gamma \rho_0}{j(\omega - u_0 \gamma)^2} E_z \quad (79)$$

and

$$i = \frac{\eta \omega \rho_0}{j(\omega - u_0 \gamma)^2} E_z \quad (80)$$

Substituting these into Eq. (68), while omitting much of the arithmetic, and using $c^2 = 1/\epsilon_0 \mu_0$ (velocity of light), yields

$$\nabla_{\perp}^2 E_z + \left[-(\gamma^2 - k^2) + \frac{\omega_p^2}{u_0^2} \frac{\gamma^2 - k^2}{(\beta_e - \gamma)^2} \right] E_z = 0 \quad (81)$$

Eq. (81) then becomes a homogeneous wave equation of the form

$$\nabla_{\perp}^2 E_z + T^2 E_z = 0 \quad (82)$$

Where

$$T^2 = (\gamma^2 - k^2) \left[\frac{\beta_p^2}{(\beta_e - \gamma)^2} - 1 \right] \quad (83)$$

With $\beta_p = \omega_p/u_0$. The propagation constant, γ , continues to be the unknown and is determined.

3.3 Determination of the Plasma Reduction Factor

To solve Eq. (82) one must specify appropriate boundary conditions. Depending on the coordinate system, the solutions will be trigonometric or Bessel functions. They will be summations over the T_n 's, with four separate β_n 's to be calculated from each T_n , since Eq. (81) is quartic in γ . Before deriving a useful solution, first consider the case of an infinite beam, with no transverse dimension variations. Then, Eq. (82) becomes

$$\nabla_{\perp}^2 E_z = 0 \quad (84)$$

which requires $T = 0$ and results in the following values for the propagation constant from Eq. (83). The first pair of roots is

$$\gamma_{1,2} = \pm k \quad (85)$$

The second pair is

$$\gamma_{3,4} = \beta_e \pm \beta_p \quad (86)$$

The first two solutions are plane waves in free space, traveling with the velocity of light. The second two are plasma waves with propagation velocities above and below the beam velocity (fast and slow space-charge waves). There are no transverse boundary conditions to be considered since the transverse space is infinite. The overall solution of equation Eq. (84) must include all four solutions, properly matched to the initial conditions at $z = 0$. If one writes for the velocity

$$u / u_0 = \sum_{n=1}^{n=4} \Lambda_n e^{-j\gamma_n z} \quad (87)$$

then from Eq. (78)

$$\frac{i}{i_0} = \frac{\omega}{\omega - u_0 \gamma} \frac{u}{u_0} = \frac{\beta_e}{\beta_e - \gamma} \frac{u}{u_0} \quad (88)$$

And hence

$$i / i_0 = \sum_{n=1}^{n=4} \frac{\beta_e}{\beta_e - \gamma_n} \Lambda_n e^{-j\gamma_n z} \quad (89)$$

where the Λ_n 's (lamdas) are constants to be determined from the boundary conditions for velocity and current at $z = 0$. At the boundary $z = 0$, the total velocity is based on the approximation first used in Eq. (4) and the current is zero. Using the definition for the β_n 's

$$\left. \frac{u}{u_0} \right|_{z=0} = \Lambda_1 + \Lambda_2 + \Lambda_3 + \Lambda_4 = \frac{MV_1}{2V_0} \quad (90)$$

and

$$\left. \frac{i}{I_0} \right|_{z=0} = \Lambda_1 + \Lambda_2 + \frac{\beta_e}{\beta_p} \Lambda_3 - \frac{\beta_e}{\beta_p} \Lambda_4 = 0 \quad (91)$$

The equations above have the solutions

$$\Lambda_1 = \Lambda_2 = 0$$

and

$$\Lambda_3 = \Lambda_4 = \frac{MV_1}{4V_0}$$

The RF current in the beam can then be found to be

$$i = -j \frac{MI_0 V_1}{2V_0} \frac{\omega}{\omega_p} \sin(\beta_p z) e^{-j\beta_e z} \quad (92)$$

This is close to the desired result in Eq. (65), except that what is ultimately needed is an expression for a cylindrical or sheet beam, not one of infinite dimensions.

For a pencil beam, not filling a cylindrical drift tube, the solution in cylindrical coordinates contains ordinary Bessel functions (J_0) within the beam (Region 1) and modified Bessel functions (I_0 , K_0) in the Region 2 between the beam and the drift tube wall.

The solutions have the form:³¹

$$\begin{aligned} E_{z1} &= B J_0(\tau_n r) \\ E_{z2} &= C [I_0(T_n r) + D K_0(T_n r)] \end{aligned} \quad (93)$$

where B, C and D are arbitrary constants to be determined by the boundary conditions. These are, $E_{z1} = E_{z2}$ and $\partial E_{z1} / \partial r = \partial E_{z2} / \partial r$ at $r = b$ (for continuity of the tangential electric and magnetic fields respectively), and $E_{z2} = 0$ at $r = a$. The wave numbers T_n and τ_n are,

In Region 1:

$$\tau_n = \sqrt{\gamma_n^2 - k^2} \quad (94)$$

In Region 2:

$$T_n^2 = (\gamma_n^2 - k^2) \left[\frac{\beta_p^2}{(\beta_e - \gamma_n)^2} - 1 \right] \quad (95)$$

The quantities τ_n correspond to waveguide modes in Region 1; and the T_n 's to space-charge waves, as well as waveguide modes in Region 2. Equation (95), as a quartic in γ_n , has 4 solutions. We shall make the assumptions that in Region 2, the space-charge wave modes have velocities almost equal to the velocity of the beam making $\gamma_n \approx \beta_e$, and hence $\gamma_n \gg k$. We can then use β_e instead of γ_n in Eq. (95) (except in the denominator term), with the result,

$$\beta_e - \gamma_n = \pm \frac{\beta_p}{\sqrt{\left(1 + \frac{T_n^2}{\beta_e^2}\right)}} \quad (96)$$

If the small difference between the electron wave number and “reduced” plasma wave number is denoted by β_q , we write

$$\gamma_n = \beta_e \pm \beta_q \quad (97)$$

And, finally

$$\gamma_{n1,2} = \beta_e \pm \frac{\beta_p}{\sqrt{\left(1 + \frac{T_n^2}{\beta_e^2}\right)}} \quad (98)$$

Where, as before the + sign corresponds to the slow space-charge wave. The ratio between β_q and β_p is the “Plasma reduction factor,” which we set out to determine. It is

$$R = \frac{1}{\sqrt{\left(1 + \frac{T_n^2}{\beta_e^2}\right)}} = \frac{\beta_q}{\beta_p} \quad (99)$$

To obtain the T_n 's we need to match boundary conditions at $r = b$. When this is done, and by substituting β_e for γ , we can obtain the transcendental equation

$$T_n \frac{J_1(T_n b)}{J_0(T_n b)} = \beta_e \frac{K_0(\beta_e a) I_1(\beta_e b) + K_1(\beta_e b) I_0(\beta_e a)}{K_0(\beta_e b) I_0(\beta_e a) - K_0(\beta_e a) I_0(\beta_e b)} \quad (100)$$

Using the lowest root T_0 and omitting the subscript, we obtain for the plasma reduction factor R

$$R = \frac{1}{\sqrt{\left(1 + \frac{T_0^2}{\beta_e^2}\right)}} = \frac{\beta_q}{\beta_p} \quad (101)$$

Equation (100) can be solved graphically as shown in (Fig. 29). (It is quickly solved in Mathcad, using the same approach). Branch and Mihran³² have published solutions and graphs for a number of geometries. For the pencil beam in a cylindrical drift tube where a and b are the drift tube and beam radii, the plasma reduction $R = \omega_q/\omega_p$ is plotted as a function of the beam radius in (Fig. 30).

Using a similar procedure as in the case of no drift tubes, it can be shown that the current is the same as in Eq. (92), with β_q substituted for β_p . The drift tube is assumed to be cut off.

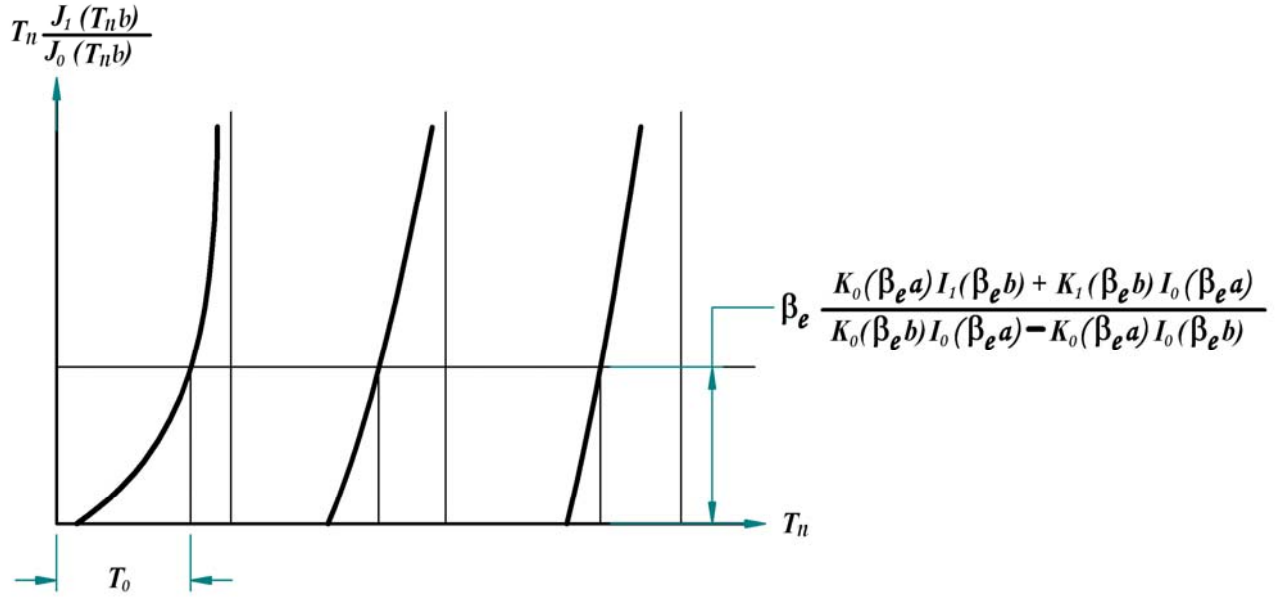


Fig. 29 Graphical solution of Eq. (99)

$$\frac{i}{V_1} = -j \frac{MI_0}{2V_0} \frac{\omega}{\omega_q} \sin(\beta_q z) e^{-j\beta_e z} \quad (102)$$

Equation (102) is the fundamental small-signal transconductance relating the modulating cavity voltage V_1 to the RF current a distance z downstream.

An equation similar to Eq. (100) can be used to determine the plasma reduction factor for a sheet beam of thickness t centered between parallel plates spaced by a distance W . In rectangular coordinates, the transcendental equation is

$$\frac{T_m t}{2} \tan\left(\frac{T_m t}{2}\right) = \frac{\gamma t}{2} \coth \frac{\gamma(W-t)}{2} \quad (103)$$

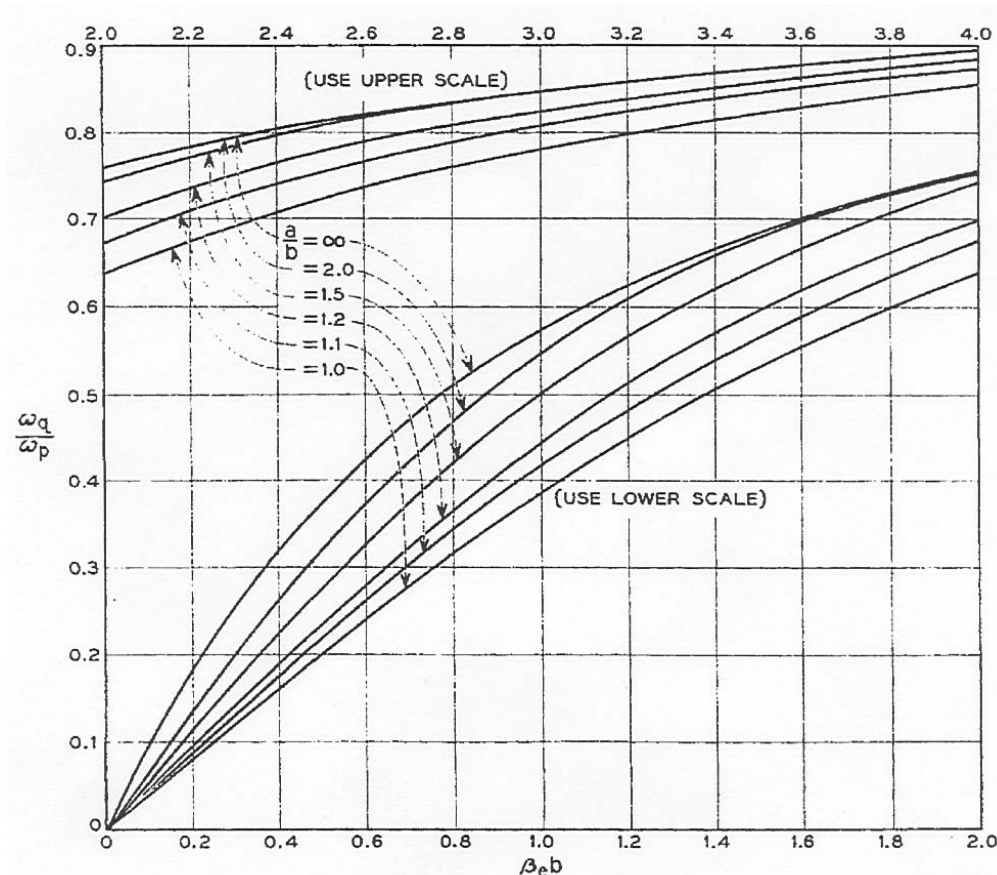


Fig. 30 Plasma reduction factors (Ref. 11)

3.4 Small-Signal Beam-Loading Analysis

Having derived expressions for the plasma reduction factor R , one can now proceed to analyze the interaction between beam and RF circuit in one dimension, using plasma theory. We shall consider only the z -dimension, along the path of the e-beam. This is not restrictive, because formulae exist, e.g. - Eq. (59), which average beam parameters over the beam, when transverse dimensions matter; and computer simulations do the same thing, even more accurately. Higher-order modes in the drift tubes or in the circuits with which the beams interact are also neglected. Drift tubes are cut off below the operating frequency. Beams are assumed “cold,” with no thermal velocities. The mathematical treatment follows Wessel-Berg but it will be followed only long enough to demonstrate the method, before jumping to the final, very useful, beam-loading derived in Chapter 2. The objective is to derive equations relating gap fields to the voltage, current and plasma density of the beam interacting with these fields. Although the mathematics are similar to those employed in the kinematic theory of Chapter 2, the concept of positive and negative energy space-charge waves provides an important insight to the operation of the klystron.

One begins as earlier in this section by using the equations for continuity, Eq. (70); current, Eq. (73); and force, Eq. (74). Wessel-Berg defined the “kinetic voltage,” $U(z)$, as

$$U(z) = \frac{u_0 u}{\eta} \quad (104)$$

Again, the z -subscripts are omitted since z is the only dimension. One can then write, after some algebra

$$\left[j\beta_e + \frac{\partial}{\partial z} \right] U = E = E_s + E_c \quad (105)$$

$$\left[j\beta_e + \frac{\partial}{\partial z} \right] i = \frac{1}{2} j\beta_e \frac{i_0}{V_0} U \quad (106)$$

where E_s is the field due to the space charge and E_c is the circuit field. These will be used to relate the detailed gap fields to electron motion and eventually to derive expressions for energy transfer and beam loading.

Notice that E_s can be related to the current i through one of the Maxwell equations

$$\nabla \times H = i + \frac{\partial D}{\partial t} = i + j\omega\epsilon_0 E_s \quad (107)$$

Taking the divergence, which is zero, one obtains for the truly 1-D case (infinite beam cross-section), where there are no transverse fields and the z -dependence of field and current are the same

$$\nabla \cdot E_s = \frac{\partial E_s}{\partial z} = -\frac{1}{j\omega\epsilon_0} \frac{\partial i}{\partial z} \quad (108)$$

Integrating this equation yields

$$E_s = -\frac{1}{j\omega\epsilon_0} i \quad (109)$$

which relates the space-charge field to the current in an infinite beam. Recall that in the earlier 3-D derivation, where there E_z was the only electric field component, but where the beam was bounded, E_z was equivalent to the present E_s , and Eq. (80) was obtained. It is reproduced (and re-numbered) here

$$i = \frac{\eta\omega\rho_0}{j(\omega - u_0\gamma)^2} E_z \quad (110)$$

This can be rewritten as

$$E_z = E_s = -\frac{1}{j\omega\epsilon_0} \frac{(\omega - u_0\gamma)^2}{\omega_p^2} i \quad (111)$$

Then, in the case where the beam does not fill the drift tube $\gamma = \beta_e \pm \beta_q$, as before, which leads to

$$E_s = -\frac{1}{j\omega\epsilon_0} \left(\frac{\omega_q}{\omega_p} \right)^2 i = -\frac{1}{j\omega\epsilon_0} R^2 i \quad (112)$$

Comparing Eq. (112) with Eq. (110) shows that for a finite beam, the effect of the radial field leakage to the walls of the drift tube is to reduce the longitudinal space-charge field E_z by R^2 , a number less than unity, as previously derived. The effect of the walls is illustrated in the (Fig. 31), which shows how the fields between bunches are weakened by the drift tube wall. Fields resulting from electron bunches are shown for, a) an infinite beam; b) a finite beam in free space; c) a finite beam in conducting cylinder. These fields are considered to be the net change in space charge (as a result of bunching) from the space charge of the unmodulated beam.¹¹

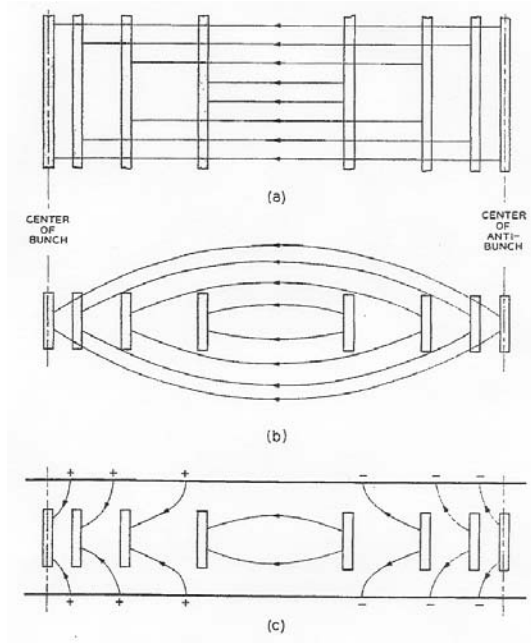


Fig. 31 Weakening of the fields between bunches due to the presence of the drift tube. (Ref. 11)

Wessel-Berg then defines a quantity \underline{W} as the “beam characteristic impedance,”

$$W = \frac{2V_0 \beta_q}{I_0 \beta_e} \quad (113)$$

Then, after manipulating Eq. (112) and the expressions for ω_p and R , one finds

$$E_s = j\beta_q W i \quad (114)$$

Furthermore, Eqs. (105) and (106) become

$$\left[j\beta_e + \frac{\partial}{\partial z} \right] U = j\beta_q W i + E_c \quad (115)$$

$$\left[j\beta_e + \frac{\partial}{\partial z} \right] i = j\beta_q \frac{1}{W} U \quad (116)$$

These equations are analogous to transmission line equations and can be used to further develop details of the space-charge theory. Combined, they form a second-order equation for the current i . Dropping the partial signs, since the only variable is z , we obtain

$$\frac{d^2 i}{dz^2} + 2j\beta_e \frac{di}{dz} - (\beta_e^2 - \beta_q^2)i = j\beta_q \frac{1}{W} E_c \quad (117)$$

Consider now a two-cavity klystron, as illustrated in (Fig. 32), with interaction Regions 1 and 2, centered at $z = 0$ and $z = l_{12}$, with lengths $\pm \frac{d_1}{2}$ and $\pm \frac{d_2}{2}$ (these are not gridded gaps, only regions with z -varying axial electric fields). We shall calculate the current at $z = l_{12} + \xi_2$ in the second cavity. Using Laplace transforms, Eq. (117) can be integrated subject to the initial conditions, $i(0) = 0$ and $\frac{di}{dz}(0) = 0$ to give

$$i(z) = j \frac{1}{W} \int_0^z E_c(\xi) e^{-j\beta_e(z-\xi)} \sin \beta_q(z-\xi) d\xi \quad (118)$$

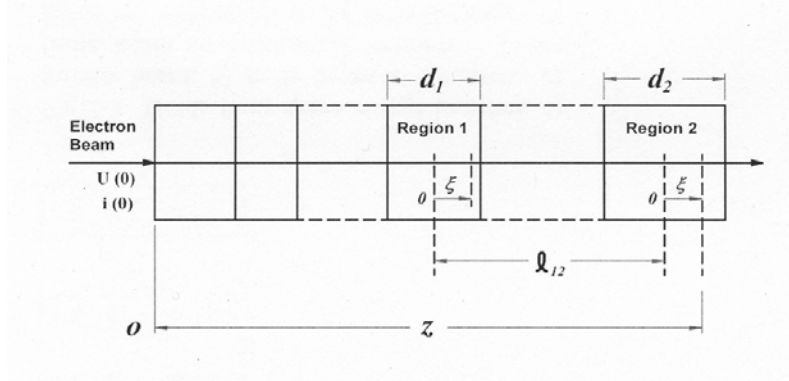


Fig. 32 Two-cavity gridless klystron formalism

The integration only needs to be performed over the two regions where the circuit fields are E_{c1} and E_{c2} . The fields are zero elsewhere. First, we introduce some shorthand to make the equations that follow manageable. Define

$$\Delta F(\beta_e) = \frac{1}{2} [F(\beta_e + \beta_q) - F(\beta_e - \beta_q)] \quad (119)$$

It can then be shown that

$$\begin{aligned} \Delta [aF(\beta_e) + bF(\beta_e)] &= a\Delta F(\beta_e) + bF(\beta_e) \\ \Delta \left[\frac{dF(\beta_e)}{d\beta_e} \right] &= \frac{d}{d\beta_e} [\Delta F(\beta_e)] \\ \Delta \int F(\beta_e, \xi) d\xi &= \int \Delta F(\beta_e, \xi) d\xi \end{aligned} \quad (120)$$

Also define coupling coefficients for the slow and fast space-charge waves, respectively, as

$$\text{Slow wave } (\beta_e^- = \beta_e + \beta_q) \quad M_1^+ = \frac{1}{V_1} \int_{-\frac{d_1}{2}}^{\frac{d_1}{2}} E_{c1}(\xi) e^{(\beta_e + \beta_q)\xi} d\xi \quad (121)$$

$$\text{Fast wave } (\beta_e^+ = \beta_e - \beta_q) \quad M_1^- = \frac{1}{V_1} \int_{-\frac{d_1}{2}}^{\frac{d_1}{2}} E_{c1}(\xi) e^{(\beta_e - \beta_q)\xi} d\xi \quad (122)$$

There should be no confusion about the plus and minus signs above, since a lower propagation constant indicates a higher velocity and hence a fast wave.

Now, we write for the fields in the two regions

$$E_{c1,2} = V_{1,2} f_{1,2}(\xi) \quad (123)$$

and normalize them as in the equation below

$$d \int_{-\frac{d}{2}}^{\frac{d}{2}} f_{1,2}(\xi) f_{1,2}^*(\xi) d\xi = 1 \quad (124)$$

It then follows that

$$V_{1,2} V_{1,2}^* = d \int_{-\frac{d}{2}}^{\frac{d}{2}} E(\xi) E^*(\xi) d\xi \quad (125)$$

where the asterisks signify complex conjugates. Eq. (125) clearly represents the square of the magnitude of the gap voltages.

Beginning with Eq. (118), and after a considerable number of steps, but no further assumptions, it can be shown that the current in region 2 can be written as shown below. The reader is referred to another Wessel-Berg text³³ for the details.

$$i(\xi_2) = -\frac{V_1}{W} \Delta \left[e^{j\beta_e(l+\xi_2)} M_2(\beta_e) \right] - \frac{V_2}{W} \Delta \int_{-\frac{d_2}{2}}^{\xi_2} f(\xi_2) e^{j\beta_e \xi_2} d\xi_2 \quad (126)$$

Expanding the first part of Eq. (126), one obtains

$$i(\xi_2) = -\frac{V_1}{2W} \left[M_1(\beta_e + \beta_q) e^{-j(\beta_e + \beta_q)(l+\frac{d}{2})} - M_1(\beta_e - \beta_q) e^{-j(\beta_e - \beta_q)(l+\frac{d}{2})} \right] \quad (127)$$

which can be rewritten as

$$i(\xi_2) = \frac{j}{W} \left[\int_{\frac{d_1}{2}}^{\frac{d_1}{2}} E_{c1}(\xi) e^{-j\beta_e(z-\xi)} \sin \beta_q(z-\xi) d\xi + \int_{-\frac{d_2}{2}}^{\xi_2} E_{c2}(\xi) e^{-j\beta_e(z-\xi)} \sin \beta_q(z-\xi) d\xi \right] \quad (128)$$

The significance of the above equation is the following: The current in the interaction Region 2 is composed of a superposition of fast and slow space-charge waves originating within Region 1, as a result of the voltage V_1 there, plus currents originating within Region 2. The complex power imparted to, or extracted from the beam at Region 2, is given by the following expression

$$P_2 = \frac{1}{2} \int_{-\frac{d_2}{2}}^{\frac{d_2}{2}} i(\xi_2) E(\xi_2)^* d\xi_2 = \frac{1}{2} V_2^* \int_{-\frac{d_2}{2}}^{\frac{d_2}{2}} i(\xi_2) f(\xi_2) d\xi_2 \quad (129)$$

This, and a great deal of additional algebra is used to arrive at the final result

$$G_b = - = \frac{1}{4W} \left[|M_2^2(\beta_e - \beta_q)| - |M_2^2(\beta_e + \beta_q)| \right] = \frac{1}{8} \frac{\beta_e}{\beta_q} \frac{I_0}{V_0} \left[|M_2^-|^2 - |M_2^+|^2 \right] \quad (130)$$

Now, compare the result above to Eq. (60), repeated (and renumbered) below

$$\frac{G_b}{G_0} = - \frac{\beta_e}{2} M \frac{\partial M}{\partial \beta_e} = - \frac{\beta_e}{4} \frac{\partial |M|^2}{\partial \beta_e} \quad (131)$$

This equation, which was first derived by kinematic theory by Tomlin, can be shown to be equivalent to Eq. (130) for no space charge ($\beta_q \rightarrow 0$) by recognizing that

$$\lim_{\beta_q \rightarrow 0} \left\{ |M_2^2(\beta_e - \beta_q)| - |M_2^2(\beta_e + \beta_q)| \right\} = -2\beta_q \frac{\partial}{\partial \beta_e} |M_2|^2 \quad (132)$$

Equation (130) is fundamental to the design of extended interaction klystrons, since it can be used not only for determining beam loading but also for testing a circuit for stability, a practice that is highly recommended in the design of extended interaction klystrons. A negative value for G_b can imply a ‘‘monotron’’ instability. This is a condition where the exchange of energy between beam and circuit is such that net energy flows to the circuit, which can then develop excessively high fields (i.e. - an oscillation) unless it is sufficiently loaded or sufficiently lossy.

In the case of single, cylindrical, gridless gaps, the values for G_b/G_0 calculated by Eq. (130) or by the kinematic formula Eq. (131) are almost identical for realistic values of the beam perveance. However, Eq. (130) is more general and can be evaluated for single and extended gap geometries by the same methods as the calculation of the coupling coefficient M (i.e. - by using Eq. (30) and numerical integrations of tabulated E_z values from a SUPERFISH simulation of the cavity fields).

Chapter 4.

Gain-Bandwidth Calculations

4.1 Introduction

The previous two sections developed most of the fundamental theory necessary to make the formulae used in practical klystron design credible and to help in applying them correctly. These dealt with electron-bunching in the beam and in the interaction between beam and circuit, and were largely based on small-signal approximations. This section will describe the use of the theory in practice and will illustrate it with numerical examples and with the design of a practical klystron.

The classic klystron circuit, with which a pencil beam interacts, is a direct descendant of the Hansen “rhumbatron” and consists of a cylindrical cavity operating in the TM_{01} mode, providing an axial field in the direction of the beam traversing the cavity. In order to concentrate the electric field and enhance coupling to the beam, the two drift tubes are usually (but not always) reentrant. More complex interaction circuits are in use supporting multiple modes in the axial direction (extended interaction) or in a transverse direction (sheet-beam klystrons), or both. Those will require special treatment. The analysis in this section will only cover the performance of multi-cavity klystrons employing simple cylindrical cavities.

4.2. Small-Signal Stagger-Tuning Theory

A klystron cavity can be usually treated as single-tuned resonant circuit consisting of a parallel combination of a capacitance, an inductance and a resistance across the interaction gap, and driven by the RF current in the beam. That was illustrated earlier in (Fig. 27). The cavity is driven by a “constant current generator,” representing the fundamental component I_1 in a beam that has been bunched by preceding cavities. This current produces a voltage V across the gap. If I_1 is high enough, and V is comparable or higher than the beam voltage V_0 , power will be extracted from the beam. Such a circuit is fully determined by its resonant frequency, the total Q , and the “ R/Q .” The following relations apply

$$\text{Resonant frequency} \quad \omega_0 = \sqrt{\frac{1}{LC}} \quad (133)$$

$$\text{Total } Q \quad \frac{1}{Q_T} = \frac{1}{Q_b} + \frac{1}{Q_0} + \frac{1}{Q_e} \quad (134)$$

$$\text{R/Q (ohms)} \quad \frac{R}{Q} = \frac{1}{\omega_0 C} = \sqrt{\frac{L}{C}} \quad (135)$$

The beam-loading conductance and susceptance defined in Chapter 2 were shown in (Fig. 27) as an admittance $G_b + jB_b$. The three Q 's above correspond to beam loading losses, cavity ohmic losses and the external load, respectively, and correspond to resistances with similar subscripts. The calculation of R/Q must use matching values of R and Q . The physical description of R/Q is that it is the ratio of the square of the voltage V across the interaction gap of a klystron cavity and the energy W stored in the cavity, as follows:

$$\frac{R}{Q} = \frac{V^2}{2\omega_0 W} \quad (136)$$

The two definitions are equivalent (see Appendix IV).

Klystrons are resonant, narrowband devices. Nevertheless, they are usually required to have some limited bandwidth. This bandwidth is primarily set by the R/Q of the output circuit, although the front end of the tube is required to produce sufficient fundamental-frequency RF current (I_1) to drive the output circuit over the band of interest. Note that in previous sections, lower case letters were used to indicate small-signal quantities and capitals were reserved for large-signal currents. In this case, and in the formulae which follow, the current I can be either. It can also be the fundamental component I_1 of the RF current driving the output cavity. It will be made clear in the text which is the case.

In what follows, the current-producing part of the klystron is analyzed. It will usually consist of two or more “gain” cavities, tuned within the band of interest, and one or more “penultimate” cavities tuned above the band. The function of the penultimate cavities is to present an inductive load to the beam, which has the effect of shortening the length the electron bunches, thus increasing their content of RF current I_1 . The importance of the R/Q parameter is most apparent when it is considered that the output circuit must present a total impedance R_T to the RF current, such that the product $I_1 R_T$ is approximately equal to the beam voltage V_0 , a necessary condition for removing RF energy from the beam. If the output circuit is the simple resonant circuit described above, its half-power bandwidth is

$$\frac{\Delta\omega}{\omega_0} = \frac{1}{Q_T} = \frac{R}{Q} \frac{1}{R_T} \quad (137)$$

The output voltage and the overall klystron gain \mathcal{G} are proportional to R_T and since R_T is usually almost equal to R_L , the following relation usually holds

$$\mathcal{G} \times BW \propto R_L \times \frac{\Delta\omega}{\omega_0} = \frac{R}{Q} \quad (138)$$

indicating that the gain-bandwidth product of a klystron is proportional to the R/Q of the output cavity. More generally, if the output circuit is more elaborate, for instance a maximally-flat filter circuit presenting to the driving current an impedance R_T , there is a circuit theorem³⁴ for driving-point impedances with a capacitive input, which states

$$\frac{\Delta\omega}{\omega} R_T \leq \frac{\pi}{2} \frac{1}{\omega C} = \frac{\pi}{2} \frac{R}{Q} \quad (139)$$

Or, in words, if the required load impedance for best efficiency at the output cavity of a klystron is R_T , then the maximum bandwidth attainable with a single-gap output is equal to the cavity R/Q multiplied by $\pi/2$ and divided by R_T . The single-gap distinction is important because as will be shown, extended interaction (multiple-gap) output circuits do not obey this rule and make possible wider bandwidths than Eq. (139) indicates.

To describe this process analytically, we begin with the final expression for the driving current at a cavity n , resulting from the voltage across the gap of a preceding cavity m , namely,

Eq. (102). Both that current and the voltage are measured at the circuit (in this case I_n can be an either small or large-signal quantity) and are linked to the effective voltage on the beam and the RF current in it by the coupling coefficient M . The ratio of I_n to V_m is called the “transconductance” g_{mn} .

$$g_{mn}(\omega) = \frac{I_n}{V_m} = -\frac{1}{2} j \frac{I_0}{V_0} \frac{\omega}{\omega_q} M_m M_n \sin(\beta_q \ell_{mn}) e^{-j\beta_q \ell_{mn}} \quad (140)$$

The two coupling coefficients above are assigned to the two cavities and ℓ_{mn} is the drift distance between them.

The gain cavities of a wide-band klystron are usually stagger-tuned in a manner similar to low-frequency cascaded amplifiers.³⁵ However, feed-forward currents make calculation more complicated. The amplification mechanism begins with the velocity modulation being imparted on the e-beam by the RF voltage across the interaction gap in the input cavity. In the drift spaces beyond, electron bunching produces RF currents, thereby exciting subsequent cavities and introducing an additional, amplified velocity modulation on the beam. The original modulation, however, persists and RF currents originating from all previous cavities are finally summed at the output gap. A graphical rendition of the process is shown in the (Fig. 33).

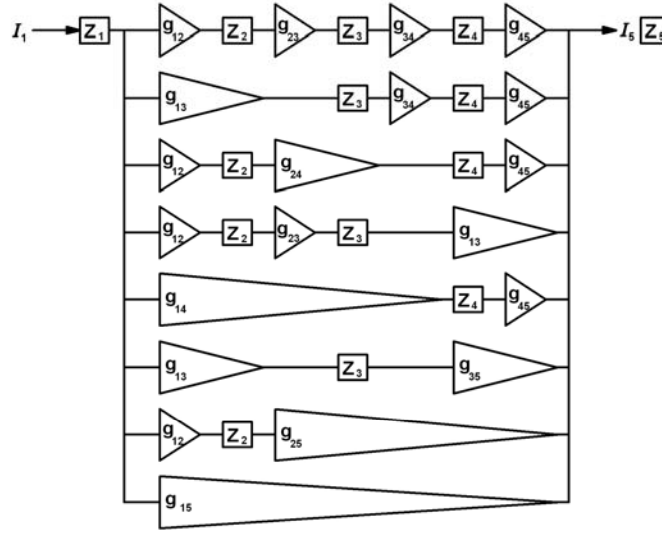


Fig. 33 Feed-forward currents in a 5-cavity klystron

The overall current gain function can be treated as a lumped constant network problem. The analysis proceeds as follows: The current gain between cavities m and n is

$$\frac{I_n}{I_m} = \mathcal{G}_{mn}(\omega) = g_{mn}(\omega) Z_m(\omega) = -\frac{1}{2} j Z_m(\omega) \frac{I_0}{V_0} \frac{\omega}{\omega_q} M_m M_n \sin(\beta_q \ell_{mn}) e^{-j\beta_q \ell_{mn}} \quad (141)$$

where, the expression for the lumped equivalent circuit for the n th cavity (at the operating TM_{01} mode) is

$$Z_n(\omega) = \left(\frac{R}{Q}\right)_n \left[\frac{1}{\frac{1}{Q_{Tn}} + j \frac{\omega^2 - \omega_{0n}^2}{\omega \omega_{0n}}} \right] \quad (142)$$

For the five-cavity klystron in (Fig. 33), the overall current gain can be written as

$$\mathcal{G}_{15}(\omega) = I_5 / I_1 = \left(\begin{array}{l} g_{12}g_{23}g_{34}g_{45}Z_2Z_3Z_4 \\ + g_{12}g_{23}g_{35}Z_2Z_3 + g_{12}g_{24}g_{45}Z_2Z_4 + g_{13}g_{34}g_{45}Z_4Z_3 + \\ + g_{12}g_{25}Z_2 + g_{14}g_{45}Z_4 + g_{13}g_{35}Z_3 \\ + g_{15} \end{array} \right) Z_1 \quad (143)$$

The first term in the brackets involves currents only between adjacent cavities. The remaining terms represent feed-forward currents skipping two, three and four cavities.

Equation (143) is rather daunting, but when programmed on the Mathcad analytical code that will be described later (Appendix I), it presents no difficulties. However, some additional insight can be gained by rewriting Eq. (142) in complex notation and reexamining the gain function Eq. (143) on the complex frequency plane. This is standard network theory³⁶ that need not be explained here in detail since the results will be fairly easy to understand intuitively.

The new (complex) variable is $p = \sigma + js$. Its imaginary part s is normalized to ω_0 and shifted in origin with respect to ω_0 according to the relations below. Here, ω_0 is the center of the klystron passband, which is assumed to be narrow (less than 10%). This is written as

$$\begin{aligned} p &= \sigma + js \\ js &= j \frac{\omega - \omega_0}{\omega_0} \\ \frac{\omega + \omega_0}{\omega_0} &\approx 2 \end{aligned} \quad (144)$$

With the above approximation, Eq. (142) becomes

$$Z_n(p) = \frac{1}{2} \left(\frac{R}{Q}\right)_n \left[\frac{1}{p - p_n} \right] \quad (145)$$

With

$$\begin{aligned} p_n &= -\frac{1}{2Q_n} + js_n \\ s_n &= \frac{\omega_n - \omega_0}{\omega_0} \end{aligned} \quad (146)$$

The above impedance function, $Z(p)$, is now a much simpler expression and the position of the root, p_n on the complex frequency plane is shown in (Fig. 34). This root, known in network theory as a “pole” of the $Z(p)$ function (marked by an “X”) has an imaginary part equal to the normalized resonant frequency, ω_n , and a real part equal to $-1/2Q_n$. The distance from the origin

to the pole is the absolute value of the impedance, $Z(p)$, and the angle to the $j\omega$ -axis is the phase. It is evident that the approximation and the change in variables have not changed the magnitude of Z . At $\omega = \omega_0$, Eq. (145) reduces to $Z = R$, as does Eq. (142)

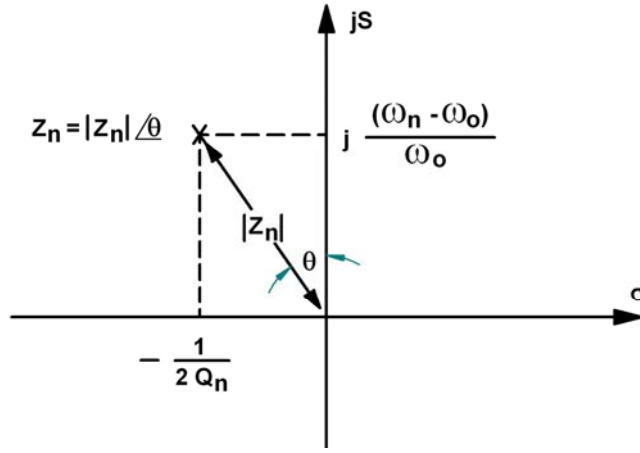


Fig. 34 The normalized complex frequency plane and the cavity impedance Z_n

Using the new variables we obtain the following expression for the absolute value of the power gain

$$G(p) = \frac{4}{Q_{e1}Q_{e5}} \frac{|Z_5 \mathcal{G}_{15}|^2}{(R/Q)_1 (R/Q)_5} = A \left| \frac{(p - z_1)(p - z_2)(p - z_3)}{(p - p_1)(p - p_2)(p - p_3)(p - p_4)(p - p_5)} \right|^2 \quad (147)$$

where A is a constant that embodies various circuit and beam parameters, the p_n 's are the poles of the five resonant circuits, and the z_n 's are the complex frequencies at which the gain function goes to zero. This happens because of the feed-forward terms. Consider the previous (Fig. 33). The various ways in which the feed-forward currents can produce zero gain do not depend on the input and output cavity tuning. All feed-forward currents from the input cavity are in phase, irrespective of its tuning, and the output cavity is the end of the line. Hence only the complex frequencies of the three middle cavities affect the position of the zeroes. This, besides algebra, accounts for the three zeroes in the $G(p)$ function. In general, the gain functions of multicavity klystrons with single-tuned cavities have two less zeroes than poles.

It is useful, and mathematically correct, to consider the poles and zeroes as positive and negative line charges into the complex frequency plane, and the logarithmic gain as the value of the electric potential due to these charges, measured along the $j\omega$ axis. It is easy then to visualize the effect of poles and zeroes on the shape of the gain response of the klystron. There will be gain peaks opposite poles and gain depressions opposite the zeroes. The steepness of both will depend on the distance of the pole or zero from the $j\omega$ axis. For the poles that distance is inversely proportional to the Q_T of the cavity concerned, hence the lower Q_T is, the less pronounced the gain peak. The problem then is to arrange the resonant frequencies of the cavities so that the gain is reasonably flat within the band of interest. Since the gain will be depressed in the vicinity of the zeros, the pole arrangement must be such that a zero is either moved outside the band or else is canceled by an adjacent pole. For drift lengths below a quarter

space-charge wavelength, the nearest zeros will be distributed toward the high frequency end of the band and will move closer towards band center as the drift angle is decreased. Consequently, tuning arrangements for the shorter drift angles will have more cavities tuned above band center to counteract the effect of the zeros. The klystron frequency response will generally fall off more sharply at the high end of the band, due to the presence of zeroes there.

The bandwidth for a given number of cavities will be rather closely related to the bandwidths of the individual cavities. It is frequently desirable to reduce the cavity quality factor by resistive loading. In the early stages where the power extracted thus from the beam is not a problem, this is satisfactory, in principle. It is, however, often mechanically inconvenient. The simplest Q factor reduction is accomplished through using the power required to velocity modulate the beam. The beam loading parameter is a function of gap geometry, and in general, the beam loaded Q of a cavity is reduced when the gap spacing is increased.

A simple example, that does not require a computer, is in order. A three-cavity klystron example will be used to illustrate the process. For $n = 3$, Eq. (143) becomes

$$\mathcal{G}(p) = I_3 / I_1 = (g_{12}g_{23}Z_2 + g_{13})Z_1 \quad (148)$$

and the power gain is

$$G(p) = \frac{4}{Q_{e1}Q_{e3}} \frac{|Z_3 g_{13}|^2}{(R/Q)_1 (R/Q)_3} = \frac{4}{Q_{e1}Q_{e3}} \frac{|(g_{12}g_{23}Z_2 + g_{13})Z_1 Z_3|^2}{(R/Q)_1 (R/Q)_3} \quad (149)$$

which is a three-pole, one-zero function. To calculate the zero, assume for simplicity that the three cavities have identical gap geometries and R/Qs, and that they are equally spaced along the beam. One would then obtain

$$\begin{aligned} g_{12}(p) &= -\frac{1}{2} j \frac{I_0}{V_0} \frac{\omega}{\omega_q} M^2 \sin(\beta_q \ell) e^{-j\beta_e \ell} = -j |g_{23}| e^{-j\beta_e \ell} \\ g_{13}(p) &= -\frac{1}{2} j \frac{I_0}{V_0} \frac{\omega}{\omega_q} M^2 \sin(\beta_q 2\ell) e^{-j2\beta_e \ell} = -j |g_{13}| e^{-j2\beta_e \ell} \end{aligned} \quad (150)$$

Setting $\mathcal{G}(p) = 0$, leads to the following expressions for the numerator “zero”

$$\begin{aligned} g_{12}g_{23}Z_2 + g_{13} &= g_{12}^2 \frac{1}{2} \left(\frac{R}{Q} \right)_n \left[\frac{1}{p - p_2} \right] + g_{13} = 0, \\ z_1 &= \frac{-\frac{|g_{12}|^2 R/Q}{2} + j |g_{13}| p_2}{j |g_{13}|} = p_2 + j \frac{|g_{12}|^2 R/Q}{2 |g_{13}|}, \\ z_1 &= -\frac{1}{2Q_2} + j \left[s_2 + \frac{1}{2} \frac{|g_{12}|^2}{|g_{13}|} R/Q \right] \end{aligned} \quad (151)$$

To illustrate the pole-zero technique for calculating the logarithmic current gain, it is worthwhile to work out a numerical example. A three-cavity klystron operating at 3 GHz, at about 25 kW power output could reasonably have the following set of parameters: $V_0 = 28$ kV, $I_0 = 3.6$ A, $\beta_q l_{12} = \beta_q l_{23} = 60^\circ$, $|g_{12}| = |g_{23}| = 0.0003$, $(R/Q)_1 = (R/Q)_2 = (R/Q)_3 = 120$, $Q_1 = 150$, $Q_2 = 350$, and $Q_3 = 50$. It can be shown that the power gain can be written, in terms of the poles and zeroes as

$$G(p) = \left[\frac{g_{13}}{2} R/Q \right]^2 \frac{1}{Q_{e1} Q_{e3}} \left| \frac{(p - z_1)}{(p - p_1)(p - p_2)(p - p_3)} \right|^2 \quad (152)$$

See (Fig. 35), which shows the changes in the gain response with the single zero position. As the cavity spacings change from 15° to 30° , to 60° , to 90° , the zero z_1 goes to infinity and has no longer any effect on the shape of the passband. That also maximizes the gain at the center frequency $\omega = 0$.

Taking the log of both sides yields the power gain in db as

$$G(p)_{db} = 10 \log \left(\left[\frac{g_{13}}{2} R/Q \right]^2 \frac{1}{Q_{e1} Q_{e3}} \right) + 20 (\log |p - p_1| + \log |p - p_2| + \log |p - p_3| - \log |p - z_1|) \quad (153)$$

One can make a rough estimate of the bandwidth of a single gain cavity in order to gain some insight to the design of broad-band klystrons. The maximum beam loading conductance that can be attained for ordinary gaps ($\beta_e d \approx 1$, $\gamma_a \approx 1$) is equal to about 0.15 times the DC beam conductance

$$G_b \approx 0.15 G_0 = 0.15 \frac{I_0}{V_0} \quad (154)$$

If one assumes a commonly encountered $R/Q = 100$ ohms, then

$$Q_b = \frac{1}{G_b \times R/Q} = \frac{1}{0.15 \frac{I_0}{V_0} \times 100} \approx 0.07 \frac{V_0}{I_0} \quad (155)$$

For an example that follows (the BFK 1.2 MW klystron), where $V_0 = 83$ kV and $I_0 = 24$ A, a Q_b of about 240 can then be expected from Eq. (155). That, together with ohmic losses would produce an approximate 3-db bandwidth 0.4% for that gain cavity. If there are three cavities in the gain section of the klystron, it should be possible to stagger-tune these cavities with as much as a 2% bandwidth in the current driving the output cavity. That cavity, however, must have that bandwidth by itself, at the correct impedance, in order for the saturated klystron bandwidth to be that wide.

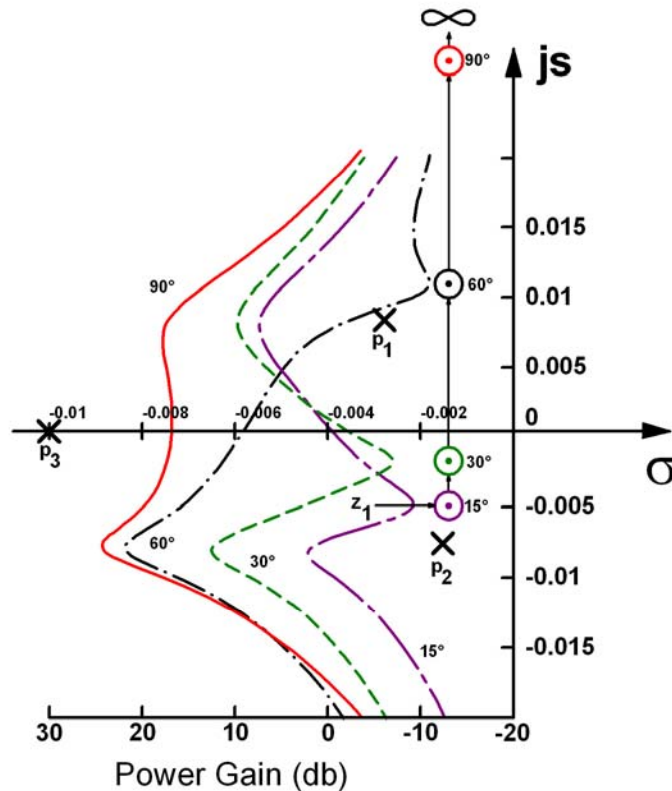


Fig. 35 Effect on zero and overall response of changing drift angle in a 3-cavity klystron

A comprehensive theory does not exist which would allow direct design for a specified gain bandwidth product. Optimization is obtained by trial-and error stagger-tuning through the use of an analytical Mathcad code such as the one described below. Alternatively, the zeroes can be calculated by solving for the roots of the numerator polynomial. A graphical method can then be used to obtain the logarithmic gain response directly from the locations of poles and zeroes on the complex frequency plane.

Qualitatively, one can say that the gain-bandwidth product of the driver section can be improved almost indefinitely by adding cavities. This can, however, lead to an excessively long klystron. The usual design procedure is to determine the bandwidth that can reasonably be expected of the output stage, and then design a driver section having adequate bandwidth with the required total gain. In doing so, one must remember to allow 3 to 5 dB reduction in gain due to saturation.

4.3 Large-Signal Methods

This discussion now turns to the output circuit, which, as explained earlier, must have adequate impedance and bandwidth to take advantage of the RF current provided by the driver section of the klystron. Analytical treatments of the problem, although in existence³⁷ are simply not accurate enough to bother with, given the availability of codes that are capable of simulating

the physics in 1-D, 2-D, or even 3-D. Simulation codes first became available in the mid-50's, when computers became powerful enough to handle the quantities of data involved. Some of the first results were published by Webber,³⁸ who was followed by Rowe³⁹ in treating klystron bunching through an iterative process involving an analytic description of the fields and a simulation of the beam by charged disks. The Webber and Rowe codes were the forerunners of modern one-dimensional codes, of which the "AJ-Disk" is an example now in use at SLAC. Such codes involve a relatively small number of disks, usually 64 or less, but can quickly assess the frequencies and spacings of the penultimate and output cavities, as well as the input power to drive the klystron to saturation. They can therefore be used for design, as opposed to design verification, which comes later in the development of a new klystron. For this phase, the codes usually employed are of the "particle in cell" variety. These rely on the simulation of the actual electric and magnetic fields by tracing the outlines of cavities, drift tubes and magnetic polepieces on closely spaced grids, "pushing" thousands of simulated electrons clumps (generating their own space charge) through these simulated fields, and iterating to convergence.

These methods will be examined in detail in the Appendices, where a high-power klystron will be analyzed and simulated by a variety of codes, and the results compared to the tube's actual performance.

For now, a simple formula is proposed for determining the loading required for a single-gap output cavity, since that sets the bandwidth of the klystron.

Assume that the RF current driving the output cavity is estimated to be I_1 and that the R/Q and the coupling coefficient M are known. Then the current induced in the output circuit will be $M \times I_1$. That current will develop a voltage V_1 across the parallel-resonant equivalent circuit, whose impedance is $Q_t \times R/Q$. In a general and rather simplistic way, that voltage must be sufficient to bring beam electrons to a stop, extracting the kinetic energy they acquired by being accelerated by the beam voltage V_0 . If a voltage across the circuit capacitance (the cavity gap) is to produce a voltage V_0 at the beam, one must have $V_1 M = V_0$. Expressing the foregoing in an equation, yields

$$I_1 Q_t \frac{R}{Q} M \approx \frac{V_0}{M} \quad (156)$$

which, rewritten in a more convenient form, provides a value for the desired Q_{ext}

$$Q_e \approx \frac{\frac{V_0}{I_0}}{M^2 \frac{R}{Q} \frac{I_1}{I_0}} \quad (157)$$

In Eq. (157), Q_e has been substituted for Q_t , since in most cases the coupling will be sufficiently strong (and Q_0 will be sufficiently high) to make the approximation $Q_e \approx Q_t$ valid. Equation (157) is intended only as a guide for the approximate value of the output cavity external Q . It is, as the gain is, very sensitive to the value of the coupling coefficient at the output gap, which in turn is very sensitive to the beam size.

4.4 Design of the SLAC "B-Factory" Klystron

The tools are in place now to illustrate the foregoing theory with an example making use of the methods actually used at SLAC for klystron design. These are the small-signal analytical

Mathcad gain-bandwidth calculator, the “AJ-Disk” 1-D simulation code, and 2-D and 3-D MAGIC codes. (Note that the AJ-Disk is named after Aaron Jensen, a Stanford University graduate student, who rewrote the original “Japandisk” code⁴⁰ in C++ and rendered it user-friendly.) Because of its complexity and the time required to run it, MAGIC is considered as a check on the other two codes, rather than as a design tool.

The example below is for a klystron currently in production at SLAC for use in the PEP-II (B-Factory) electron-positron asymmetrical storage ring collider. The original specifications for this tube (B-Factory klystron, or BFK) were as follows:

- Frequency = 476 MHz
- Output power = 1.2 MW CW
- Beam Voltage = 83.5 kV
- Beam Current = 24 A
- Efficiency > 60%,
- Gain > 43 dB
- Bandwidth (1-dB) = 6 MHz
- Group Delay <100 nsec (in ± 0.5 MHz)

A mechanical drawing of this klystron is shown in (Fig. 36). For reasons of linearity (necessary because of feedback systems in the PEP-II rings) the klystron was to be operated at drive levels well below saturation. The linearity specification required good efficiency and a collector designed to accept the full 2-MW beam power. The delay specification was found in simulation to be attainable as long as the specified bandwidth was realized.

It was decided to design a klystron with three gain cavities, followed by a second harmonic cavity to improve bunching and efficiency, followed by two “penultimate cavities” (to limit the total voltage necessary for the final bunching), and an output cavity with loop coupling and a coaxial output window. For the purposes of the Mathcad calculations, this is a total of six cavities (the 2nd harmonic cavity does not affect the small-signal calculations).

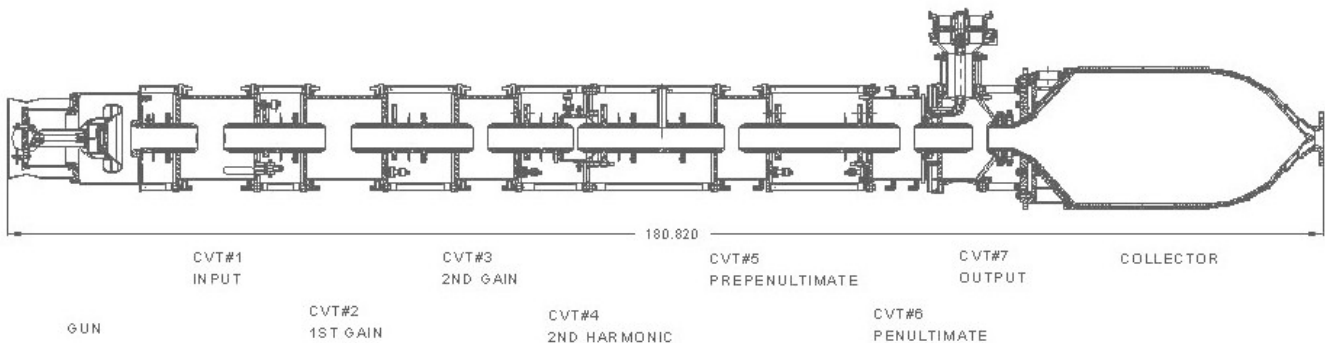


Fig. 36 Mechanical design of the BFK

The perveance of 1×10^{-6} was chosen as a compromise between good efficiency and a reasonable DC voltage. The gun does not present a serious challenge, since at this frequency, reasonable choices of beam and drift tube diameters do not require a large beam convergence. The electron gun was designed for a maximum current density of 0.3 A/cm^2 . Computer simulations predicted a beam diameter of 0.45 cm and the beam tunnel was chosen at 7 cm. This

resulted in a $\gamma a = 0.6$, which produced good coupling coefficients and hence good gain bandwidth. None of the cavities were loaded, but the first two had wider gaps for a lower Q_b and improved bandwidth. Notice that the empirical calculation Eq. (157) gives $Q_{e6} = 33$. However, the operating value of $Q_{ext} = 38.9$ was determined by a more accurate large-signal simulation.

All cavities except the output are made of stainless steel cylinders and end plates that are copper plated. The output cavity is all copper for good circuit efficiency and cooling. All cavities except the output are tunable over approximately 3 MHz by deforming an end wall slightly, thus changing the gap length (capacitive tuning). The 2nd harmonic cavity can be tuned over twice that range.

It is now highly instructive to compare the actual performance of the above BFK klystron to the small-signal Mathcad calculations, the “A-J Disk” 1-D simulation, and a 2-D MAGIC simulation. The CD Appendices afford the opportunity to follow the step-by-step klystron design process currently in use at SLAC. As a preview, the results of the various small-signal calculations/simulations for the BFK gain are compared in (Fig. 37) below. The drive power is the same for all traces except for Mathcad, where it is not pertinent.

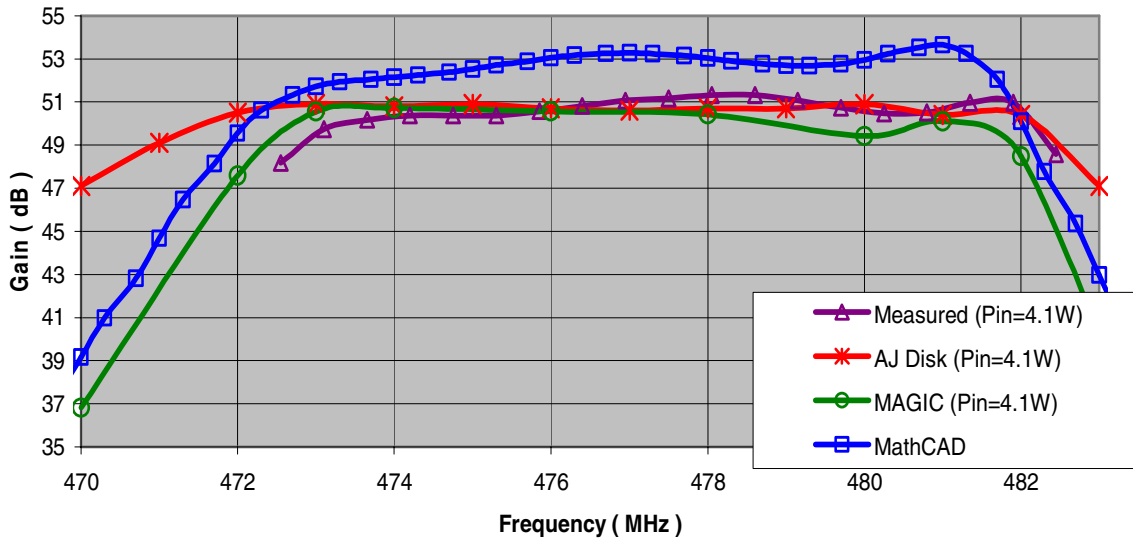


Fig. 37 Simulation results and experimental performance of the BFK

Chapter 5.

Advanced Klystron Configurations

5.1 Introduction

Unlike the previous three, this chapter deals more with work in progress than with established theory and designs. Previous chapters provided the basic theory and the computation and simulation tools necessary for the design of “classical” klystrons, consisting of a single pencil beam interacting with several single-gap cavities. For many years, such klystrons served well the purposes of radar, communications, and accelerator applications. Eventually, however, the combined needs for wider bandwidth, higher frequencies and higher power, have led to a number of klystron variants in which beams become multiple or flat, and single gap cavities become multiple-gap, or “extended-interaction.” At SLAC, Extended Interaction Klystrons (EIKs), Multiple Beam Klystrons (MBKs) and Sheet-Beam Klystrons (SBKs), as well as permutations of them, have been studied extensively, and this research continues.

5.2 Extended Interaction Klystrons (EIKs)

Because of the high-peak power needs of a future e+e- linear collider, which if funded will require thousands of 11.4 GHz, 75-MW klystrons, both solenoid and PPM-focused EIKs have been designed at SLAC. They have also been manufactured, and put into service.

Extended interaction theory is no more than a generalized theory of klystrons, where the restrictions of single and/or gridded gaps are removed and beam interaction takes place with a generalized field. Such a field may consist of several discrete regions, corresponding to cavities placed closely together, or it may be the continuous field of a shorted helix or a coupled cavity structure. Most of the published theory is due to Wessel-Berg, who began his work at Stanford and continued it in Norway. The theory is 1-D, but can be applied to 2-D situations by the averaging methods discussed earlier in this chapter. More often than not, however, numerical simulations are necessary to complete the design process and to avoid expensive cold-test procedures.

The Wessel-Berg theory is based on the assumption that as long as the cavities are resonant with high Qs, the extended cavity (or standing-wave structure) fields are unaffected by the RF fields of the bunched beam. The EIK cavities can be analyzed independently of the beam, using the methods described earlier to calculate coupling coefficients and R/Q analytically, or through simulation. Overall EIK small-signal frequency response can be calculated using the analytical Mathcad program by treating the extended cavities as simple resonant circuits, as in the case of single-gap cavities. However, the AJ-Disk 1-D code cannot be used because it does not simulate accurately the large signal behavior of extended cavities. The use of PIC codes is mandatory (see Appendix III).

Extended interaction cavities offer several advantages: The most important is that they make possible R/Q values that cannot be attained with single-gap cavities. This is a direct result of the fact that these circuits are no longer driving-point impedances as single-gap cavities are and hence not subject to the bandwidth limitation described by Eq. (139).⁴¹ Hence EIKs can attain bandwidths modestly superior to ordinary klystrons. High R/Q output circuits also imply low external Qs, and higher circuit efficiency. Extended interaction output cavities made possible the 1-MW CW X-Band klystron built at Varian in the 60's.⁴² Finally, extended interaction cavities can distribute the necessary retarding RF voltage at an output cavity over

several gaps, thereby reducing the RF gradient and the danger of RF breakdown. This is the principal reason for the use of extended cavities in the SLAC pulsed klystrons, though circuit efficiency was also a consideration.

The original Wessel-Berg research on extended interaction at Stanford⁴³ involved shorted sections of ring-bar structures, which are relatively low-voltage (and low power) circuits. The SLAC high-power EIKs operate at 400-500 kV and their output circuits are ordinary accelerator structures (i.e. iris-loaded round waveguide). In the SLAC EIKs, these circuits are usually operated in the π -mode and consist of three to five sections. The detailed design of the XP-3, a SLAC PPM 75-MW klystron is described in Part 2 of this report, but it is useful to present here an example of an earlier SLAC EIK, in which the design of a four-section output cavity proved to be unstable. It should have been predicted to be so, had the detailed simulation of the beam loading conductance been performed. This example will also illustrate the method of obtaining the R/Q, coupling coefficient and G_b/G_0 for an extended interaction cavity.

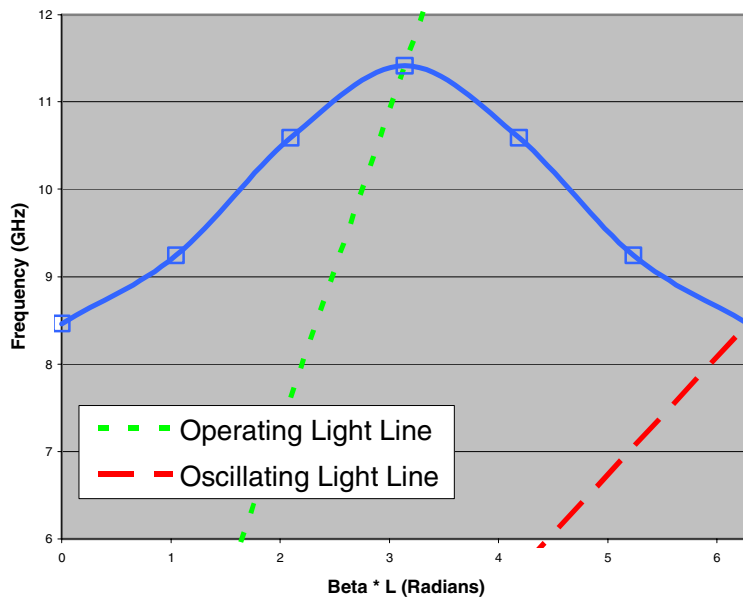


Fig. 38 ω - β diagram for the XC-8

In the early 90's, SLAC research for NLC X-band klystron sources was centered on extended interaction klystrons which could be operated by existing modulators to reach an output of 100 MW. This approach required a microperveance of 2 and was soon to be abandoned because it did not produce a satisfactory efficiency and was not compatible with PPM beam confinement. The last klystron in this series, designated as XC-8, suffered from a fatal oscillation at a lower than operating frequency, corresponding to the 2π mode. Figure 38 shows the ω - β diagram for the disk-loaded waveguide used. The four-cell output cavity of the XC-8 is shown to be operating at the π mode, with the intersection of the ω - β diagram and the light line at 11.4 GHz. The light-line at the 2π mode has an intersection at about 8.4 GHz, which would occur in operation as the beam voltage was raised through about 200 kV. A SUPERFISH simulation of the cavity was performed and the four modes, 0 (2π), $\pi/3$, $2\pi/3$ and π , are shown in (Fig. 39).

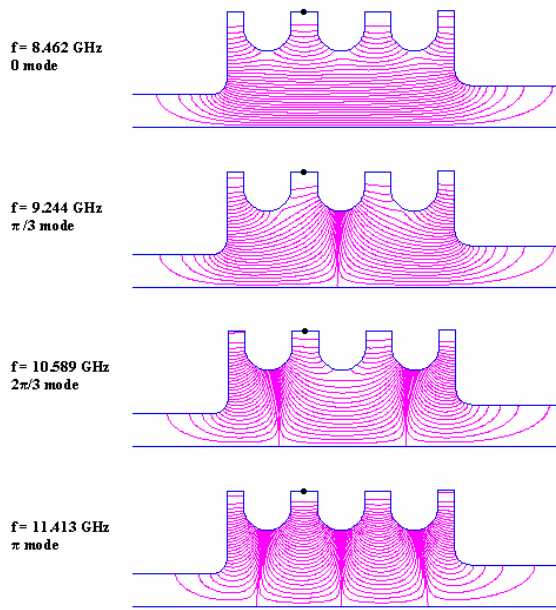


Fig. 39 Field patterns for the four modes in the XC-8 extended cavity

A Mathcad program shown in Appendix IV was used to calculate coupling coefficients and R/Qs for each of the four modes, as well as the Wessel-Berg M^+ and M^- coupling coefficients which, together with the other parameters in Eq. (130) are used to calculate G_b . From the G_b s and R/Qs of the four modes the beam-loaded Qs of the four modes were plotted in (Fig. 39) as a function of the beam voltage.

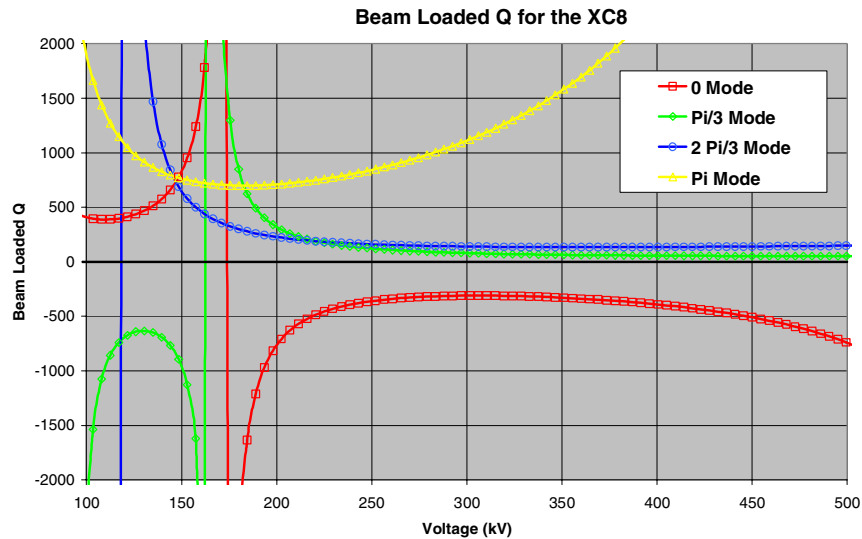


Fig. 40 Beam-loaded Q vs. beam voltage for the XC-8 EIK

The problem with the cavity is immediately evident. The beam-loaded conductance Q at the 0 (or 2π) mode is negative, and quite low. Since there is a window matched at 11.4 GHz between the cavity and the matched load, there is no simple way to evaluate the loading of the cavity at the much lower frequency of the 0-mode. The loading was light at 8.5 GHz and the cavity oscillated as the voltage was raised, and continued oscillating at higher voltages.

The NLC EIKs, strictly speaking, are not klystrons but “twystrons.” No mention of these devices has been made so far in this report, largely because they have not been at the forefront of device development in recent years. The term is a composite of “TWT” and “klystron.” Both the word and the device were invented at Varian in the 60’s, when some very high-power radars being deployed at the time required more bandwidth than a conventional klystron could deliver. At Varian, an engineering team of klystron coupled cavity and klystron engineers used the front end of a megawatt-level klystron and the output section of a cloverleaf TWT to make the first Twystron, with a bandwidth of 12 to 15 per cent. Subsequently, a number of classified “superpower” Twystrons were developed and put into production. Subsequently, some of the original, lower-power, twystrons were replaced by EIKs which were easier to manufacture since they did not require the distributed Kanthol loss that the cloverleaf output of the twystrons employed.

The output circuit design of the NLC EIKs was initially a 4-cell resonant cavity, along the lines described above. After a series of 8 unsuccessful microperveance 2 klystrons, the perveance was reduced to 1.2×10^{-6} and two solenoid-focused 50-MW klystrons were built, successfully. At that point, since the beam voltage had been increased due to the lower perveance and because of concerns about RF breakdown, it was decided to migrate to a disk-loaded waveguide output circuit that would be specifically designed to divide the RF voltage developed across it equally among its 4 cells. This was accomplished with the aid of a little computer code, which provided dimensions of the cells such as to decrease the impedance of the circuit as seen by the beam by a factor of 2 as one proceeded from the first cell to the 4th cell, which coupled to the output waveguide. The idea was due to Symons and Begum⁴⁴ and was based on the assumption that, since additional RF current was fed to the output circuit at each gap, the impedance there should be decreased to keep all gap voltages equal. The result of this operation was that, the final gap, the impedance required was so low that the last cell was effectively matched to the output load, making the output a TWT section. The difference from a twystron output circuit is that there is no loss and no reverse termination. This is definitely not a resonant cavity, which means that there is the additional benefit that bandwidth and circuit efficiency are both improved for the EIK.

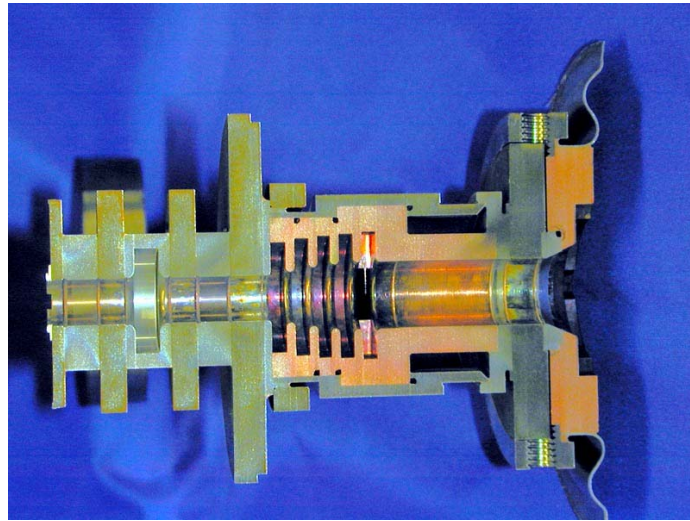


Fig. 41. A sectioned copper XP output circuit (collector to the right). Note the expanding iris openings, decreasing the circuit impedance toward the output. The last of three “penultimate” cavities is visible on the left. This and all other cavities are made of stainless steel. Larger iron polepieces are shown on either side of the output cavity.

A total of thirteen EIKs (XL4s), producing 50-MW, 1.2 μ s pulses with a 60 Hz repetition rate were built at SLAC and have been in operation for a number of years in several experimental installations. These are all solenoid-focused klystrons and hence not suitable for the NLC. For that future machine, a number of PPM-focused klystrons were also designed and built, to more demanding specifications. These are the following:

Power output: 75 MW
Pulse length: 1.6 μ s
Pulse repetition rate: 120 Hz
Beam voltage: 515 kV
Beam current: 260 A
Efficiency: 56 %
Gain: 60 dB

At this writing, the output circuit for these EIKs (designated as XPs and requiring 5 cells at the output) must be designed on the computer, using the MAGIC code. The “little code,” which provided approximate circuit dimensions for the XL4s falls short for the XPs and requires drastic revisions.

The experimental performance of XP4, the latest in the series of PPM NLC klystrons is described in the figures below.¹

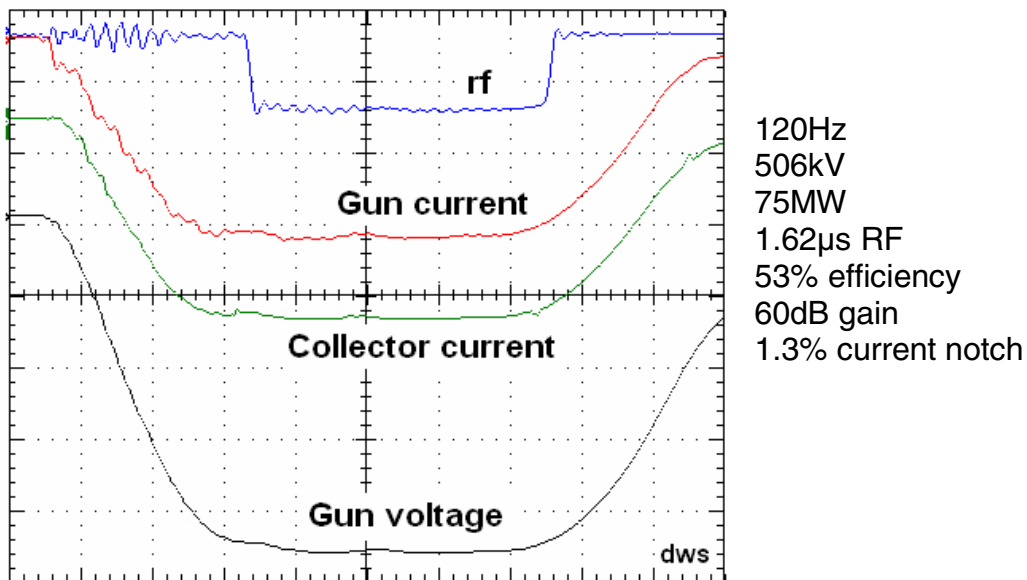


Fig. 42. Oscilloscope traces of XP4 experimental data. “Current notch” refers to beam interception at full power, as measured by reduced collector current

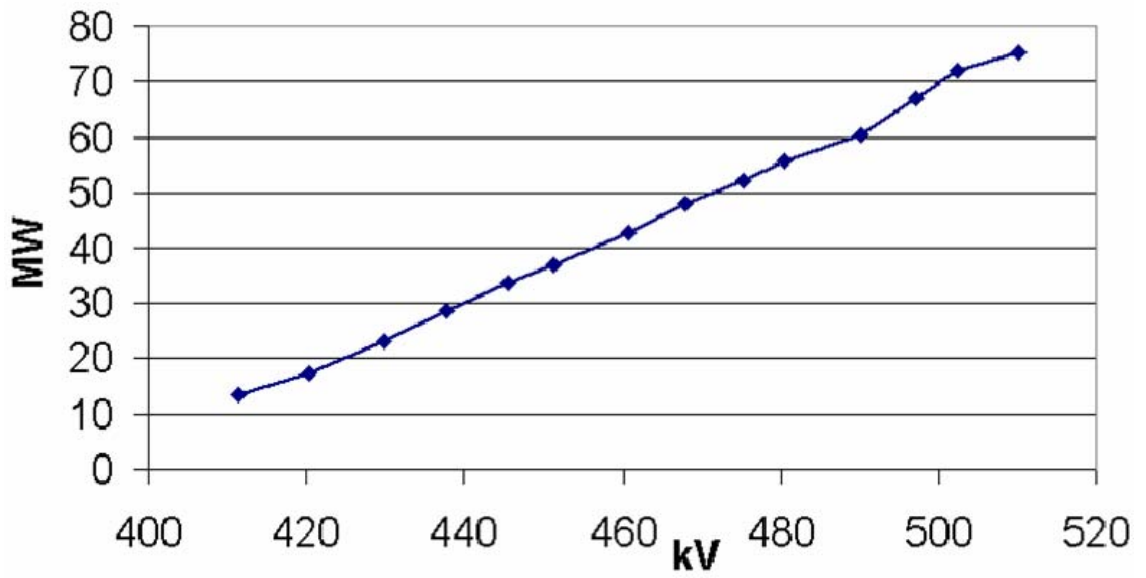


Fig. 43 XP4 output power vs. voltage

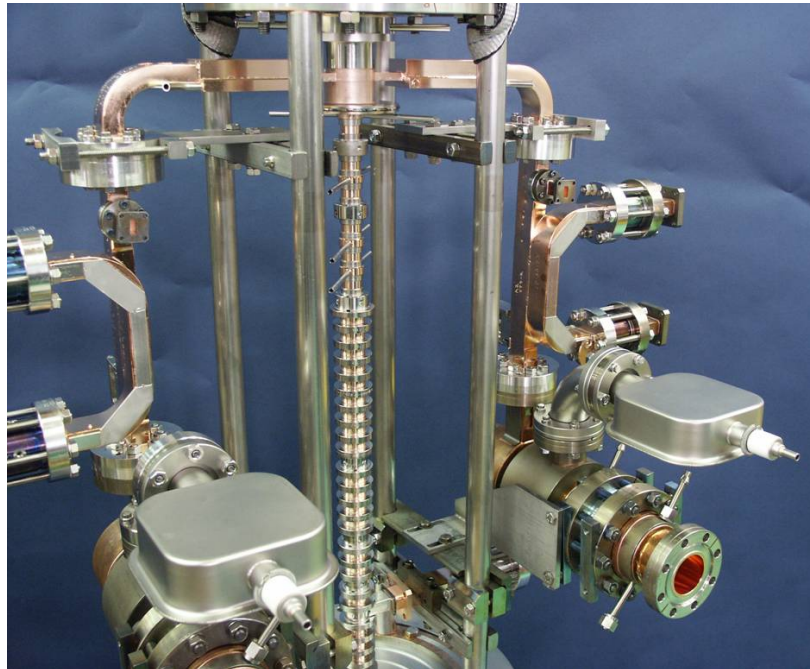


Fig. 44 Detail of XP4 construction showing polepieces and cavities at the output end. The tube has a double output for symmetry in the output cavity fields, and to reduce window power. The magnets are not yet in place

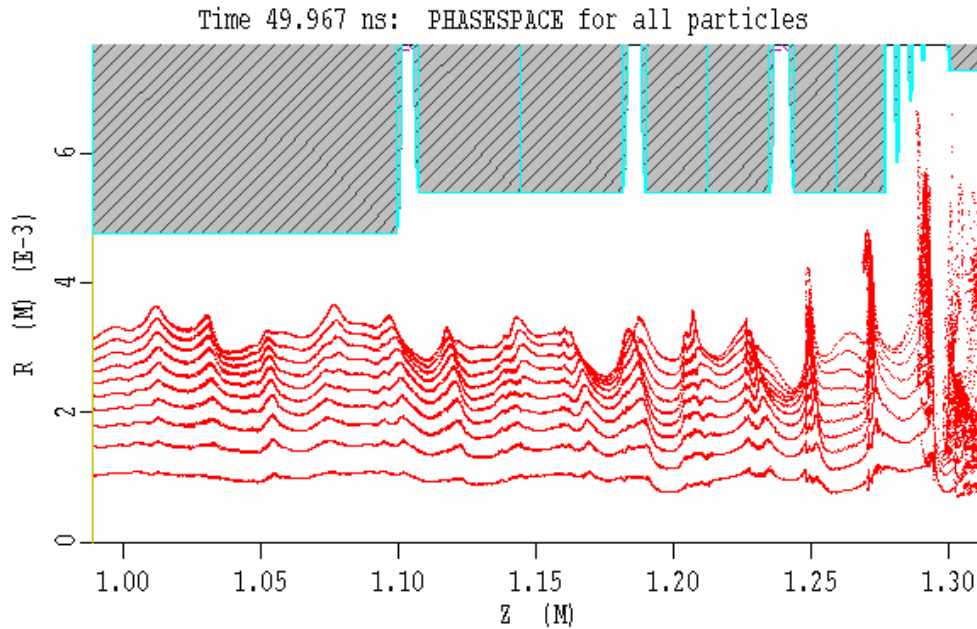


Fig. 45. MAGIC simulation of the RF current at the output end of the XP4, showing three “penultimate” cavities and an extended output circuit. The RF current shown is approximately 1.6 times dc beam current. The last two cells of the output are not visible. The plot axes are for radial and axial (z) distance.

It should be pointed out that PPM focusing of 500-kV klystrons is surprisingly forgiving, assuming of course that gun and beam optics are very good. Unlike TWTs, whose PPM stacks often require shunting on the test bench, the XP klystrons PPM stacks do not require any “tuning.” This is fortunate, since these klystrons are operated behind several inches of lead on test, and their PPM stacks are completely inaccessible. This performance is partly due to the fact that the ratio of plasma wavelength to the PPM period in the XP4s is about twice that of typical TWTs.

5.3 Multiple Beam Klystrons (MBKs)

In Russia, where tube development followed different paths than the West during the Cold War, MBKs have been in production for 30 years or more and are used for two reasons: a) because they make possible lower voltages, particularly in airborne applications and b) because the lower beam impedance of the MBK results in a wider bandwidth. The Russians appear to have opted for MBKs rather than coupled-cavity TWTs for applications requiring 10-20% bandwidth. Their designs call for as many as 60 beams. The principal shortcoming of the Russian MBKs is that the large number of closely-spaced “beamlets” allows little room for focus electrodes around the multiple cathodes of the electron gun. This results in very low area convergence for the beamlets and often requires high-current densities at the cathodes. As a consequence, one can speculate that Russian-style MBKs may have lower life expectancies than conventional pencil-beam klystrons.

In 1998, an experienced Russian MBK designer, Yuriy Besov from Svetlana Electronics in St. Petersburg, Russia, was invited to work at SLAC for several months. The motivation was for SLAC klystron engineers to gain some insight into Russian MBK technology. Besov worked out a paper design of a 1-MW, 12% bandwidth klystron at S-band. The idea was to compare this MBK design to that of a conventional klystron used in a military system.

Besov patterned his design after a lower power MBK that he had previously built in Svetlana. He used 19 beams, and extended interaction cavities at the input and output, with seven cavities in total. The output cavity operated in the 2π mode was also part of a filter circuit in the output waveguide. The design was accomplished with the aid of a Russian disk-model, large-signal program called "KLYSTRON."⁴⁵ It predicted 50% efficiency for the TUBE, a reasonable result given the individual beams perveances (0.33×10^{-6} each beam, total perveance 6.25×10^{-6}). The voltage was only 40 kV, the current 50 A.

This particular MBK is offered here only as an example of the Russian technology, not as a tutorial on this technology. There are no details available on critical parameters used in the Besov design, such as R/Q and the coupling coefficients. Besov's sketches of the MBK and the response simulated by the KLYSTRON are shown on (Figs. 41 and 42) respectively. The gain-bandwidth of the tube is impressive and requires an in-line filter circuit, in addition to a two-gap extended output cavity.

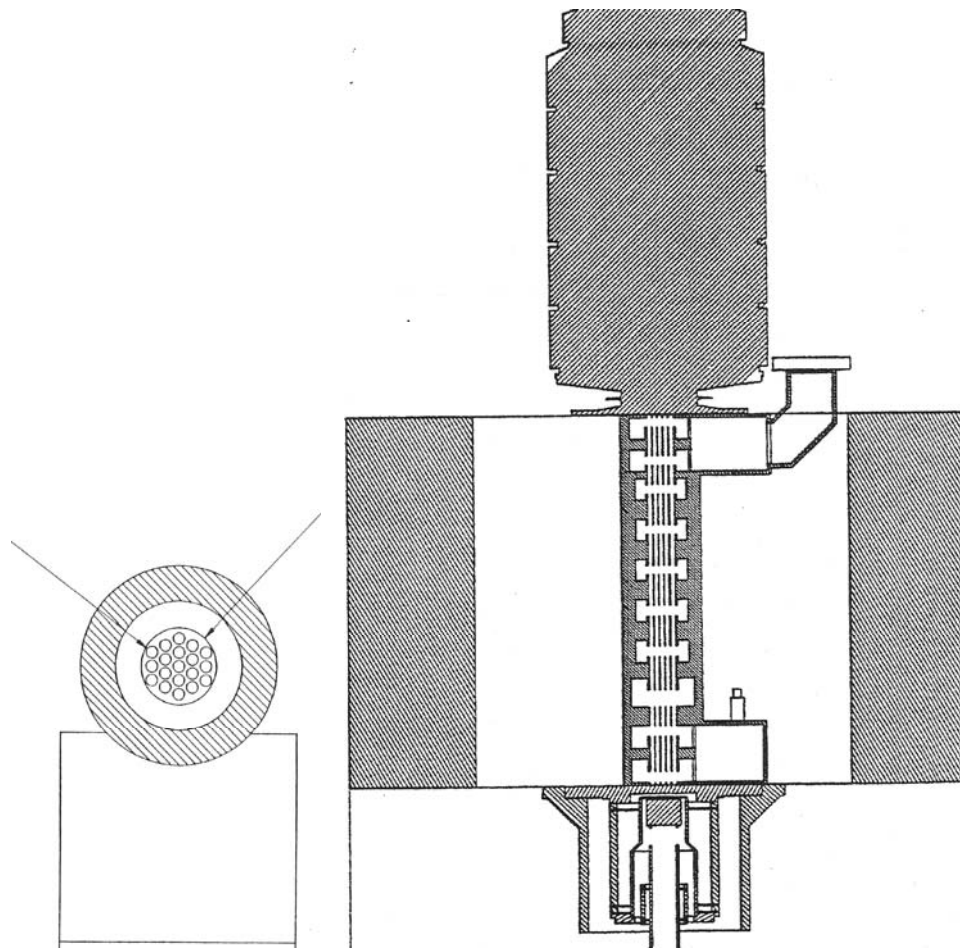


Fig. 46 Besov MBK and beam bundle cross section

The Russian approach of forming a tight bundle of drift tubes and beams at the center of common cavities is simply a way to employ a quasi-high-perveance beam for low voltage and bandwidth, without incurring the penalty of the potential drop that would exist in the center of a

single high-perveance beam. However, the price paid is a very low beam convergence, higher cathode current densities and a shorter tube life. A better approach may be to use a higher (TM_{02} , instead of TM_{01}) mode in the cavities and place cathodes and beams on a larger “bolt circle.” This allows some room at the guns for individual focus electrodes, and therefore more convergence. However, with this approach, the axes of the beams are farther from the central axis of the tube and its solenoid. This necessitates extensive magnetic polepiece shaping to provide symmetrical magnetic fields around the individual beam axes.

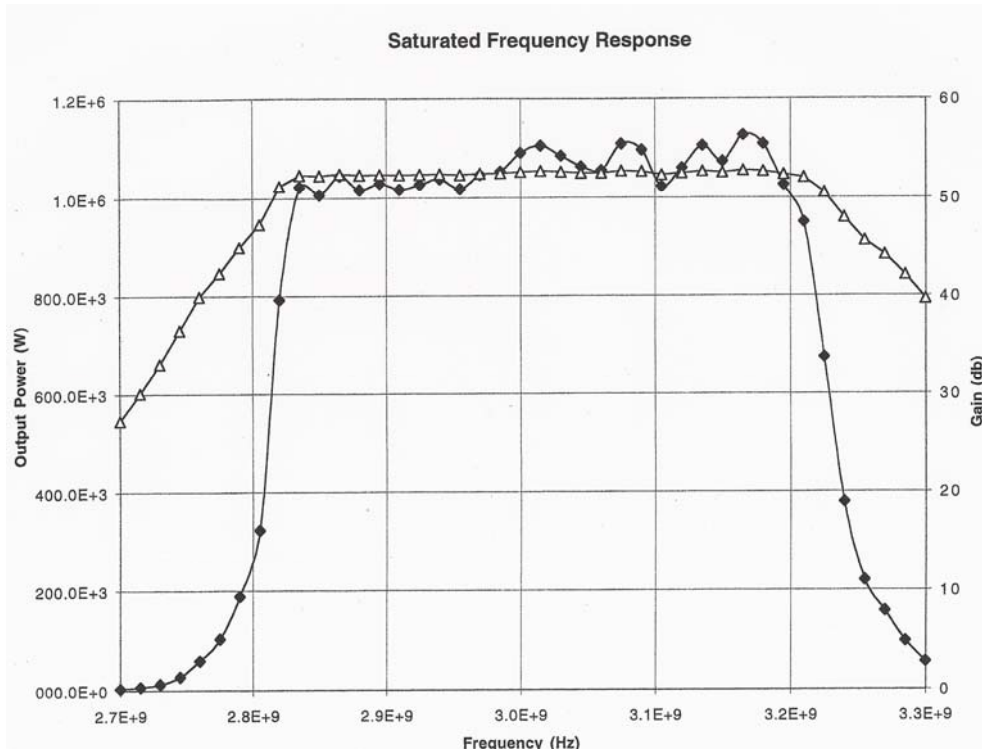


Fig. 47 Frequency response (power and gain) of the Besov MBK

A novel form of MBK was investigated at SLAC, under the following circumstances: For the past 30 years or more, high-power microwave (HPM) researchers in a number of US government and university laboratories have been attempting to develop L-band microwave sources capable of generating 1-kilojoule, one-microsecond pulses. Since a 500-kV beam voltage was considered the maximum practical, which forces the required beam current to be in the thousands of amperes, the HPM community approach has been to employ field emission cathodes, capable of very high current densities. For this and other reasons the devices which have been built (MILOs, “Relativistic klystrons”) have operated with a poor vacuum, a condition not consistent with the necessity to hold off the very high RF and dc gradients encountered at these power levels. As a result, the microsecond/kJ goal has never been attained. Although in some cases several gigawatts have been generated, pulse durations have been limited. This condition has been known as “pulse shortening.”

As a participant in an HPM Air Force research program, SLAC addressed the kilojoule problem with a periodic permanent magnet focused (PPM) MBK. This was an outgrowth of work performed at SLAC for the NLC klystrons. It finessed the need for extensive magnetic field shaping and substantially reduced the weight of the device. The new tube, dubbed GMBK for “Gigawatt Multiple Beam Klystron” was entirely within the state-of-the-art and depended

only on good vacuum practice to perform to its specifications. It would have employed thermionic cathodes, loaded to about 30 A/cm², a current density which was consistent with 1-microsecond pulses, and with the expendable character of the device.

The proposed GMBK is pictured in (Fig. 48). It was to consist of ten 1.4-microperveance beams. The beams traversed four common cavities and ten individual second harmonic cavities, to enhance efficiency. Each beam would have been focused in a periodic magnet stack, with magnetically compensated openings to accommodate the cavities. Neodymium iron boron magnets were to be used. Unlike ordinary multi-beam klystrons, where a single solenoid is used to focus several beams, each GMBK beam would have occupied the axis of symmetry of the field focusing it. The first three cavities were toroidal (hollow) and operated in the TM₀₁ coaxial mode (which would be a TM₀₂, if the cavities were not toroidal). The last cavity was to be full and support the TM₀₂ mode. It coupled to a circular waveguide in the TM₀₁ mode, which terminated in a quarter-wave ceramic window.

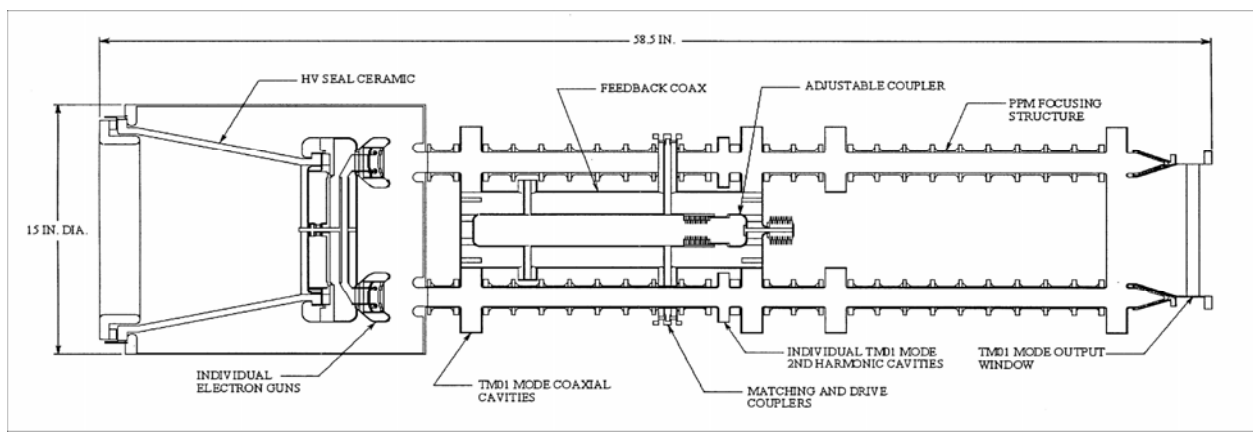


Fig. 48 A PPM-focused MBK

The two examples above illustrate the two principal reasons for using MBKs (i.e. broader bandwidth or higher power than conventional klystrons). In a current accelerator application, the German TESLA linear collider at DESY, two different tube companies, Thales in France and CPI in the US, used the Russian and US approaches respectively to design a 10-MW peak, 100-kW average, 2-millisecond-pulse MBK, at L-Band. In this case, the principal reasons for opting for an MBK were the expectation of higher efficiency with lower perveance beams, and a more favorable distribution of beam and circuit losses. The French design (see Fig. 21a) calls for seven beams at the center of its TM₀₁ cavities, which are common to all the beams. The CPI design (see Fig. 21b) is very similar to the GMBK design above, and places its six beams on the periphery of TM₀₂ common input and output cavities. All other cavities, including those at 2nd harmonic are individual to each beam. The beams of both MBKs are focused with single electromagnets. Since, in both tubes, the beams are off the electromagnet axis, the pole-pieces must be properly shaped in order for the beam trajectories to be straight inside the individual drift tubes.

Small-signal calculations for an MBK do not present any new problems compared to those for pencil-beam klystrons, although a number of papers have been published suggesting the need for new design techniques. If all the cavities (input, gain and output) are common to the beams, one simply uses the same transconductance and cavity impedance equations Eqs. (140 and 142) as if there were a single beam. The currents I_n/I_m and I_0 in Eq. (141) should be the total

currents, and the R/Q in Eq. (142) the total cavity R/Q . The ω_q and β_q beam parameters, however, are calculated for a single beamlet. The use of 3-D codes is necessary to explore competing modes in common cavities, to design solenoid pole-pieces, and for overall large-signal tube performance.

5.4 Sheet-Beam Klystrons (SBKs)

As stated previously, as many as 4000 X-Band klystrons, each delivering 75 MW, may be required for the projected Next Linear Collider (NLC). The extraordinary requirement of mass-producing such complex klystrons has led to an investigation of lower cost and/or higher power alternatives. Since it is considered impractical to increase the beam voltage much above 500 kV the beam current must be increased. Higher perveance beams were ruled out since the low perveance employed in the 75-MW prototypes ($0.7 \mu\text{P}$) is essential to both good efficiency (50-55%) and to effective PPM focusing, without which the power budget for the collider could not be met. MBKs were investigated, but were provisionally excluded because the multiplicity of parts they require is not consistent with low manufacturing costs. It appeared that a Sheet Beam Klystron (SBK) could be produced with many fewer parts than the current SLAC 75-MW pencil-beam prototypes (See Appendix VII). At the same time the beam current density and focusing magnetic field could be substantially reduced. Those improvements over the present prototypes should result in both lower acquisition and operating costs. Most importantly, the SBK should be more reliable since the surface area from which waste average power must be removed would be higher by a factor of approximately five compared to the pencil-beam prototype. As a consequence, the SBK is currently the object of intensive research at SLAC, with the goal of eventually designing a PPM-focused Double Sheet-Beam Extended Interaction Klystron (DSBK) capable of an output of 150 MW. This would reduce by a factor of two the number of tubes in the collider. Furthermore, assuming that improved pulse compression methods are developed in the future, and since average power would not be an issue with the DSBK, a doubling of the pulse length to 3.2 microseconds would further reduce the collider klystron requirement by a total factor of four to a total of perhaps as few as 1000 klystrons. The design of a single sheet beam version of this tube is presented below as a work in progress, not a completed design.

In an SBK, the central design issue is to form a beam that is as thin and as wide and with as much current as is consistent with: a) the optics of the electron gun which forms it, b) the method used to confine it, c) an appropriate M^2R/Q of cavities which interact with it. Those requirements are often conflicting, and must be reconciled in 3-D. This perhaps explains why, without the 3-D codes now available, SBKs were not extensively investigated in the past.

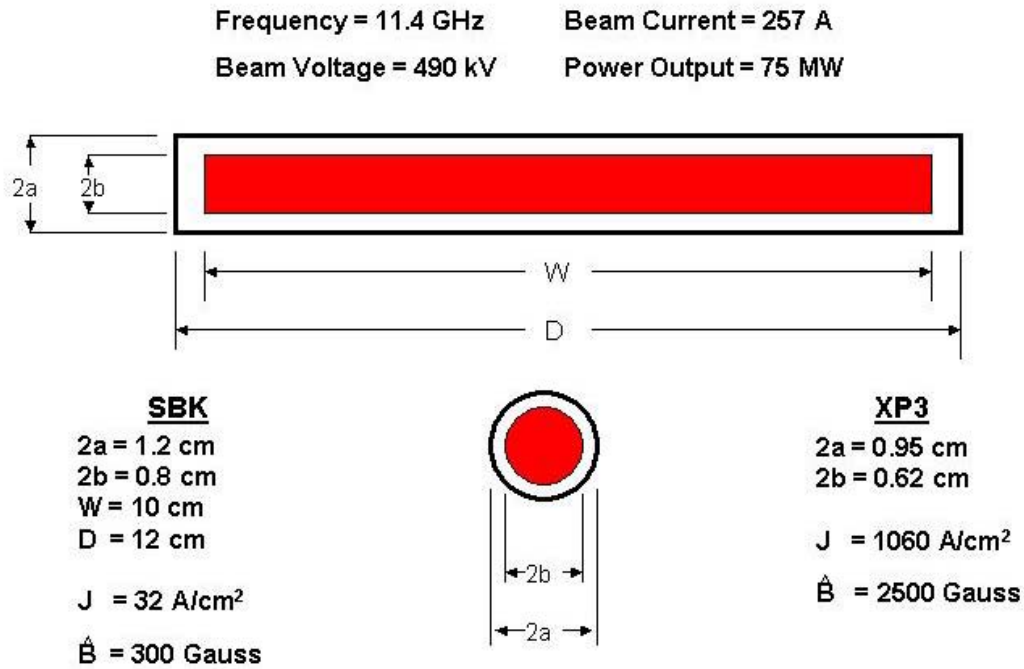


Fig. 49 Comparison of pencil-beam and sheet beam klystron parameters

The proposed NLC SBK is being designed for the same voltage and current as the XP-3 so that can be “plug-compatible” in the XP-3 sockets. Comparing the pertinent parameters of the two tubes, their most striking difference is in their current densities (Fig. 49). The consequences are: a) a very low magnetic field required for beam confinement and; b) very weak debunching forces. Both are beneficial effects. Even more important, however, are the thermal and mechanical benefits from the flat, overmoded cavities of the SBK. These are: a) much larger surfaces on which to dissipate beam interception and I^2R losses and; b) a considerably simplified fabrication of the klystron RF circuits, resulting in many fewer parts than the manufacture of the XP-3 will require.

A serious penalty would be incurred in choosing the SBK approach if one were interested in wideband performance. This is not the case for the NLC klystron application. The single cell SBK cavity is essentially a TE_{10} rectangular waveguide positioned transverse to the direction of beam transport. The broad dimension of the waveguide cross section, (the ‘a’ dimension), is chosen so the waveguide is cutoff at the SBK operating frequency. The electron beam traverses the narrow dimension of the guide. Since the waveguide section is cutoff, the electric field seen by the beam is constant across the width of the cavity. The cutoff waveguide is terminated at both ends by quarter wave matching sections to produce a resonant structure. The R/Q of such a cavity, which in the NLC case has an aspect ratio of 10:1, is about 50 ohms, and the coupling coefficient is about 0.5. Those values are to be compared to 80 and 0.8 respectively for an XP-3 “gain” cavity. Even if bandwidth were not an issue, these single-cell SBK cavity parameters are still dismal. The solution is to use extended cavities, synchronous with the e-beam. These greatly enhance the critical parameter M^2R/Q by increasing both M and R/Q. A quarter-symmetry MAGIC model of a three-cavity SBK, showing a single-cell input, and two three-cell cavities, all with matching networks to external waveguides is shown in (Fig. 50).

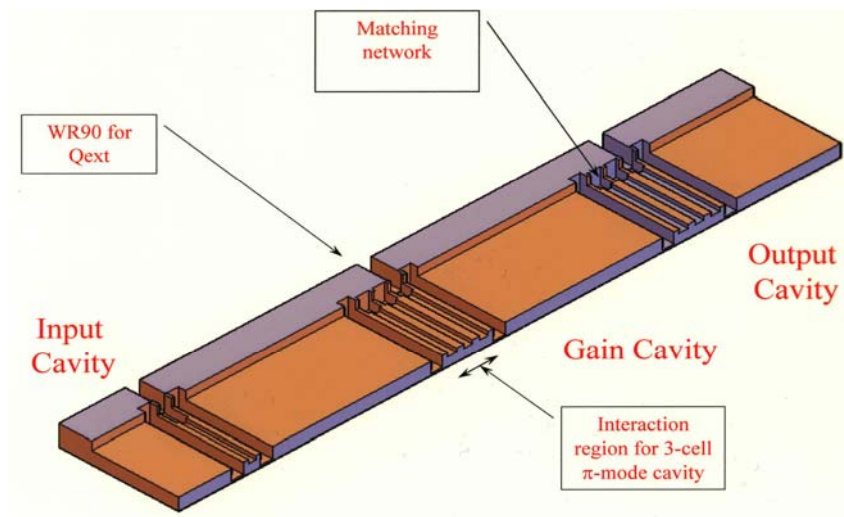


Fig. 50 A 3-cavity SBK quarter-block

The design of a sheet beam electron gun presents the usual 3-D problems. For the NLC SBK, the gun design was developed using two codes, 3-D MAGIC and the Russian 3-D code, "TOPAZ."⁴⁶ The gun has a 10:1 convergence in one dimension only, and a cathode current density of 3.2 A/cm^2 (Fig. 51).

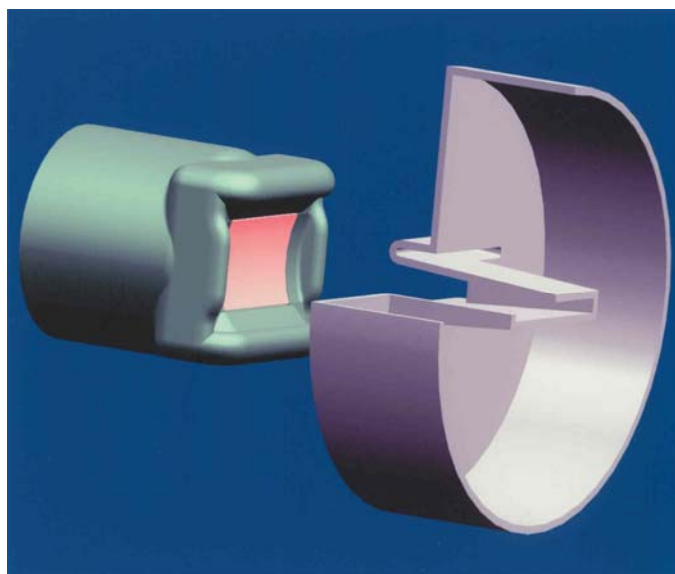


Fig. 51 A sheet beam gun design

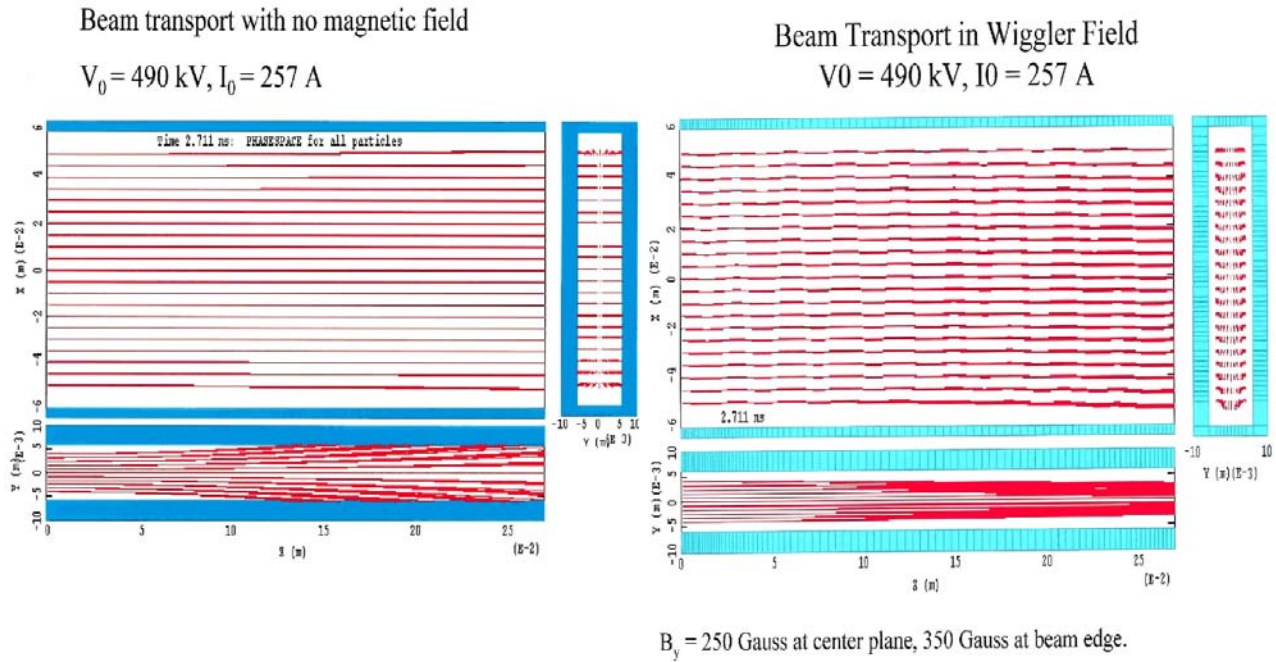


Fig. 52 MAGIC simulation of sheet beam transport

As indicated above, the current density in the sheet beam is quite low. Simulations have shown that a 490-kV, 257A beam artificially launched into the drift tube expands very little laterally, even when no magnetic field is applied (Fig. 52). Furthermore, with a 250-Gauss wiggler field at the center and 350 gauss at the beam edges, the beam is well confined.

The SBK overmoding problem manifests itself with the formation of mode “forests” for one, three and five-cell sheet beam cavities (Fig. 53). Cavity TE and TM modes in the extended interaction waveguide structures are a result of coupling between all structural components—resonant waveguide, matching elements, and guard cavities. (“Guard cavities” are off-frequency cavities added at the two ends of an extended interaction cavity to prevent field spreading into the drift tube and to improve the coupling coefficient). The waveguide TE modes are seen by the beam as TM modes, which velocity-modulate the beam. The operating frequency is 11.4 GHz and the desired mode is the TE_{01} ($N=0$). All TM drift-tube modes below 11.4 GHz are cut off in the drift-tube; TE cavity modes, if converted to TE drift tube modes by a displacement in z of symmetrical components, can propagate in the drift tube but do not readily couple to the beam. Note that in every one of the three cases simulated above, mode-free 100-MHz bands were achieved on either side of the operating frequency. This is the bandwidth required in the NLC for phase switching in pulse-compression.

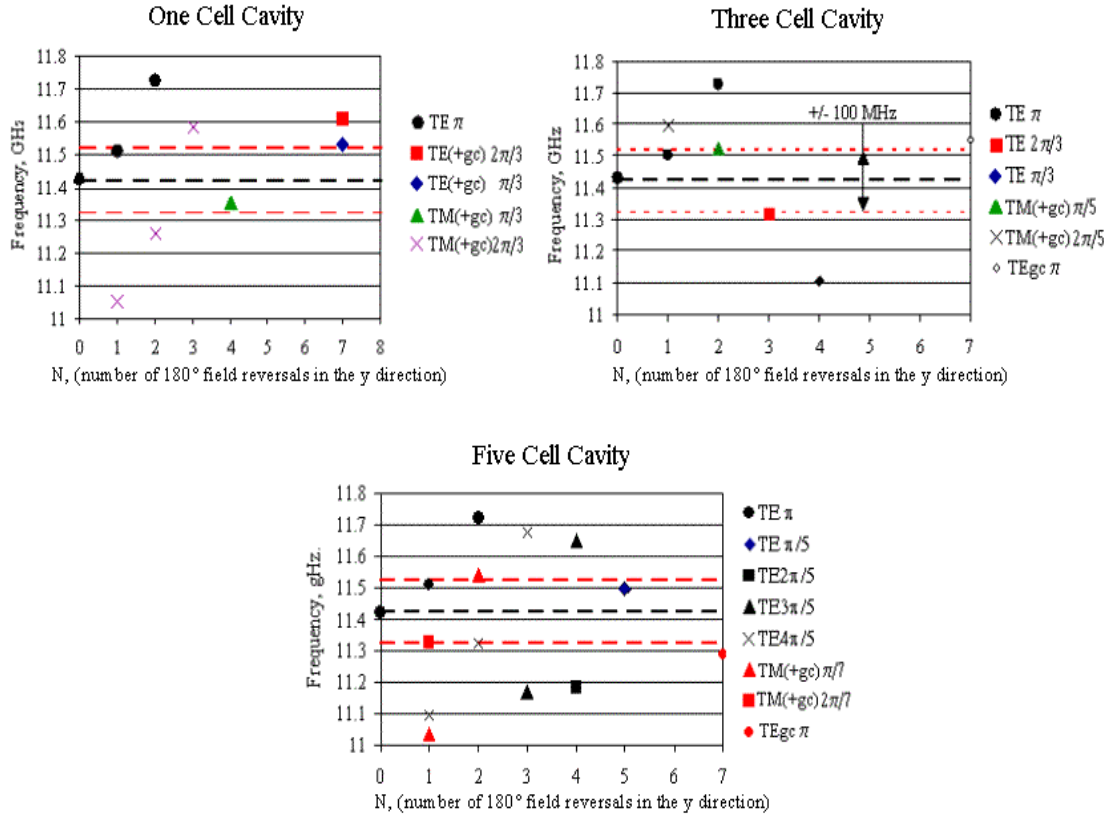
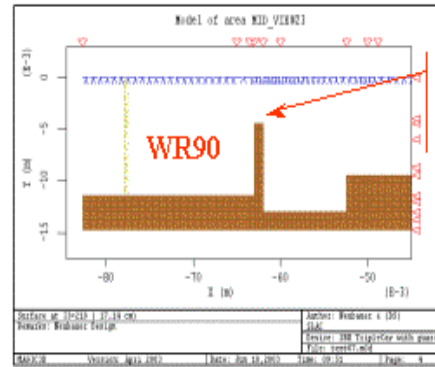
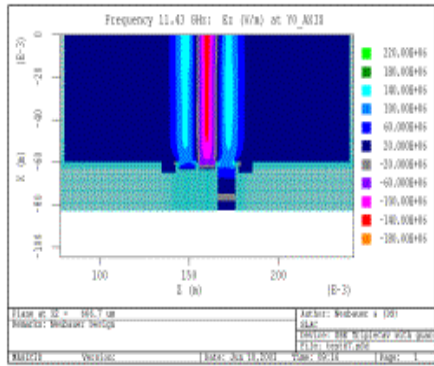


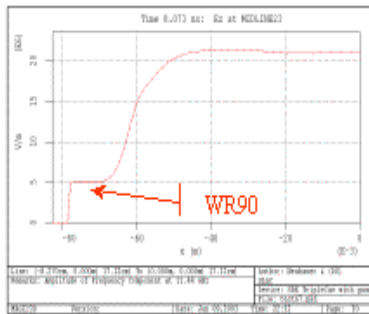
Fig. 53 Mode “forests” for one, three, and 5-cell cavities

It is important in general to obtain agreement between the analytical formulae in Mathcad and MAGIC PIC simulations. For the SBK studies, G_b was calculated from a MAGIC simulation, and used subsequently to “plug” the reduction factor $R (= \beta_e / \beta_q)$ so that the MAGIC-simulated G_b agreed with the G_b calculated from Eq. (130). The reduction factor R calculated from Eq. (103) is 25% lower than the MAGIC calculation. That, of course, is not a satisfactory process and the issue will be settled when MAGIC 3-D simulations are refined further. To obtain G_b from MAGIC and subsequently Q_b , an eigenmode solution was done in MAGIC, with a port plane in the WR90 waveguide external load to the cavity (Fig. 54). That plane acted as a magnetic field boundary during the simulation. A $Q_0=6897$ was determined in the above example, and the fields saved for the next calculation. This consisted of loading the cavity with the eigenmode field solutions and allowing the fields to decay through the external waveguide, with the port plane set for zero reflections. From the time constant, a $Q_{ext}=550$ was determined. In a third step, the previous calculation was repeated with the beam present. A $Q_t=327$ was then determined. Those Q 's were then used to calculate a $Q_b=900$.

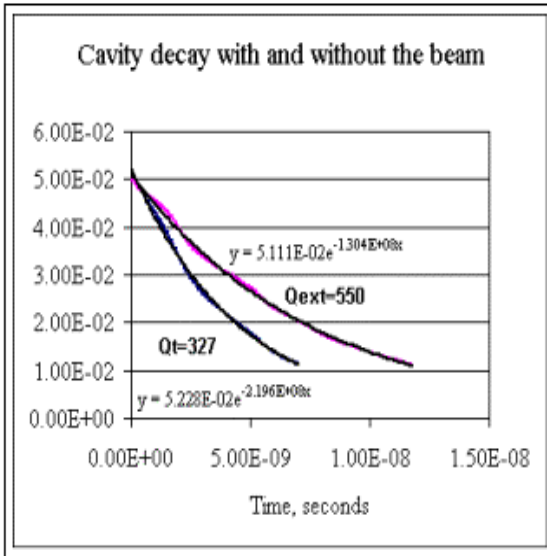


iris

Eigenmode solution with waveguide port plane ($v_p=0$): 11.4264 GHz, $Q_0=6897$



Ez in cell 3 @ 8ns without beam



$$\frac{1}{Q_b} = \frac{1}{Q_r} - \frac{1}{Q_o} - \frac{1}{Q_{ext}}$$

$$Q_b = 900$$

Fig. 54 Calculation of Q_b

Figure 55 shows a small-signal 3-D MAGIC simulation of the three-cavity front end of an SBK (Fig. 50), using a 256A artificial beam in a strong, straight magnetic field. The input cavity was loaded to $Q_{ext}=150$, and the two gain cavities were loaded to 1200 and centered at the operating frequency. An input signal of 1 kW was applied to the input waveguide of the first cavity. The RF current in the beam was shown to grow to about 25A after the 3rd cavity. The fields in third cavity represented an overall power gain of about 30 db. A Mathcad calculation of the same SBK section (Fig. 56) predicts a comparable (32.3 dB) gain with the same parameters, if the length l_{mn} between cavities entered in Mathcad is taken as the length from the end of one interaction region to the beginning of the second interaction region, and the extended cavities was thus located at single points. In the Mathcad model the extended interaction region's parameters, (R/Q and M) were averaged over a beam cross-section.

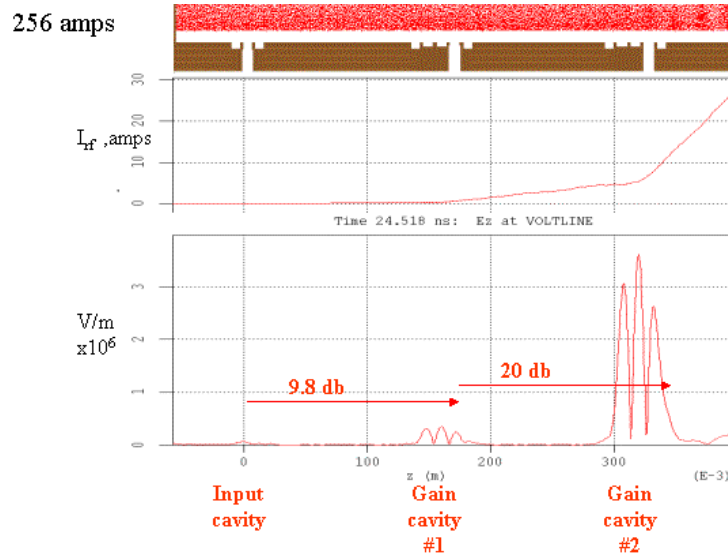
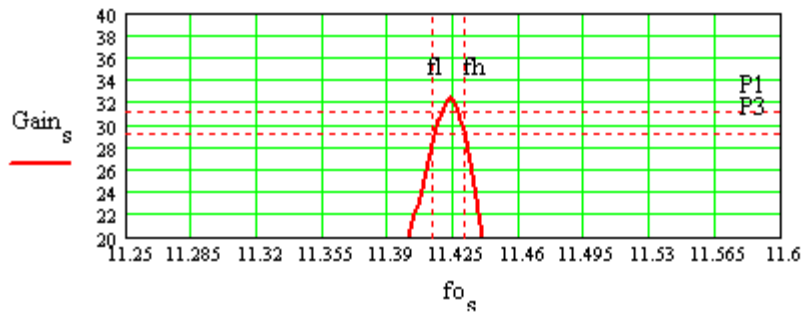


Fig. 55 Simulation of RF current and small-signal gain



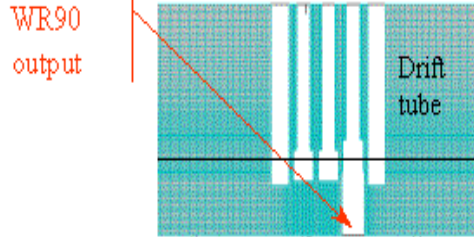
External Q and Q _o	Cavity Frequency (GHz)	Gap-Gap L (m)	$\beta_{q1} = \begin{bmatrix} 0 \\ 28.029 \\ 23.357 \end{bmatrix}$
$Qe_1 \approx 150$	$f_1 \approx 11.424$	$l_1 \approx 0$	
$Qe_2 \approx 1200$	$f_2 \approx 11.424$	$l_2 \approx .12$	
$Qe_3 \approx 1200$	$f_3 \approx 11.424$	$l_3 \approx 0.1$	

Fig. 56 Mathcad calculation of small-signal gain

As a proof-of-principle of SBK potential efficiency, a pre-bunched beam was simulated using MAGIC with $I_1/I_0=1.8$ exciting a five-cell output cavity. The cavity was loaded to a Q_{ext} of 163, which is close to the value required by the empirical formula. The efficiency predicted was 40% (Fig. 57).

Desired Q_{ext} for single cell output in
3-cell cavity

$$Q_{\text{ext}} = \frac{V_{\text{a}}}{\frac{R}{Q} M^2 I_{\text{r}}} = \frac{490000}{18.24 \cdot 66^2 \cdot 1.8} = 133$$



$P_0 = 50 \text{ MW} @ I_{\text{RF}}/I_0 = 1.8$
with $Q_{\text{ext}} = 163$
for 40% eff.

Pseudo bunches

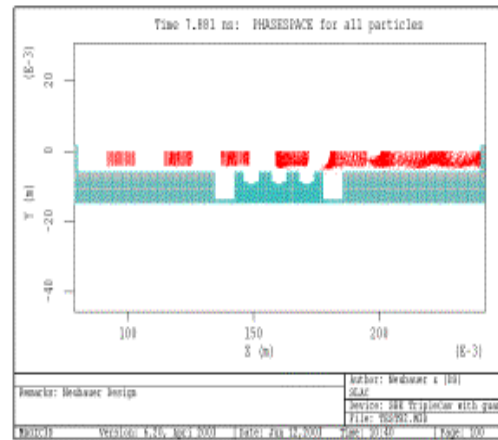
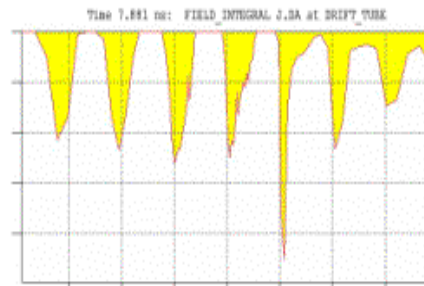


Fig. 57 Large-signal simulation with pre-bunched beam

In order to obtain a preliminary frequency response for the six-cavity SBK, cavities with one, three, and five cells were simulated with the GdfidL code and their R/Q and M parameters were calculated by averaging over the beam cross-section (Fig. 58). The Q_{b} s were determined independently from MAGIC runs as above. The results were fed into a small signal Mathcad calculation using an overall length for the SBK of about 75 cm (plus the length of the interaction regions). The small-signal gain was found by Mathcad to be about 42.7 dB (Fig. 59).

SHEET BEAM PLUG-COMPATIBLE KLYSTRON
(COUPLING COEFFICIENTS & BEAM LOADING OBTAINED DIRECTLY FROM SIMULATIONS)

$\beta_{cq} = 4077$ From MAGIC Qb calculations

$V_0 = 490000$	Beam Voltage (V)	$Qb_i := \frac{1}{RQ_i Gb_i}$	$Gb_i := \frac{I_0 \cdot \beta e}{8 \cdot \beta_{cq} \cdot V_0} \cdot \left[\left(M_{minus_i} \right)^2 - \left(M_{plus_i} \right)^2 \right] \cdot \frac{2}{\sigma \cdot (\sigma + 1)}$
$I_0 = 256$	Beam Current (A)		
$f_0 = 11.424$	Center Frequency (GHz)		
$W = 0.12$	Tunnel width		
$Y = 0.012$	Tunnel height (m)		
$w = 0.1$	Beam width (m)		
$t = 0.008$	Beam thickness (m)		
$P_{out} = 75 \cdot 10^6$	Desired Output Power (W)		

$RQ = \begin{bmatrix} 12.8 \\ 18.24 \\ 18.24 \\ 18.24 \\ 18.24 \\ 25.26 \end{bmatrix}$	i/p	$M = \begin{bmatrix} 0.49 \\ 0.66 \\ 0.66 \\ 0.66 \\ 0.66 \\ 0.7 \end{bmatrix}$	One cell cavity
			Three cell cavities
	o/p		Five cell cavity

R/Q, M, M+, and M- from GdfidL calculations
averaged over the beam cross section

Fig. 58 SBK parameters obtained by simulation for use in Mathcad calculation

Gun Microperveance	$\beta e = 278.437$
$K = 0.746$	$\gamma = 142.139$
	$\gamma \cdot Y = 1.706$

Average Cathode Loading	
$J_{cmax} = 15 \text{ (A/cm}^2\text{)}$	
$Qe_N := \frac{V_0}{RQ_N \cdot \left[\left(\frac{M_N}{M_N} \right)^2 \cdot Irf \right]}$	
$Irf = 1.5$	$Qe_N = 103.094$
$Bbr = 284.982$	

1dB Bandwidth (GHz)	$Bndwth_{db} = 0.141$	
3dB Bandwidth (GHz)	$Bndwth = 0.161$	
		$PPmax = 42.707$

Cavity Rs/Q (Ohms)	External Q and Qo	Cavity Frequency (GHz)	Gap-Gap L (m)			
$Qe_1 = 150$		$f_1 = 11.424$	$L_1 = 0$	$Qt = \begin{bmatrix} 120.723 \\ 241.423 \\ 343.485 \\ 280.059 \\ 466.83 \\ 81.087 \end{bmatrix}$	$Qb = \begin{bmatrix} 1.709 \cdot 10^3 \\ 906.399 \\ 906.399 \\ 906.399 \\ 906.399 \\ 459.32 \end{bmatrix}$	$\beta_{cq} = \begin{bmatrix} 0 \\ 30.365 \\ 30.365 \\ 30.365 \\ 53.722 \\ 23.357 \end{bmatrix}$
$Qe_2 = 500$		$f_2 = 11.353$	$L_2 = 0.13$			
$Qe_3 = 1300$		$f_3 = 11.50$	$L_3 = 0.13$			
$Qe_4 = 700$		$f_4 = 11.455$	$L_4 = 0.13$			
$Qe_5 = \infty$		$f_5 = 11.53$	$L_5 = 0.23$			
$Qe_6 = 100$		$f_6 = 11.424$	$L_6 = 0.10$			

Fig. 59 Mathcad calculation for 6-cavity SBK

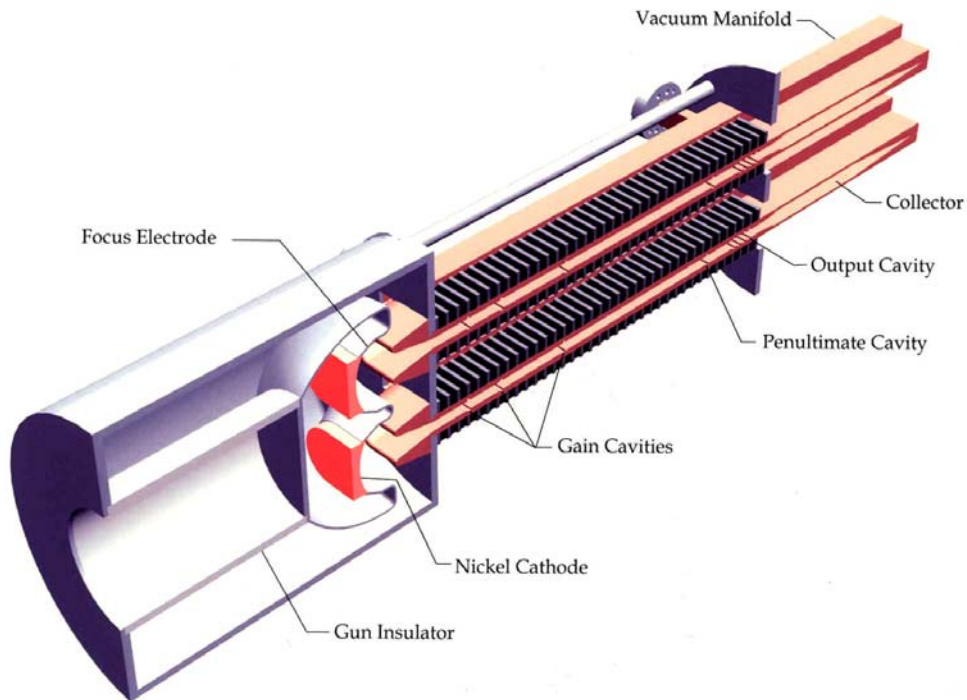


Fig. 60 Conceptual double sheet beam klystron

It should be possible to design a double power SBK, using a single middle rack of magnets. A cartoon of such a 150-MW Double-Sheet Beam klystron is shown in (Fig. 60) above.

Note that the entire RF portion the tube (and the collectors) can be machined from four copper plates, with the cavity circuitry on one side and water-cooling passages on the other. The focusing magnets can be pre-assembled in four (or three) racks and attached to the rest of the tube. This design is obviously entirely preliminary. A great deal of development will be required before this DSBK can be produced, but it is considered that, largely because of the considerable reduction in the number of parts, the production cost of this 150-MW klystron should be lower than a pencil-beam klystron of half that power.

Appendix I:

The Mathcad Small-Signal Code (A. Jensen, C. Wilsen)

Below is a complete description of the code, as it applies to the BFK design. A working 7-page listing is provided as an attachment. It can be followed using the text below. The content of the code is largely self-explanatory, with Mathcad (Version 8 or later) displaying the operational equations in an easily readable format. Key equations used in Mathcad and derived in the main text are numbered as in the text (in blue). The “input file” is located on page 6 of the listing. The following variables, defined in the Mathcad code, should be initialized:

- V_0 – DC beam voltage (V)
- I_0 – DC beam current (A)
- f_0 – operating frequency (GHz)
- a – tunnel radius (m)
- b – beam radius (m)
- $npoints$ – the number of frequency points within the bandwidth
- BW – the bandwidth over which the frequency response is calculated
- N – the number of klystron cavities
The number of rows at the bottom of the page (containing variables RQ , Q_e , Q_o , etc.) should be changed to match this input.
- RQ_n – the cavity R/Q’s
- Q_e_n – the external Q’s (set to ∞ for those cavities with no external coupling)
- Q_o_n – the ohmic Q’s
- f_n – the cavity center frequencies (GHz)
- L_n – the gap-to-gap spacing, from center to center (m)
- d_n – the gap width (m)
- Ma_n – the coupling coefficient at $r = a$

The major elements of the code are now outlined on a page-by-page basis, with reference to the highlighted text equations.

Page 84 of the code defines constants and contains the calculation of some basic quantities, such as the perveance. Some other equations on the first page include the “depressed beam voltage” (voltage at $0.707 * b$, the beam “center of mass”) and the Brillouin field.

Page 85 includes the calculation of the reduced plasma frequency. The method of Branch and Mihran is followed. The variable RI is an initial guess required by the Mathcad solving routine. The value of RI is used in the highlighted equation (100), from which the reduction factor is calculated. The result is in the blue background box. After computing the reduced plasma wavelength, the remainder of the page is devoted to initializing several matrices to be used in the gain calculations that follow.

Page 86 contains calculation of the coupling coefficient, in equation (58), and beam loading, in equation (62).

The calculation of the klystron’s frequency response is critically dependent on the evaluation of the coupling coefficient. There are three possible approaches: The first is to use Eq. (59), which can be done by Mathcad alone and is the quickest approach.

This yields,

$$M = J_0 \left(\frac{\beta_e d}{2} \right) \frac{\sqrt{I_0^2(\gamma_e b) - I_1^2(\gamma_e a)}}{I_0(\gamma_e a)} = 0.8167 \times 0.9345 = 0.7633$$

Another method, which does not rely on the approximation involved in equation (37), is to simulate the cavity field by HFSS or Superfish (Superfish is available at <http://laacg1.lanl.gov/laacg/services/psann.html>), and use equation (29), evaluated at the $r = a$ to calculate $M_a(\beta_e)$. This yields

$$M_a(\beta_e) = 0.8334 \quad \text{and} \quad M = 0.7788$$

Finally, in order to compare the Mathcad calculated result with the AJ-disk simulation (which follows) we use the HFSS or Superfish simulation above and match the E_z field variation with z to the Gaussian assumed by AJ-disk (see below). We then calculate a coupling coefficient at $r = 0.707 * b$ (rather than average it over the beam), which is how AJ-disk evaluates M . This yields, $M = 0.7333$. Since M appears in the gain equation in powers as high as 10, the above 5% spread in the calculation of M produces substantially different frequency responses for the klystron. These are compared in Figure I-1 on page 90.

The beam-loading conductance represents the energy transfer from the cavity to the beam. In Equation (62), this is calculated using the formula for the field in a knife-edge gap as was used to calculate a coupling coefficient. The beam-loaded, Q_b is determined from G_b and the cavity R/Q . An alternative calculation is to use equation (130), which requires that the fast and slow-wave coupling coefficients be calculated by using equation (59) with β_e replaced by $\beta_e \pm \beta_q$, and γ by $\gamma(\beta_e \pm \beta_q) / \beta_e$. In this case, equation (62) of Mathcad is used. This calculation results in a slightly different value for G_b , which makes little difference to the klystron frequency response. Equation (62), however, is important in determining the stability of extended interaction cavities, which must have a positive total Q , when it is calculated as a parallel combination of Q_b , Q_e and Q_0 . A Q_b with a low negative value may lead to a cavity monotron oscillation.

On Page 87 is the definition of the gap impedance: the highlighted equation (142). The definition of the total klystron transconductance is shown in Equation (140). Finally, the klystron power gain is computed in the highlighted Eq. (147).

Page 88 includes curves of the gain response at each cavity, allowing the evolution of the klystron gain to be monitored. The remainder of this page is programming to determine 1-dB and 3-dB bandwidths.

The input fields on Page 89 have been discussed previously and are highlighted in green. Equation (157), which is highlighted in yellow, is an empirical expression for the desired Q_e of the output cavity. If the reader wishes to use the optimal Q_e value, the second column of the cavity inputs at the bottom of the page should be modified. The blue fields contain the maximum gain, the gain at the center frequency, and the 3 dB bandwidth. The 1 dB bandwidth is also calculated.

The program concludes with a listing of beam-loading conductance (ohms), beam-loaded Q , gap location (m), total coupling coefficient, the reduced gap-to-gap transit angle (degrees), the gap transit angle (radians), and the unloaded Q (Q_e in parallel with Q_0) on Page 90.

+

Appendix I: The MathCAD Small-Signal Code (A. Jensen, C. Wilsen)

ORIGIN = 1

(MathCAD Version 8 or Later)

Define Constants:

$$c := 2.997925 \cdot 10^8$$

$$m_e := 9.109 \cdot 10^{-31}$$

$$e := 1.602 \cdot 10^{-19}$$

$$\epsilon_0 := 8.8541878 \cdot 10^{-12}$$

Speed of Light**Electron Rest Mass****Electron Charge****Permittivity of Free Space****Initialize Variables:**

$$\eta := \frac{e}{m_e}$$

Electron Charge to Mass Ratio

$$\eta = 1.759 \times 10^{11}$$

$$J_0 := \frac{I_0}{\pi \cdot b^2}$$

Beam Current Density (A/m²)

$$J_0 = 1.483 \times 10^4 \quad \text{A/m}^2$$

$$J_{\text{beam}} := \frac{J_0}{100^2}$$

Beam Current Density (A/cm²)

$$J_{\text{beam}} = 1.483 \quad \text{A/cm}^2$$

$$K_{\text{w}} := \frac{I_0}{V_0^{1.5}} \cdot 10^6$$

Microperveance

$$K = 1.004$$

$$V_d := .0304 \cdot V_0 \cdot K \cdot \left(\frac{1}{4} + \ln \left(\frac{a}{b} \right) \right)$$

**Potential Beam Depression
(@ r = 0.707 * b)**

$$V_d = 1722.394$$

$$V_{od} := V_0 - V_d$$

Depressed Beam Potential

$$V_{od} = 8.1278 \times 10^4$$

$$G_0 := \frac{I_0}{V_{od}}$$

(Depressed) Beam Admittance

$$G_0 = 2.953 \times 10^{-4}$$

$$\sigma := 1 + \frac{V_{od}}{511000}$$

Relativistic Mass Factor

$$\sigma = 1.159$$

$$v_{on} := \frac{1}{\sigma} \cdot \sqrt{\sigma^2 - 1}$$

**v/c for a Relativistic Particle
with Potential Depression**

$$v_{on} = 0.506$$

$$\beta_e := \frac{2 \cdot \pi \cdot f_0 \cdot 10^9}{v_{on} \cdot c}$$

Electron propagation constant

$$\beta_e = 19.732$$

$$\gamma := \beta_e \cdot \sqrt{1 - v_{on}^2}$$

Radial propagation constant

$$\gamma = 17.024$$

$$B_{br} := 8.304 \cdot \frac{I_0^{.5}}{(b \cdot V_{od}^{.25})} \cdot \left[\frac{2}{(1 + \sigma)} \right]^{.25}$$

Brillouin Flux (Gauss)

$$B_{br} = 104.128$$

MCAD pg 1

----- PLASMA REDUCTION FACTORS -----

Calculation of the Plasma Reduction Factor, R, for the Pencil Beam Geometry, Using the Method of Branch and Mihan.

$$\gamma_b := \gamma \cdot b \quad \gamma_b = 0.386$$

$$\gamma_a := \gamma \cdot a \quad \gamma_a = 0.594$$

Plasma Frequency $\omega_p := \sqrt{\eta \cdot \frac{J_0}{\epsilon_0 \cdot \nu_{on} \cdot c} \cdot \left(\frac{1}{\sigma} \cdot 1.5 \right)}$ $\beta_p := \frac{\omega_p}{\nu_{on} \cdot c}$ $\lambda_p := 2 \cdot \frac{\pi}{\beta_p}$

As a First Estimate of R, Use: $R1 := \sqrt{1 - 2 \cdot I1(\gamma_b) \cdot K1(\gamma_b) - 2 \cdot \frac{K0(\gamma_a)}{I0(\gamma_a)} \cdot I1(\gamma_b)^2}$ $R1 = 0.219$

$$T_0 := \gamma \cdot \sqrt{\frac{1}{R1^2} - 1} \quad \text{(Initial Guess)}$$

Solve the Transcendental Equation for the Plasma Frequency Reduction Factor, R:

Given

$$T_0 \cdot \frac{J1(T_0 \cdot b)}{J0(T_0 \cdot b)} = \beta_e \cdot \frac{K0(\beta_e \cdot a) \cdot I1(\beta_e \cdot b) + K1(\beta_e \cdot b) \cdot I0(\beta_e \cdot a)}{K0(\beta_e \cdot b) \cdot I0(\beta_e \cdot a) - K0(\beta_e \cdot a) \cdot I0(\beta_e \cdot b)} \quad (100) \quad T := \text{Find}(T_0) \quad T = 73.973$$

$$\underline{\underline{R}} := \frac{1}{\sqrt{1 + \left(\frac{T}{\gamma} \right)^2}} \quad \underline{\underline{R}} = 0.224$$

Reduced Plasma Frequency, Propagation Constant, and Wavelength

$$\omega_q := \omega_p \cdot R \quad \beta_q := \frac{\omega_q}{\nu_{on} \cdot c} \quad \lambda_q := \frac{2 \cdot \pi}{\beta_q}$$

$$w := 1..npoints - 1$$

$$i := 1..N \quad j := 1..N - 1$$

$$s := 1..npoints$$

$$n := 1..N \quad \underline{\underline{m}} := 1..N - 1$$

Indices for Calculating Group Delay

Indices for Calculating the Various Drift Lengths

npoints is the Number of Frequency Points to Calculate Within the BW

N is the Number of Klystron Cavities

$$Z_{g_i} := \sum_{i=1}^i L_i$$

Z_g is the Position of the Gap Centers where L is the Gap-to-Gap Spacing

$$l_{m,n} := Z_{g_n} - Z_{g_m}$$

Distance from a Given Gap to all the Others

$$\beta_{q_i} := \left(\beta_q \cdot L_i \cdot \frac{360}{2 \cdot \pi} \right)$$

Gap-to-Gap Transit Angle in Degrees

$$f_{o_s} := f_0 + s \cdot \frac{BW}{npoints} - \frac{BW}{2}$$

Assign Frequencies Symmetrically About the Center Frequency

----- CALCULATE BEAM COUPLING COEFFICIENTS -----

$$M_{\text{bar}} = \sqrt{\frac{I_0(\gamma \cdot b)^2 - I_1(\gamma \cdot b)^2}{I_0(\gamma \cdot a)^2}} \quad (58)$$

Mbar is the radial averaging factor which averages M over the crosssection of the beam.

Total Coupling Coefficient:

$$M_1 := \begin{cases} J_0\left(\frac{\beta e}{2} \cdot d_1\right) \cdot M_{\text{bar}} & \text{if (Switch = 1)} \\ M_{a_1} \cdot M_{\text{bar}} & \text{otherwise} \end{cases} \quad (59)$$

----- CALCULATE BEAM-LOADING CONDUCTANCES -----

Calculate Beam-Loading Conductance Using the Formula for a Knife-Edge Gap with a Hyperbolic Field Distribution:

$$G_{b_1} = \left[\frac{\beta e \cdot d_1}{4} \cdot J_1\left(\frac{\beta e \cdot d_1}{2}\right) \cdot J_0\left(\frac{\beta e \cdot d_1}{2}\right) \cdot M_{\text{bar}}^2 + \frac{1}{2} \cdot J_0\left(\frac{\beta e \cdot d_1}{2}\right) \cdot \left[\gamma \cdot a \cdot \left(\frac{I_1(\gamma \cdot a)}{I_0(\gamma \cdot a)}\right) \cdot M_{\text{bar}}^2 - \frac{I_1(\gamma \cdot b)^2}{I_0(\gamma \cdot a)^2} \right] \right] \cdot \frac{I_0}{V_{od}} \left[\frac{2}{\sigma \cdot (\sigma + 1)} \right] \quad (62)$$

Calculate Q:

$$Q_{b_1} := \frac{1}{RQ_1 \cdot G_{b_1}} \quad Q_{t_1} := \left(\frac{1}{Q_{e_1}} + \frac{1}{Q_{b_1}} + \frac{1}{Q_{o_1}} \right)^{-1} \quad Q_{u_1} := \left(\frac{1}{Q_{e_1}} + \frac{1}{Q_{o_1}} \right)^{-1}$$

Define the Impedance of the nth Gap:

$$Z_{n,s} := \frac{RQ_n}{\frac{1}{Qt_n} + \frac{(f_{o_s})^2 - (f_n)^2}{f_{o_s} \cdot f_n} \cdot i} \quad (142)$$

----- DEFINITION OF THE KLYSTRON SMALL SIGNAL POWER GAIN -----

$$MM_{m,n} := \frac{2}{\sigma \cdot (\sigma + 1)} \cdot M_m \cdot M_n \cdot \sin(\beta q \cdot l_{m,n})$$

Circuit Transconductance:

$$g_{m,n} := -\frac{1}{2} \cdot j \cdot \frac{I_o}{V_{od}} \cdot \frac{2 \cdot \pi \cdot f_o \cdot 10^9}{\omega q} \cdot (MM_{m,n}) \quad (140)$$

Definition of Transconductance: Ratio of the RF Current at the nth Gap to the RF Voltage at the mth Gap which Produced the Modulation.

$$G_{1,s} := 1$$

$$q := 2 \dots N$$

$$Qe_N = 38.900$$

$$RL := RQ_N \cdot Qe_N$$

$$Rgen := RQ_1 \cdot Qe_1$$

$$G_{q,s} := \sum_{j=1}^{q-1} \left[(g_{j,q})_s \cdot Z_{j,s} \cdot G_{j,s} \right]$$

G_{q,s} is the Transfer Function i_q/i_1 at Frequency f_o ,

Calculate the Gain:

$$P_s := (G_{N,s})^2 \cdot 4 \cdot \frac{(Z_{N,s})^2}{Rgen \cdot RL} \quad (147)^*$$

$$G_{dB_s} := 10 \cdot \log(|P_s|)$$

* Note: P_s is the power gain as a function of the frequency point "s". It does not refer to the pole / zero approach for calculating gain.

Find the Maximum Gain, PPmax:

$$P_{test_s} := |P_s|$$

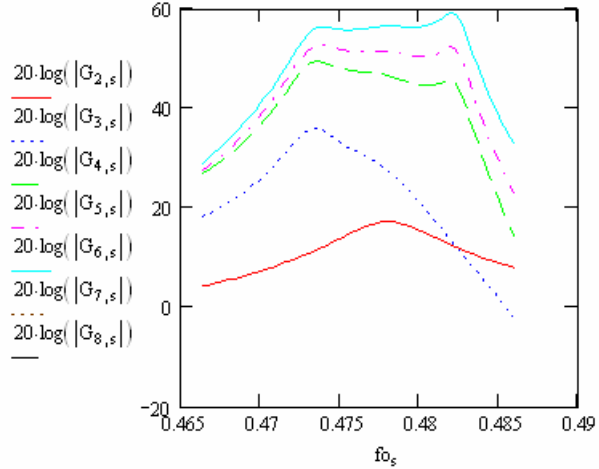
$$PP_{max} := 10 \cdot \log(\max(P_{test}))$$

Find the Gain at the Center Frequency:

$$PP_{f0} := \frac{G_{dB_{npoints}}}{2}$$

Find the Index, s, at Which the Maximum Gain Occurs:

$$sP_{max} := \begin{cases} j \leftarrow 1 \\ \text{while } G_{dB_j} < PP_{max} \\ j \leftarrow j + 1 \end{cases}$$



Find the 3dB Bandwidth and Fractional Bandwidth:

$$f_l := \begin{cases} sP1 \leftarrow sP_{max} \\ \text{while } [G_{dB_{sP1}} \geq (PP_{max} - 3)] \wedge (sP1 > 1) \\ sP1 \leftarrow sP1 - 1 \\ f_l \leftarrow fo_{sP1} \end{cases}$$

$$f_h := \begin{cases} sPh \leftarrow sP_{max} \\ \text{while } [G_{dB_{sPh}} \geq (PP_{max} - 3)] \wedge (sPh < npoints) \\ sPh \leftarrow sPh + 1 \\ f_h \leftarrow fo_{sPh} \end{cases}$$

$$\underline{f_l} := \begin{cases} 0 & \text{if } (f_l = fo_1) \\ f_l & \text{otherwise} \end{cases}$$

$$\underline{f_h} := \begin{cases} 0 & \text{if } (f_h = fo_{npoints}) \\ f_h & \text{otherwise} \end{cases}$$

$$Bndwth := \begin{cases} 0 & \text{if } |f_h - f_l| > BW \\ (f_h - f_l) & \text{otherwise} \end{cases}$$

$$f_{bw3} := (Bndwth) \cdot \frac{100}{f0}$$

Find the 1dB Bandwidth and Fractional Bandwidth:

$$f_{ldb} := \begin{cases} sP1 \leftarrow sP_{max} \\ \text{while } [G_{dB_{sP1}} \geq (PP_{max} - 1)] \wedge (sP1 > 1) \\ sP1 \leftarrow sP1 - 1 \\ f_{ldb} \leftarrow fo_{sP1} \end{cases}$$

$$f_{hdb} := \begin{cases} sPh \leftarrow sP_{max} \\ \text{while } [G_{dB_{sPh}} \geq (PP_{max} - 1)] \wedge (sPh < npoints) \\ sPh \leftarrow sPh + 1 \\ f_{hdb} \leftarrow fo_{sPh} \end{cases}$$

$$\underline{f_{ldb}} := \begin{cases} 0 & \text{if } (f_{ldb} = fo_1) \\ f_{ldb} & \text{otherwise} \end{cases}$$

$$\underline{f_{hdb}} := \begin{cases} 0 & \text{if } (f_{hdb} = fo_{npoints}) \\ f_{hdb} & \text{otherwise} \end{cases}$$

$$Bndwth_{db} := \begin{cases} 0 & \text{if } |f_{hdb} - f_{ldb}| > BW \\ (f_{hdb} - f_{ldb}) & \text{otherwise} \end{cases}$$

$$f_{bw1} := (Bndwth_{db}) \cdot \frac{100}{f0}$$

Calculate the Marker Locations for the 1dB and 3dB Bandwidth Power Levels:

$$P3 := PP_{max} - 3 \quad P1 := PP_{max} - 1$$

B-Factory Klystron

$V_0 \equiv 83000$	Beam Voltage (V)	Number of Data Points	npoints = 60
$I_0 \equiv 24$	Beam Current (A)	Calculation Bandwidth (GHz)	BW = .02
$f_0 \equiv 0.476$	Center Frequency (GHz)	Gain (Max)	PPmax = 53.428 dB
$a \equiv 0.0349$	Tunnel Radius (m)	Gain at Center Frequency	PPf0 = 52.577 dB
$b \equiv 0.0227$	Beam Radius (m)	Plot Markers	f1 = 0.473 f2 = 0.483

Remember to update the shape factor d2 if the fill-factor changes.

$\beta e = 19.732$
 $\beta q = 1.653$
 $\gamma \cdot a = 0.594$

1dB Bandwidth (GHz)	Bndwithdb = 0.002	% BW(1dB)	fbw1 = 0.350
3dB Bandwidth (GHz)	Bndwth = 0.010	% BW(3dB)	fbw3 = 2.171

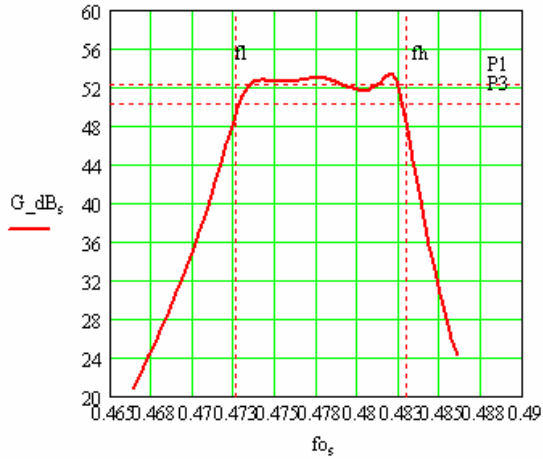
Empirical expression for Q_e of the output cavity - not used in the gain calculation:

$I_{ff} \equiv 1.8$ (157)

$$Q_{eN} := \frac{\frac{V_0}{I_0}}{RQ_N \cdot \left[\frac{2}{\sigma \cdot (\sigma + 1)} \cdot (M_N)^2 \cdot I_{ff} \right]}$$

$Q_{eN} = 33.008$

Number of Klystron Cavities:	$N \equiv 6$
Gun Microperveance ($\mu A/V^{1.5}$)	$K = 1.004$
Brillouin Field (gauss)	$B_{br} = 104.128$
Beam Current Density (A/cm^2)	$J_{beam} = 1.483$
Cathode Current Density (A/cm^2)	$J_{cathode} := 5$
Gun Convergence	$\frac{J_{beam}}{J_{cathode}} = 0.30$



Set "Switch" equal to 1 to use the JO knife edge approximation for Ma. Set "Switch" equal to 0 to use the Ma defined below.

Switch = 0

Cavity Rs/Q (Ohms)	External Q	Qo	Cavity Frequency (GHz)	Gap-Gap L (m)	Gap Length (m)	Coupling Coef. (@ r=a)	Coupling Coef. (Total)
$RQ_1 \equiv 146.8$	$Q_{e1} \equiv 175.5$	$Q_{o1} \equiv 4000$	$f_1 \equiv 0.478$	$L_1 \equiv 0$	$d_1 \equiv 0.0889$	$Ma_1 \equiv 0.8334$	$M = \begin{pmatrix} 0.7788 \\ 0.7783 \\ 0.8823 \\ 0.8819 \\ 0.8846 \\ 0.8854 \end{pmatrix}$
$RQ_2 \equiv 143.4$	$Q_{e2} \equiv \infty$	$Q_{o2} \equiv 4000$	$f_2 \equiv 0.4732$	$L_2 \equiv 0.4445$	$d_2 \equiv 0.0889$	$Ma_2 \equiv 0.8328$	
$RQ_3 \equiv 125.6$	$Q_{e3} \equiv \infty$	$Q_{o3} \equiv 4000$	$f_3 \equiv 0.4823$	$L_3 \equiv 0.4953$	$d_3 \equiv 0.05$	$Ma_3 \equiv 0.9441$	
$RQ_4 \equiv 111.1$	$Q_{e4} \equiv \infty$	$Q_{o4} \equiv 4000$	$f_4 \equiv 0.499$	$L_4 \equiv 0.8788$	$d_4 \equiv 0.05$	$Ma_4 \equiv 0.9437$	
$RQ_5 \equiv 110.3$	$Q_{e5} \equiv \infty$	$Q_{o5} \equiv 4000$	$f_5 \equiv 0.4915$	$L_5 \equiv 0.6096$	$d_5 \equiv 0.05$	$Ma_5 \equiv 0.9466$	
$RQ_6 \equiv 92.91$	$Q_{e6} \equiv 38.9$	$Q_{o6} \equiv 20000$	$f_6 \equiv 0.475856$	$L_6 \equiv 0.254$	$d_6 \equiv 0.05$	$Ma_6 \equiv 0.9474$	

MCAD pg 6

$$G_b = \begin{pmatrix} 3.842 \times 10^{-5} \\ 3.842 \times 10^{-5} \\ 2.344 \times 10^{-5} \\ 2.344 \times 10^{-5} \\ 2.344 \times 10^{-5} \\ 2.344 \times 10^{-5} \end{pmatrix} \quad Q_b = \begin{pmatrix} 177.306 \\ 181.510 \\ 339.713 \\ 384.050 \\ 386.836 \\ 459.240 \end{pmatrix} \quad Z_g = \begin{pmatrix} 0.000 \\ 0.445 \\ 0.940 \\ 1.819 \\ 2.428 \\ 2.682 \end{pmatrix} \quad M = \begin{pmatrix} 0.779 \\ 0.778 \\ 0.882 \\ 0.882 \\ 0.885 \\ 0.885 \end{pmatrix} \quad \beta q_l = \begin{pmatrix} 0.000 \\ 42.093 \\ 46.904 \\ 83.220 \\ 57.727 \\ 24.053 \end{pmatrix} \quad \beta e \cdot d = \begin{pmatrix} 1.754 \\ 1.754 \\ 0.987 \\ 0.987 \\ 0.987 \\ 0.987 \end{pmatrix} \quad Q_u = \begin{pmatrix} 168.124 \\ 4000.000 \\ 4000.000 \\ 4000.000 \\ 4000.000 \\ 38.824 \end{pmatrix}$$

$$Q_t = \begin{pmatrix} 86.296 \\ 173.631 \\ 313.120 \\ 350.407 \\ 352.724 \\ 35.798 \end{pmatrix}$$

MCAD pg 7

BFK (Small Signal)

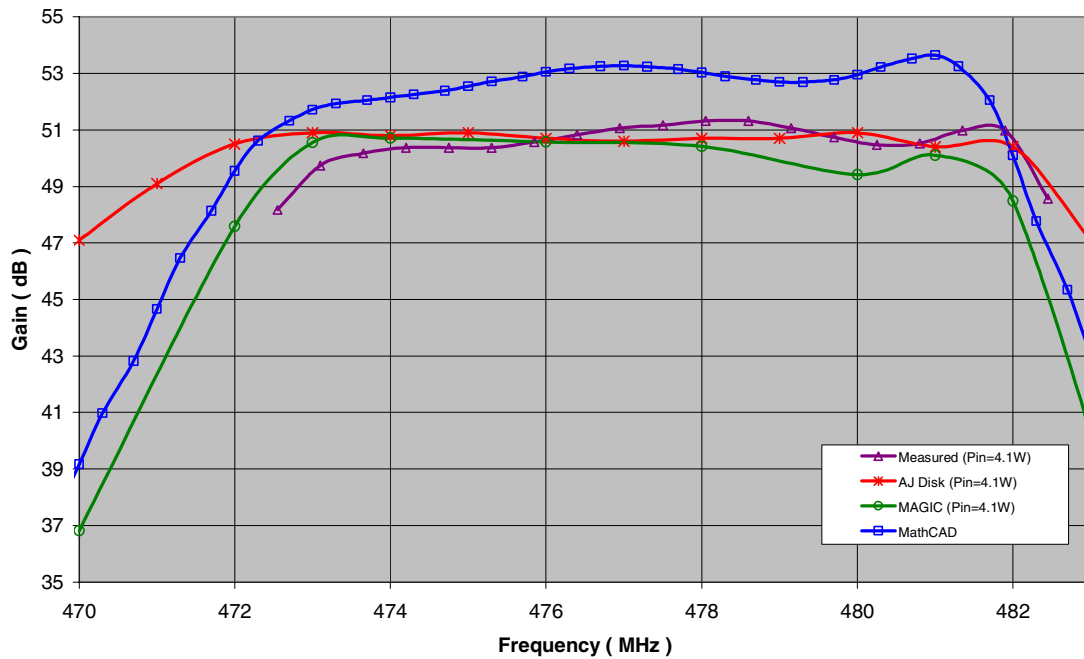


Figure I-1. Small Signal Code Comparison

Appendix II:

The AJ-Disk 1D Code (A. Jensen)

Introduction & User's Guide

The following is an introduction and user's tutorial for AJ Disk. Each step necessary to open AJ Disk and simulate a klystron will be discussed in detail.

- To get started, first, double click on the AJ Disk executable in the CD.
- Next, select "file" from AJ Disk's menu, and from within the "file" menu select "open." Now, select the BFK.dsk file and press the "open" button. AJ Disk should now display the window shown in Figure II-1.

Open / Update *.dsk...

Project Title: Author:

Vo (kV) Io (A) f (MHz) f (Carrier)

Drift Tube Radius (m) Beam Radius (m) Beta Pin (W)

Disks # Steps Max Iter. # Cavities Delta Frequency k DELTA^2

Cavity Frequency

Cavity:	1	2	3	4	5	6	7	8	9	10
Type	1	1	1	2	1	1	-1	0	0	0
Qe	175.50	9368.00	9434.00	5249.00	9388.00	9323.00	38.90	0.00	0.00	0.00
Qo	4000.00	4000.00	4000.00	4000.00	4000.00	4000.00	20000.0	0.00	0.00	0.00
R/Q	146.800	143.400	125.600	67.610	111.100	110.300	92.910	0.000	0.000	0.000
d (m)	0.08890	0.08890	0.05000	0.01840	0.05000	0.05000	0.05000	0.00000	0.00000	0.00000
z (m)	0.0000	0.4445	0.9398	1.2725	1.8186	2.4282	2.6822	0.0000	0.0000	0.0000
CAVF	478.000	473.200	482.300	938.813	499.000	491.500	475.856	0.000	0.000	0.000
k	17.918	17.888	27.456	37.101	27.535	27.058	26.900	0.000	0.000	0.000

Save as *.plt file:

Save as *.out file:

Save as *.dsk file:

Figure II-1 AJ Disk's Input Deck

The input parameters seen in Figure II-1 are for the B-Factory klystron. Now, click the “OK” button. At the top of the window a number is counting upwards. This number represents the number of iterations (the number of times a set of disks has been sent through the klystron in an attempt for cavity voltage convergence). AJ Disk should now display a plot similar to that shown in Figure II-2.

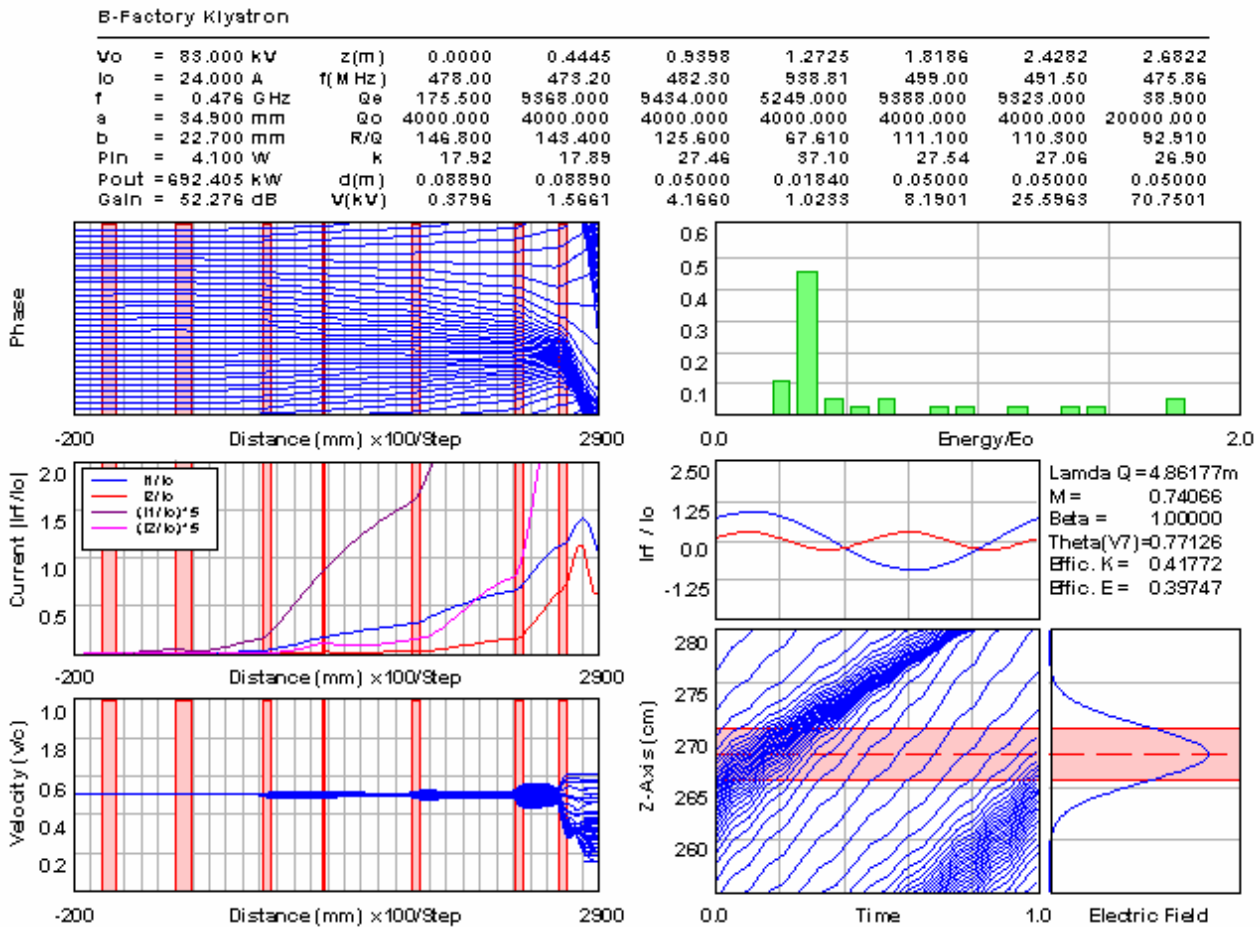


Figure II-2 AJ Disk's Simulation Results

Figure II-2 can be broken down and described section by section as follows:

- Text Block: The text block at the top of Figure II-2 shows what the user input as well as some of the numeric results of the simulation, such as, gain, cavity voltage, and output power.
- Phase Diagram: Shows the disks in one period and how their phase changes as a function of axial distance.
- Current Diagram: Shows the fundamental and second harmonic components of the beam current as a function of axial distance.
- Velocity Diagram: Shows the velocity spread as a function of axial distance.
- Energy Distribution: The energy distribution of the spent beam.
- I_{rf}/I_0 Diagram: The fundamental and second harmonic of the induced current at the output cavity as a function of time.
- Electric Field Diagram: The approximated Gaussian distribution of the electric field at the output gap.
- Applegate Chart: Disk position as a function of time in the vicinity of the output cavity.

Figure II-2 is the primary display used for analyzing the results of each simulation. The next step is to further explore AJ Disk and how it works:

- Select “view” from the menu. From within this menu select “plots.” Select “current.” This same procedure may be used to view the velocity and phase diagrams as well. AJ Disk should be displaying something similar to Figure II-3. This is a good way to view the plots in greater detail.

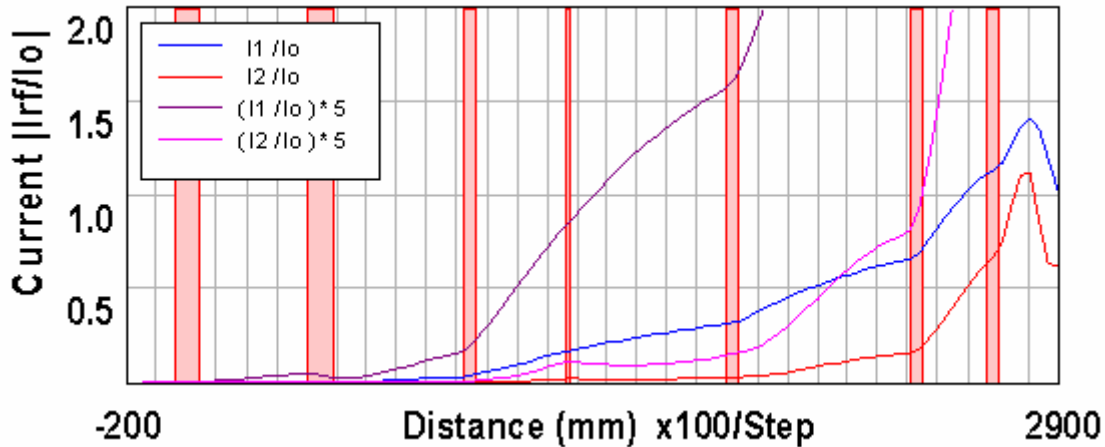


Figure II-3. A Larger Version of the Current Diagram

- Next, close the window containing the current diagram.
- Select “update” from the “file” menu. AJ Disk should now be displaying a window similar to Figure II-1, again. Using, the “update” option allows the user to update input variables from the last simulation without actually saving the changes to the original file.

At this point it is appropriate to discuss the inputs used in Figure II-1. Following is a line by line discussion:

- The 1st line contains the project’s title and the author’s name.
- The 2nd line contains,

Vo (kV)	- the beam voltage in kV
Io (A)	- the beam current in Amps
f (MHz)	- the drive frequency in MHz
f (Carrier)	- this variable is no longer used (set to zero)
- The 3rd line contains,

Drift Tube Radius (m)	- the radius of the drift tube in meters
Beam Radius (m)	- the radius of the beam in meters
Beta	- the radial coupling coefficient (set to one)
Pin (W)	- the drive power in watts
- The 4th line contains,

# Disks	- the number of disks
# Steps	- the number of integration steps per RF cycle
Max Iter.	- the maximum number of iterations
# Cavities	- the number of klystron cavities
- The 5th line contains the cavity type which is,

1 for fundamental mode cavities
 2 for 2nd harmonic cavities
 -1 for output cavities
 0 for unused cavities

- The 6th line contains the Qe's (the external Q's)
- The 7th line contains the Qo's (the ohmic Q's)
- The 8th line contains the R/Q's
- The 9th line contains the gap widths in meters, d (m)
- The 10th line contains the distances of the cavities from the input gap in meters, z (m), and is measured from gap center to gap center.
- The 11th line contains the cavity frequencies, if "Cavity Frequency" has been selected or cavity detuning from the drive frequency if "Delta Frequency" has been selected.
- The 12th line contains the parameter "k," which determines the shape of the electric field distribution across the klystron gap, according to the following Gaussian equation,

$$f(z) = \frac{k}{\sqrt{\pi}} e^{-k^2(z-z_{center})^2}$$

Where, f(z), represents a normalized field shape as a function of z. In practice, k has been found by using a program called SUPERFISH (use SF7) to simulate the field at 0.707 times the beam radius (one method of averaging). SUPERFISH may be downloaded at <http://laacg1.lanl.gov/laacg/services/psann.html> (the use of SUPERFISH and SF7 is briefly discussed in appendix IV). The field can then be loaded into AJ disk by selecting the "import Gaussian k" button as shown in Figure II-1. AJ disk will prompt the user for the center of the cavity (if the cavity is symmetric then only half of the cavity can be simulated and the center can then be input as zero). AJ Disk will then supply a value for "k" which can be used in line 12 of Figure II-1.

The last topic to cover is the concept of sweeping data. AJ Disk can sweep gain as a function of frequency or power out as a function of power in. In the following exercise gain will be swept as a function of frequency.

- First, select "sweep data" from Figure II-1.
- Next, enter values for start, stop, and step. For the BFK example the starting frequency will be 470, the stopping frequency is 484, and the step is 1. This tells AJ Disk to sweep from 470MHz to 484MHz and to sample the gain at every 1MHz step.
- Press "OK." The simulation may take a few moments since it must simulate the klystron at several different frequencies.
- Once the simulation is complete, select "view>>plots>>sweep" to see the results of the sweep. The result is shown in Figure II-4.

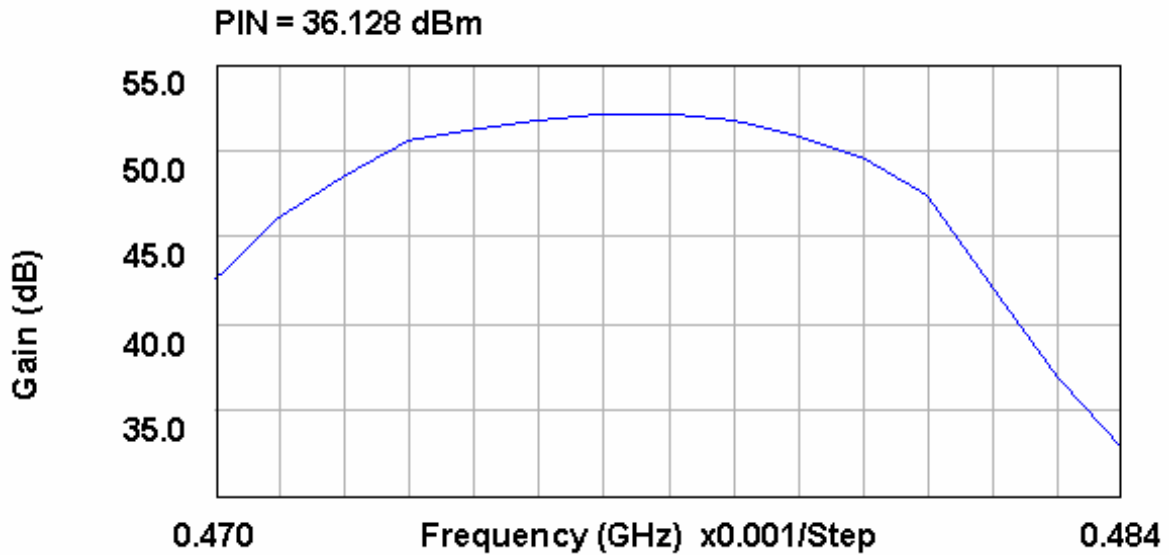


Figure II-4 Frequency Sweep of the B-Factory Klystron

The main features of AJ Disk have now been covered. However, on a final note, to save a file, use the checkboxes in the lower left hand corner of Figure II-1. *.dsk corresponds to the input file, *.plt corresponds to the output file with all the plotted data, and *.out corresponds to a file which contains data about the simulation. These boxes must be checked prior to simulation for a file to be saved.

The AJ Disk Algorithm

The algorithm for AJ Disk is fundamentally simple. To show this, AJ Disk, in its simplest form, can be broken into the following procedures:

- 1) Prompt the user for input.
- 2) Initialize data such as beam loading, gap impedance, etc.
- 3) Calculate the input gap voltage based on the desired input power.
- 4) Set all other cavity voltages close to zero.

After the first four steps, AJ Disk is ready to move the beam through the tunnel. To do this the electron beam is sliced into a set of charged disks. The motion of each disk is governed by the space charge from other disks and/or the electric field associated with each cavity.

The equations for these fields are:

$$E_s = -\frac{q_{disk}}{\pi \cdot b^2 \cdot 2 \cdot \epsilon_0} \cdot \sum_{d=0}^{N_{disk}} \sum_{i=0}^{\infty} 4 \cdot \left[\frac{J_1(\mu_i \cdot b/a)}{\mu_i \cdot J_1(\mu_i)} \right]^2 e^{\left(\frac{-\mu_i \cdot |z-z_0|}{r^a} \right)} \cdot sign(z - z_0)$$

$$E_c = |V_n| \cdot f(z) \cdot \cos(2 \cdot \pi \cdot f \cdot t + \theta)$$

where E_s is the space-charge field from all the other disks and E_c is the circuit field associated with a cavity. It should also be noted that μ_i is the i^{th} zero of the J_0 Bessel function and γ is the radial propagation constant.

The space-charge field can be broken down. The first part of the equation before the summation corresponds to the magnitude of the space-charge electric field at the location of the disk (the maximum value). The second summation, simply corresponds to an exponential decay with axial distance (the magnitude is equal to one at the location of the present disk). The first summation just sums the fields from all the other disks. For further discussion see Rowe³⁹. The cavity field is much simpler to understand. The field is described by multiplying the gap voltage by the shape of the field and by an oscillating term. The field oscillation is represented by the cosine term and the field shape is given by the Gaussian approximation:

$$f(z) = \frac{k}{\sqrt{\pi}} e^{-k^2(z-z_{center})^2}$$

where k can be found as described in the previous section.

Next, returning to the algorithm:

- 5) Evaluate the equation of motion based on the field $E = E_s + E_c$
- 6) Calculate the induced current for each cavity,

$$I_{ind} = \int_{-\infty}^{\infty} \rho \cdot v \cdot f(z) \cdot dz$$

where ρ is the one dimensional charge density, v is the velocity found in step 5 and $f(z)$ is used to represent coupling.

- 7) Calculate the fundamental component of the induced current using a Fourier expansion and the induced current from step 6.
- 8) Calculate the induced voltage in each cavity, where the induced voltage is the gap impedance times the fundamental component of the induced current.
- 9) Repeat steps 5 through 8 until the resulting voltage from the last iteration is the voltage from the present iteration to within some predefined percentage error.
- 10) Calculate gain & efficiency.

The kinetic efficiency is:

$$\eta_k = 1 - \frac{\sum_{d=0}^{N_{disk}} \left(1 - \left(\frac{v_{exit,d}}{c} \right)^2 \right)^{-1/2} - 1}{\sum_{d=0}^{N_{disk}} \left(1 - \left(\frac{v_{inlet,d}}{c} \right)^2 \right)^{-1/2} - 1}$$

where v_{exit} is the velocity at the end of the output region and v_{inlet} is the velocity at the beginning of the output region. A simple way to look at this equation, is to break it down, into the form $(KE_{\text{inlet}} - KE_{\text{outlet}})/KE_{\text{inlet}}$.

The electronic efficiency is:

$$\eta_e = \text{real} \left\{ \frac{V_N \cdot I_{\text{ind},N}^*}{2 \cdot V_0 \cdot I_0} \right\}$$

where N refers to the output cavity and * denotes the complex conjugate. This equation finds the percentage of the beam power which is converted to RF power in the output gap.

11) The final step is to display the results.

Appendix III.

Magic 2D Simulation of the B-Factory Klystron (L. Ludeking, D. Smithe)

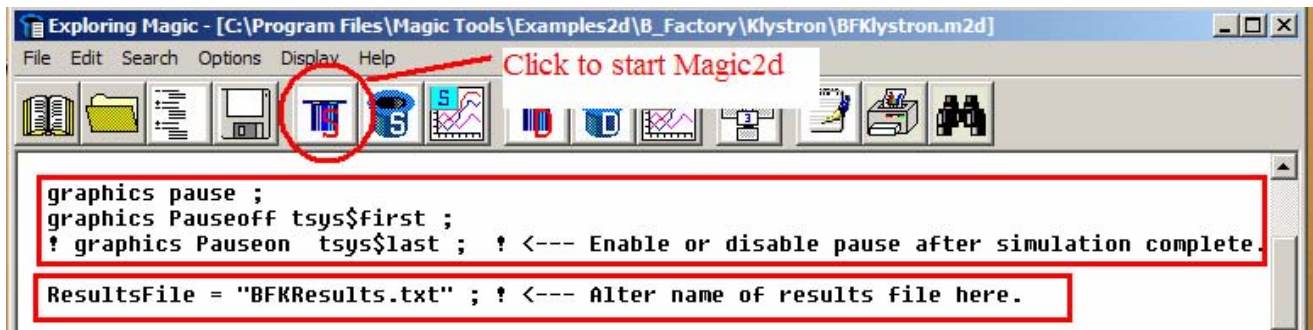
To begin double click on MugSetupDemo.exe in the CD to install Magic on your computer. MugSetupDemo.exe and associated files are also available for download at <http://www.mrcwdc.com/Magic/toolsuite.html>. Some users may also need to place the two *.dll files from the CD into the directory "C:\Program Files\Magic Tools" for Magic to operate.

Once the Magic Tool Suite is installed open Mugman.exe as follows:

- Begin with the Windows START menu button,
- Select the PROGRAMS menu,
- Select the Magic Tool Suit folder,
- Click on "Mugman.exe"

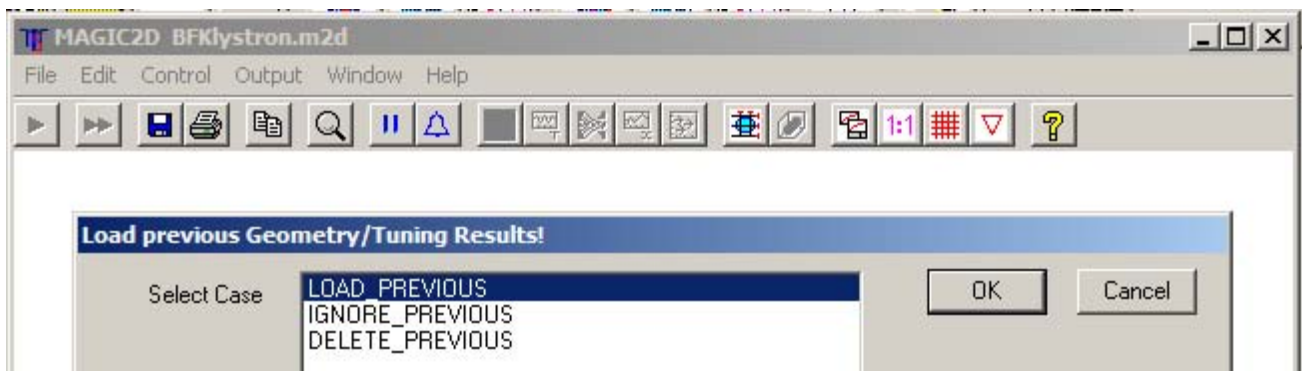
The magic start file for the klystron template is located on the CD under the name BFKlystron.m2d.

Open this file with MUGMAN. You should see a screen that looks like the following,



This file includes the user modifiable input and tuning parameters. Once these are set the file calls the internal coded klystron template embedded in MAGIC2D. This document indicates the procedure and order in which the various tuning parameters should be used. *You do not need modify any of this text file.* This file and the template are setup to allow you to interactively respond to several screens to select the type of simulation and modify elements of the klystron geometry.

Click on the Magic2d Button to start the template. The next screen that looks like this,



The Magic klystron template automatically saves the results from each run in a results file with the name “BFKResults.txt.” By default it reloads this file. The previous results file contains a record of all the parameters used for each run in sequence. Thus all changes (and pertinent results) are recorded in this file. You may delete this file (or change its name in the template text file, see first figure) when you are starting a new design sequence. If this is your first time through then you may choose any of the three options. Otherwise select “IGNORE_PREVIOUS” to ignore the results from the last run or “DELETE_PREVIOUS” to permanently delete the results from the last run.

The next screen allows you to review various elements of the cavity definitions,



At this point the demo will branch in one of four possible directions. Each of these possibilities will be discussed one a time. Once you have selected an option, read through the associated text and then skip ahead to the dialog box which allows you to choose between HOT_TEST, COLD_TEST, and EIGENMODE_TEST.

SKIP_GEOMETRY_REVIEW

Normally, once the geometry and resolution have been set this option should be selected to skip directly to the main simulation. If you have selected this option you may now proceed to the dialog box labeled, “select simulation type.”

SET_RESOLUTION

Selecting any of the geometry options, including “SET_RESOLUTION,” leads to the following screen,



This screen allows you to select a spatial mesh resolution. The default is “STANDARD,” this is the value used for the best results. It is also the most costly of computer time and resources. Using the “VERYCOARSE” setting allows you run individual cold tests in about a minute each. And the hot test will typically take about 90 minutes on a 2 GHZ PC. In the “VERYCOARSE” setting, the frequency tuning has a greater discretization error because of the larger cells. At this point select “VERYCOARSE” for a quick simulation. You may now proceed to the dialog box labeled, “select simulation type.”

BASE_GEOMETRY_REVIEW

“SET_RESOLUTION” will automatically be chosen for you before proceeding to the “BASE_GEOMETRY_REVIEW.”

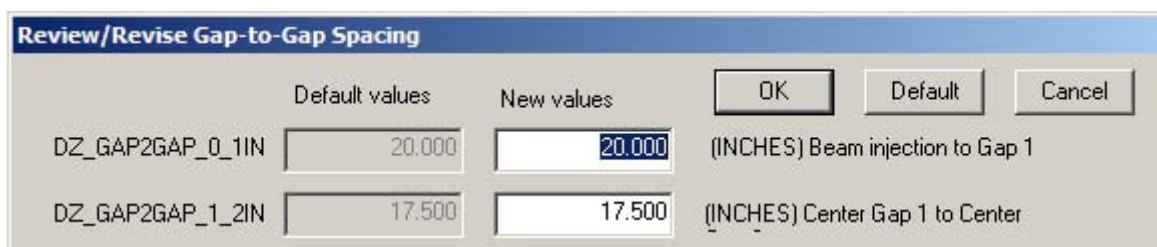
“BASE_GEOMETRY_REVIEW” allows you to review and change the geometry. Once the geometry is set the first time, you need not repeat this for the individual cavity tuning. There will be a sequence of screens that go through the various design elements. They will look like the following:

The first screen is not geometry, but the selection of cavity design frequencies.



The next set of screens allows you to set the cavity gaps and the gap-to-gap spacing.





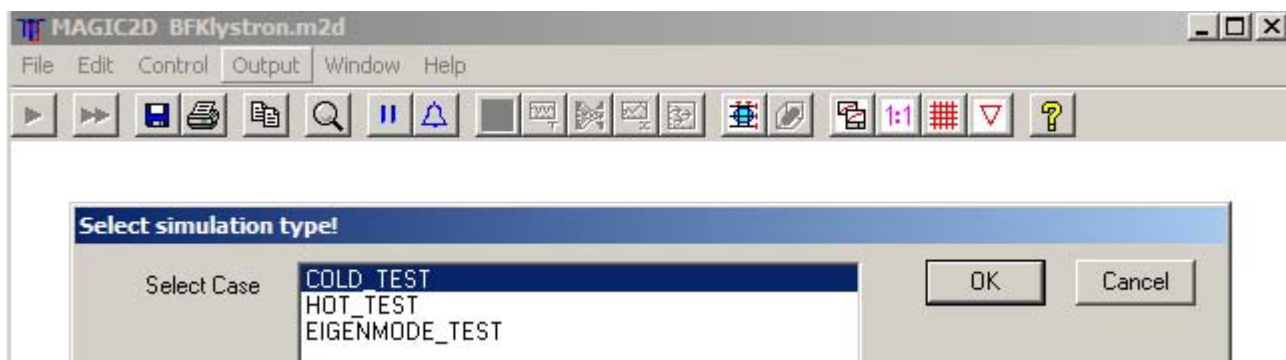
COMPLETE_GEOMETRY_REVIEW

“SET_RESOLUTION” will automatically be chosen for you before proceeding to the “BASE_GEOMETRY_REVIEW.”

In this option you will go through the same steps as the “BASE_GEOMETRY_REVIEW” but there will also be additional screens for cavity radius, tube radius, and the shape for the gap edges.

The “Select simulation type” Dialog Box

At this point the review/geometry portion of the demo has been completed and the simulation type must be selected.



This screen allows you select the type of simulation that you will be running. There are three choices.

They are:

1. COLD_TEST – in which you test the geometry and tuning effects on the frequency, Q, and R/Q of individual cavities.
2. HOT_TEST – in which you run all the finalized geometry settings, and select a hot test set of parameters. The primary output from these runs will be the measurement of gain.
3. EIGENMODE_TEST – in which you can examine the field structure after solving for an eigenmode. This would normally be used after a major geometry revision to identify the base frequency.

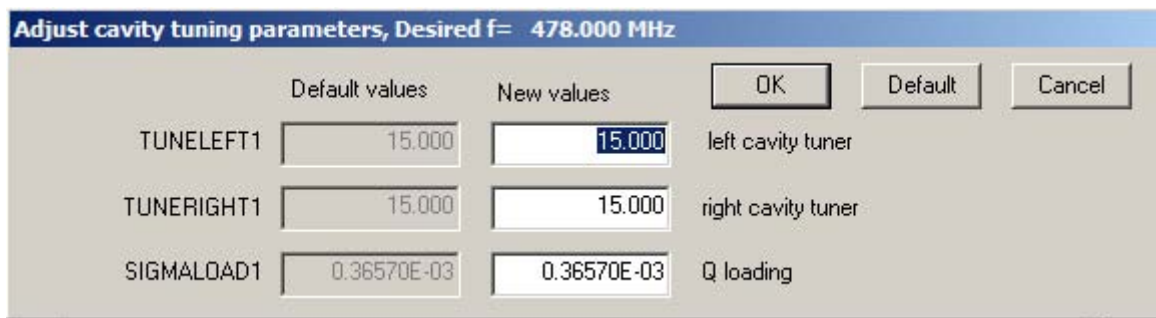
At this point we will again branch between the available options. In this case only the “COLD_TEST” and “HOT_TEST” option will be discussed.

COLD_TEST

Once COLD_TEST has been selected the next screen allows you to select which cavity to test.

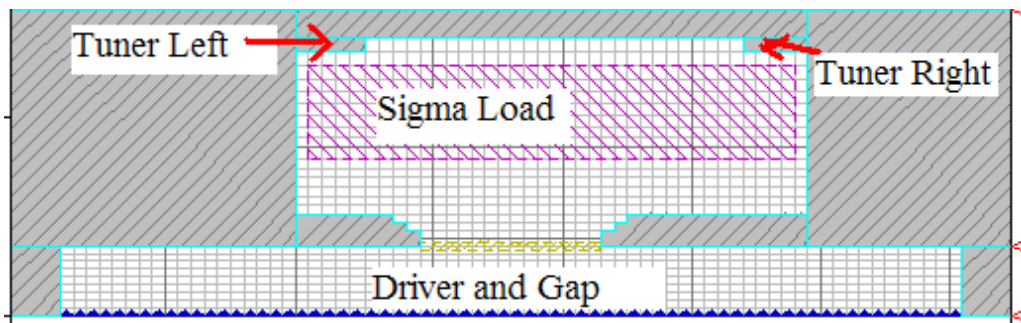


The next screen provides an opportunity to adjust the cavity tuning elements.



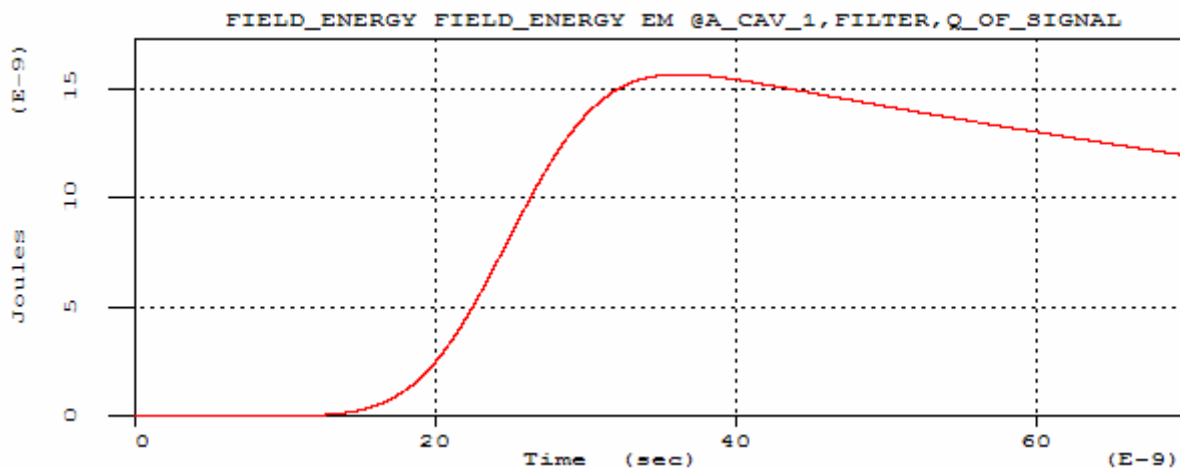
The TUNELEFT and TUNERIGHT elements are used to fine tune the frequency response of the cavity. The SIGMALOAD value is used to tune the effective Q of the cavity.

At this point when you finish the tuning parameters, the simulation will begin to run. The next screen will show the geometry that will look something like the following. The driver in the cavity gap will be used to excite that cavity at the design frequency, once that cavity has “rung-up” it will be allowed to decay and we can measure the Q, the relaxation (natural) frequency, and the R/Q of the cavity. Please remember that R/Q is basically determined by the geometry of gap. We normally do not make additional adjustments to the value obtained. The only tuning is for the load (Q) and the tuners (frequency).

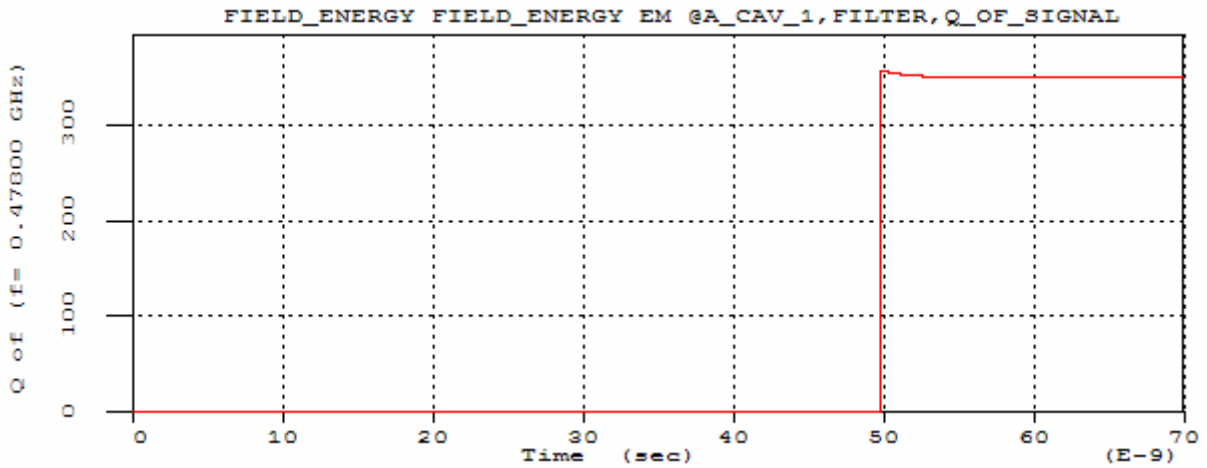


Once you have reviewed the geometry press the play button until the simulation begins.

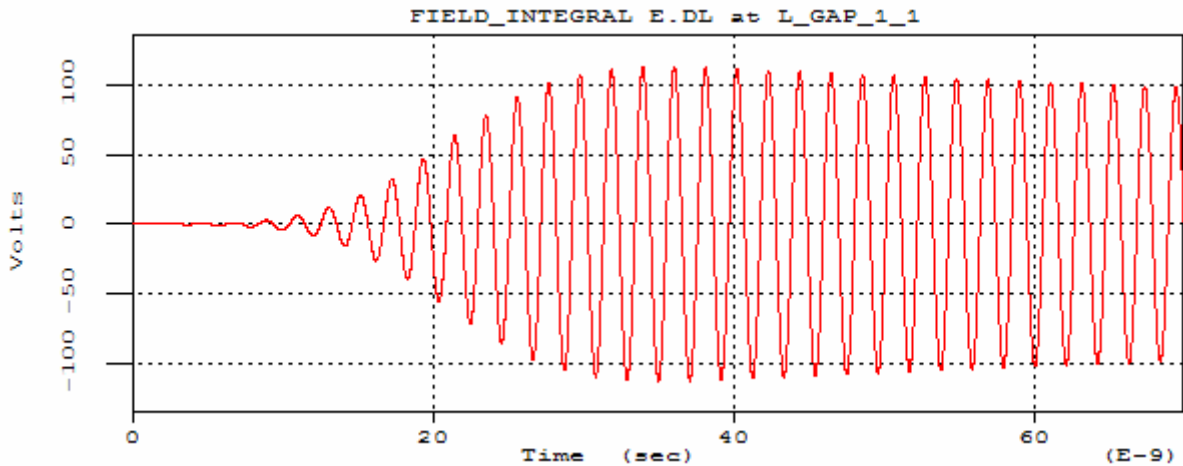
Once the simulation is complete there are several temporal diagnostics that can be examined, if the “GRAPHICS PAUSEON TSYSS\$LAST;” is enabled (this option may be modified in the BFKlystron.m2d file). The first figure is a measure of the energy in the cavity. It will look something like the following figure.



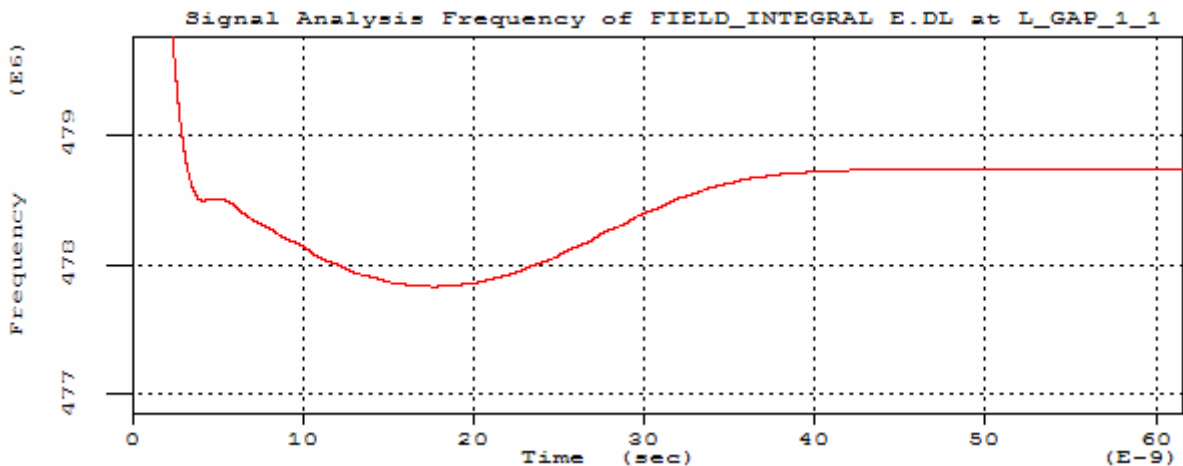
The next figure is a measurement of the effective Q, measured from the decay of the energy in the cavity. We measure Q by directly looking the energy in the cavity and the rate at which it is decreasing in time. Thus we use $Q = -2\pi f W(t)/(dW(t)/dt)$. In the measurement of Q, we start with total energy in the simulation, evaluate the derivative, and we know the driving frequency. The final value of Q is extracted automatically and entered in the results file.



The next measurement of interest is the voltage across the gap. There are several diagnostics associated with this measurement. An additional evaluation of Q, (although this determination is prone to greater error as the Q is very large.) The most significant value measured from this, however is the relaxation frequency. This is determined by a zero-crossing analysis, starting from the design frequency.



The final value of the frequency is extracted and added to the results file.

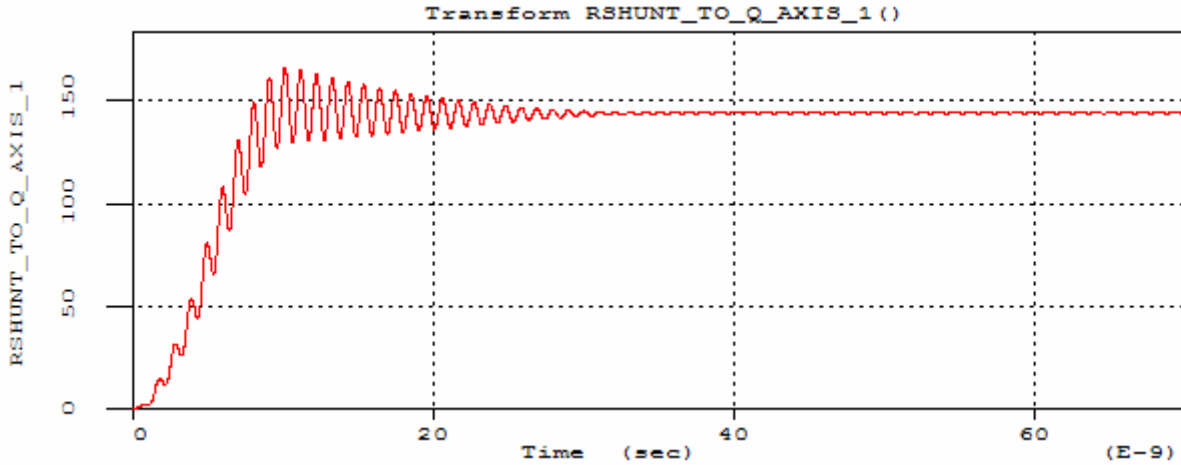


Some additional measurements are made from which we can extract the R/Q both in the gap and on the axis. To obtain R/Q we use MAGIC to measure $\langle V_{axis}^2 \rangle(t)$, the integral of the $E_z(z,r=0)$,

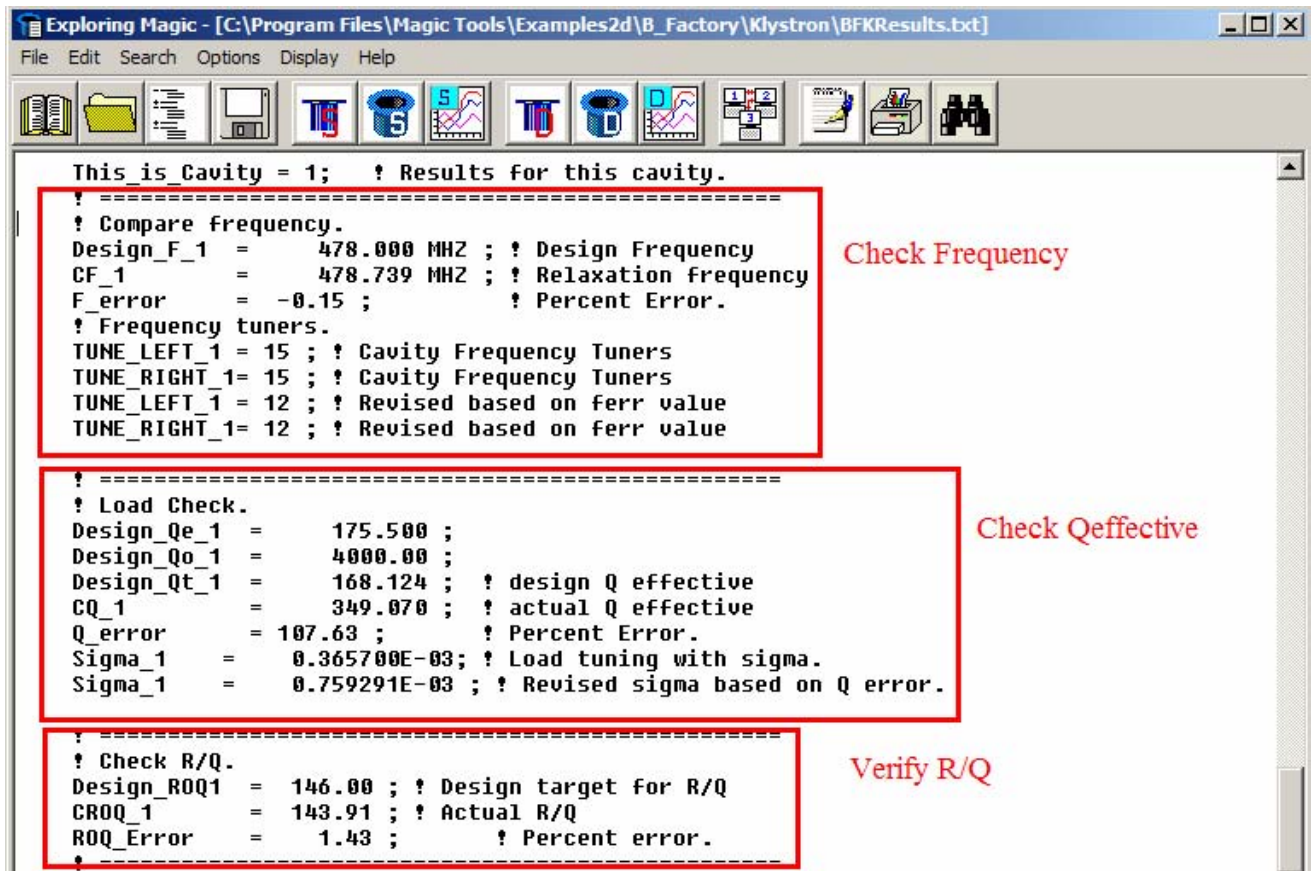
averaged over 1 RF period, and to measure $\langle W_E \rangle(t)$, the electric field energy in the cavity, averaged over 1 RF period. The ratio of these measurements gives us a measure of R/Q, as follows.

$$\langle R/Q \rangle(t) = \langle V_{\text{axis}}^2 \rangle(t) / (2\pi f \langle W_E \rangle(t)).$$

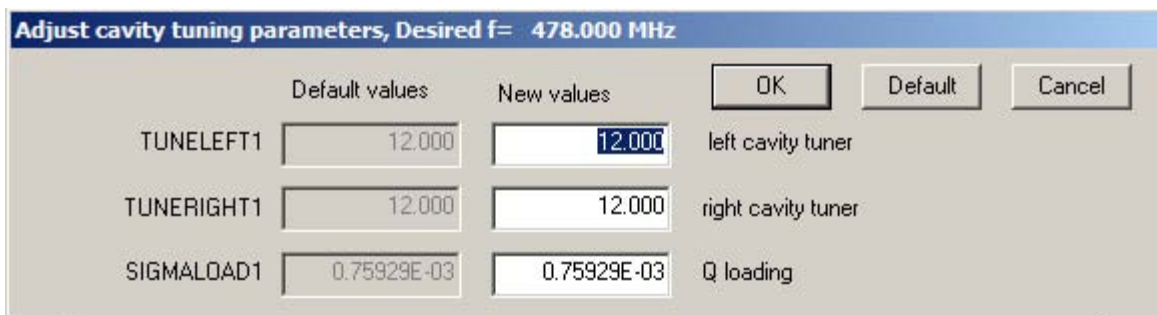
The following figure illustrates the typical result. Again the end value is automatically extracted and added to the results file.



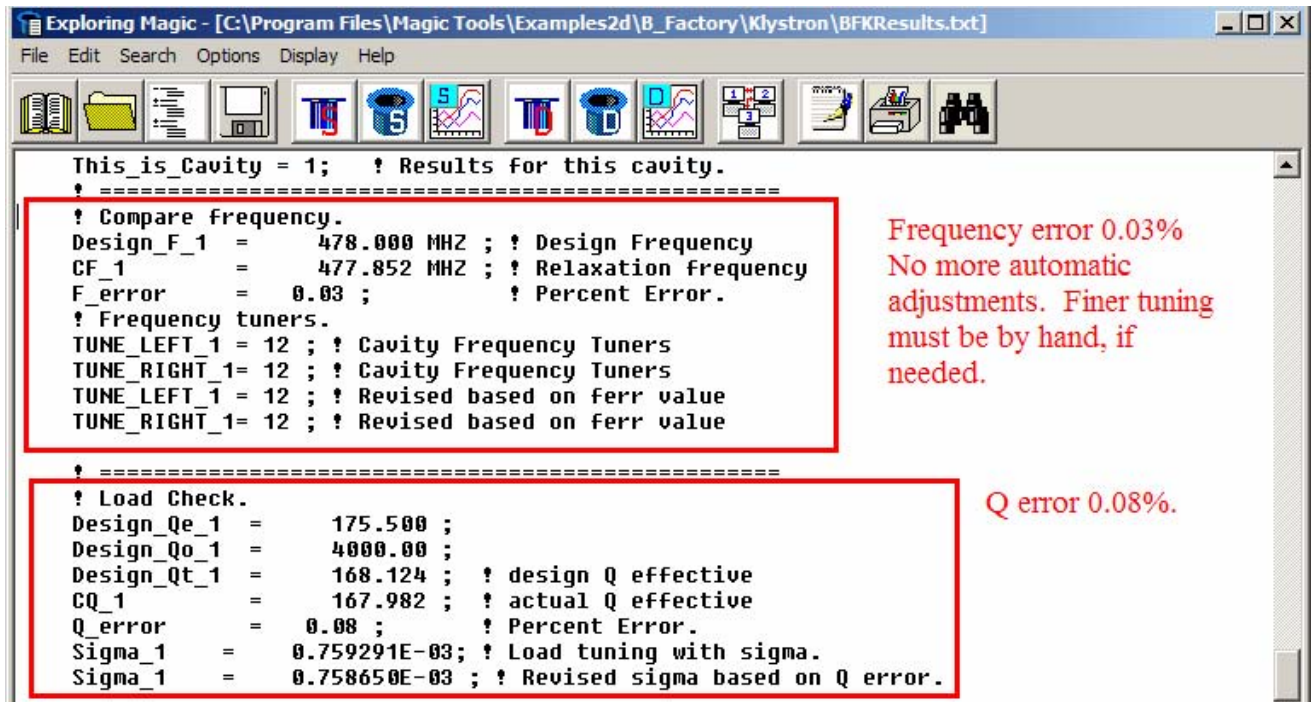
The results file, “BFKResults.txt,” will look a bit like the following, (you can use Mugman to examine this file or a text editor). Please note that the error in the frequency is about 0.15%. The template automatically calculates an adjustment for the tuners. In addition, the error in the Q is over 100%. The template also automatically calculates an adjusted value for the sigma to apply on the next simulation.



At this point we can rerun the template and select LOAD_PREVIOUS to include these corrections (or we enter them by hand at the appropriate screen). When the cavity tuning screen is displayed we will see that the adjusted parameters are being used.



We can reload the results file in Mugman and examine the frequency and Q measurements. We notice that the frequency error is 0.03% and the Q error is about 0.08%. At this point for this resolution we would declare ourselves satisfied and move on the next cavity, and so forth.



The 4th cavity is a second harmonic cavity, and is much smaller in size. Thus for the coarse resolution simulations, we have much less control of the frequency.

In general, a few cycles of cold test per cavity is required to achieve a tuned result. Once all the cavities are tuned we can proceed to the hot test.

HOT_TEST



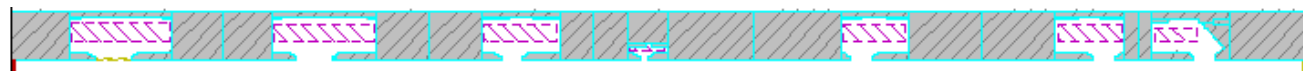
At this point you will need to rerun the simulation and select “LOAD_PREVIOUS” and “SKIP_GEOMETRY_REVIEW” when prompted to do so. Once the simulation type has been selected as “HOT_TEST” the next screen allows you set the hot test parameters. In general, you will be mostly changing the drive frequency and the power in, for the hot test.

Set hot test parameters			OK	Default	Cancel
	Default values	New values			
POWERIN	4.1000	4.1000	Input power (Watts).		
FREQ	0.47600E+09	0.47600E+09	Frequency for amplification (Hz).		
V_BEAM	81000.	81000.	Beam voltage (volt).		
BZ	0.20000E-01	0.20000E-01	Guiding magnetic field (tesla)		
A_BEAM	25.200	25.200	Beam Current (amp)		

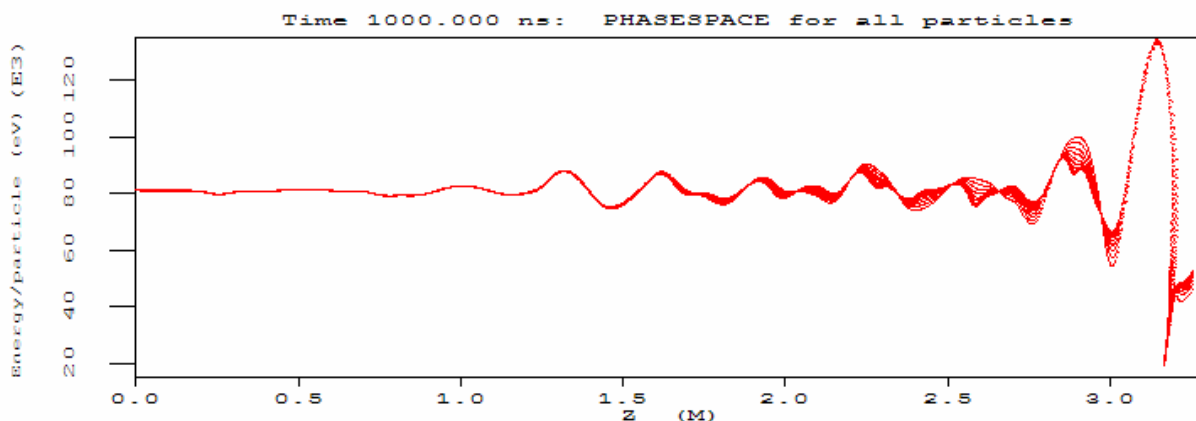
In addition, you may alter the confining magnetic field, the beam voltage and the beam current. The next screen allows you select how many of the cavities to include in the hot test.

Select number of cavities.		OK	Cancel
Select Case	ALL		
	1_THRU_6		
	1_THRU_5		
	1_THRU_4		
	1_THRU_3		
	1_THRU_2		

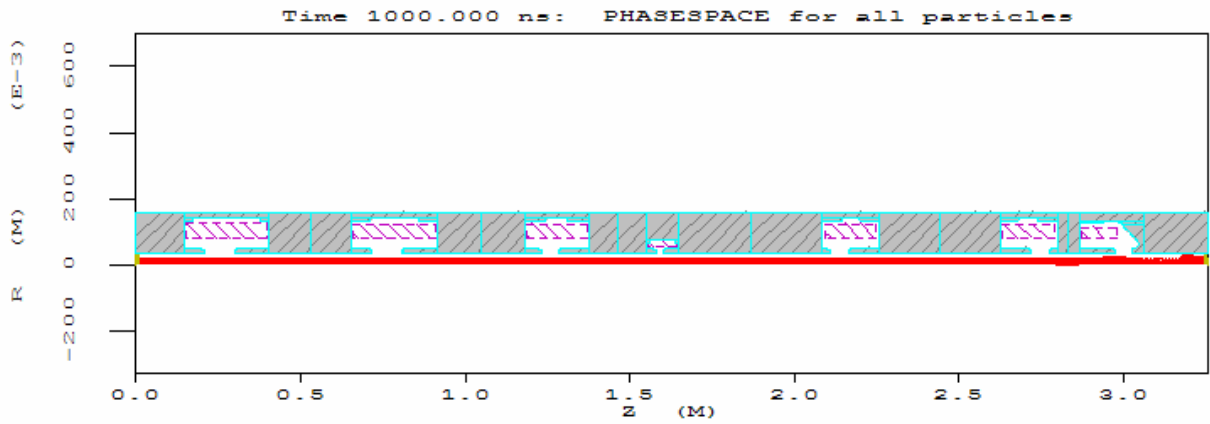
Assuming that you select all the cavities, then you will get a display of the geometry that looks like the following. At this point you start the hot test simulation.



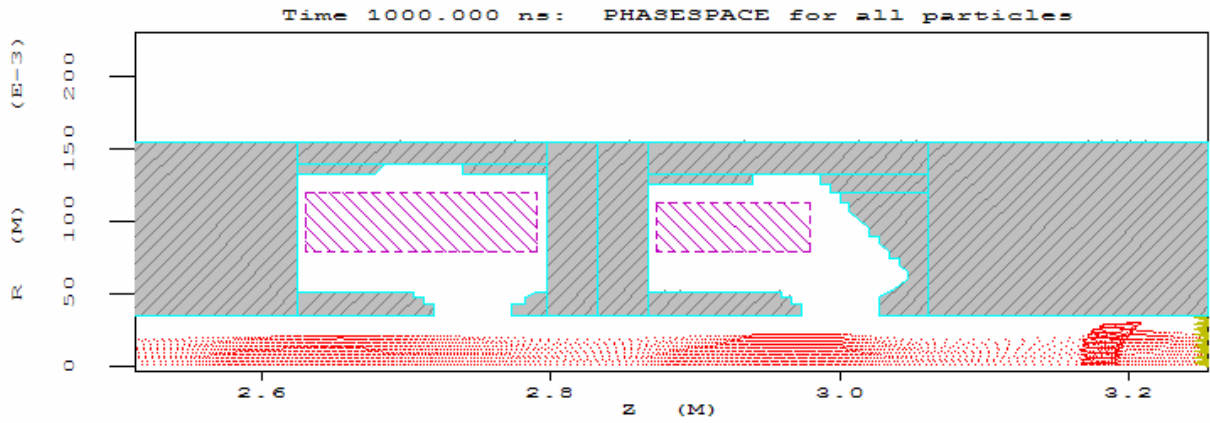
When the simulation completes, you can see several phase space figures. The following is a sample of the kinetic energy versus z of the beam.



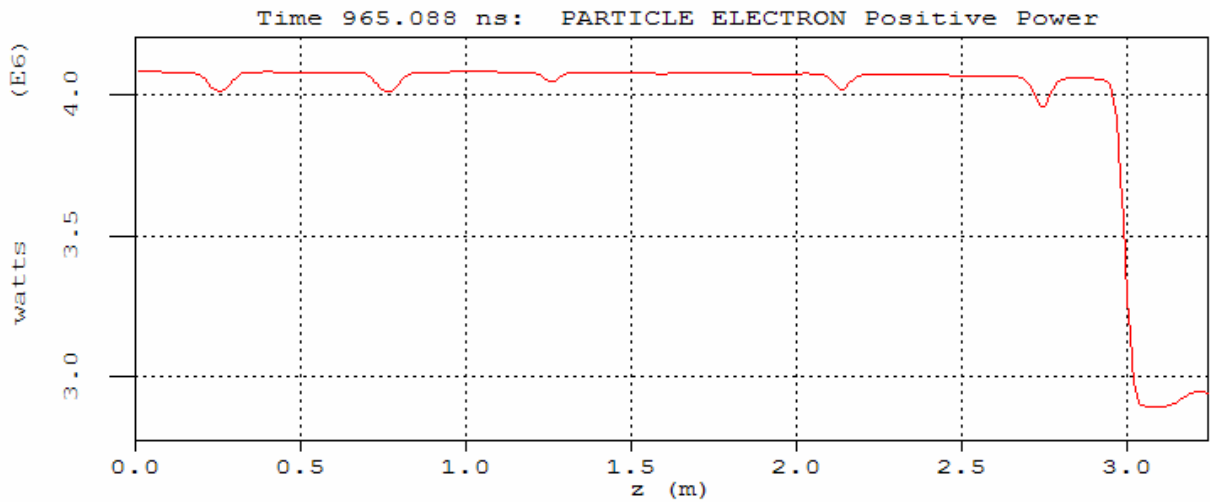
This shows the beam in the entire device.



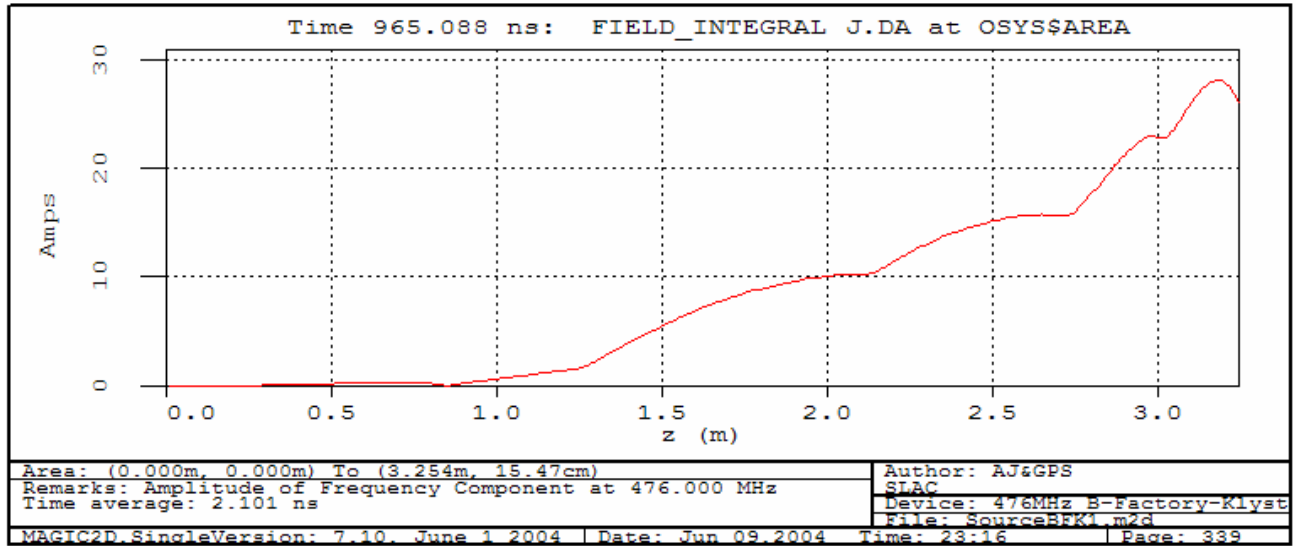
This shows a close up view of the beam at the 6th and 7th cavities. You will note the bunching of the beam is quite evident.



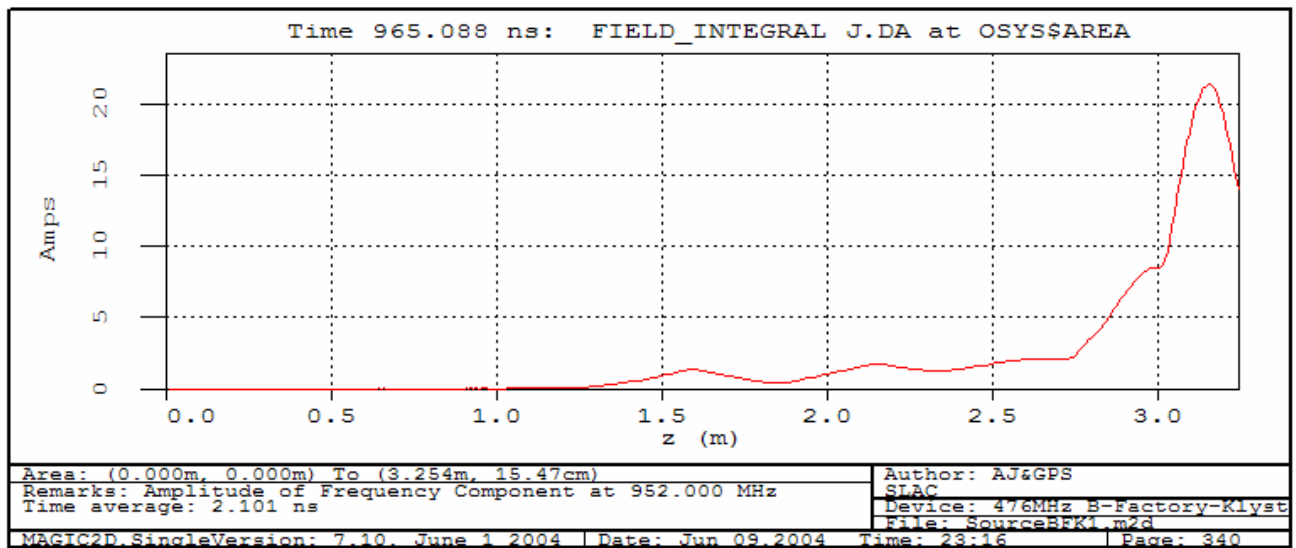
The following figure is beam power versus axial position.



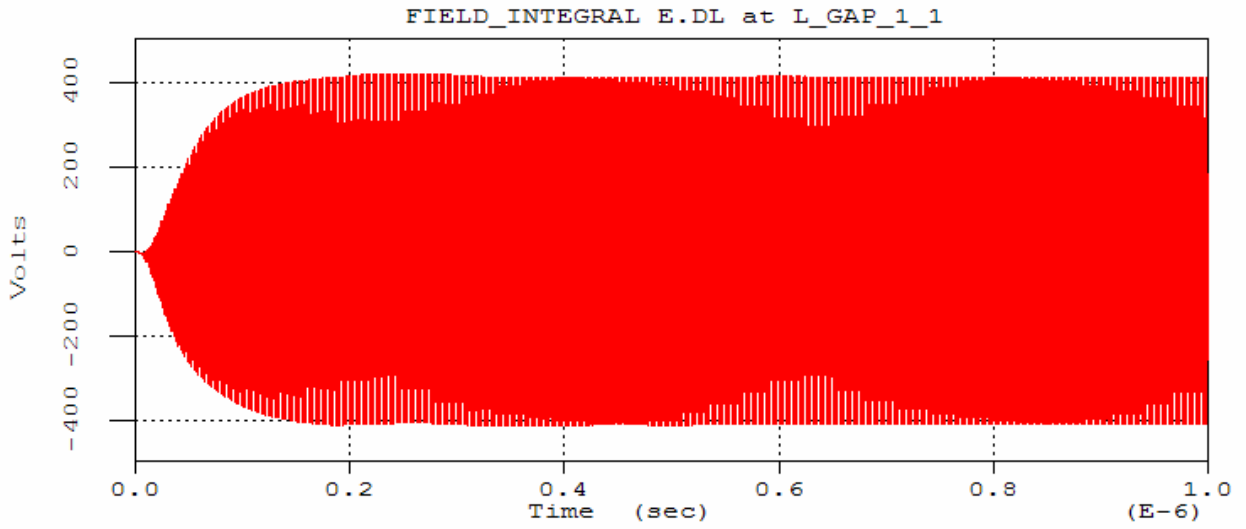
The following figure is the beam current amplitude versus z at the drive frequency of 476 MHz.



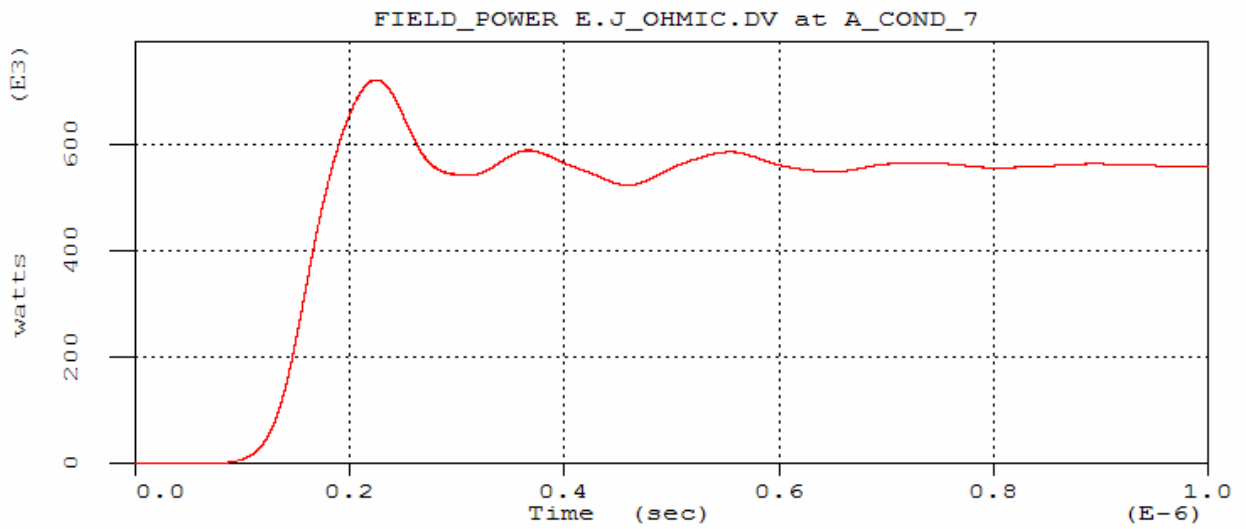
The following figure is the beam current amplitude versus z at the 2nd harmonic frequency of 952 MHz.



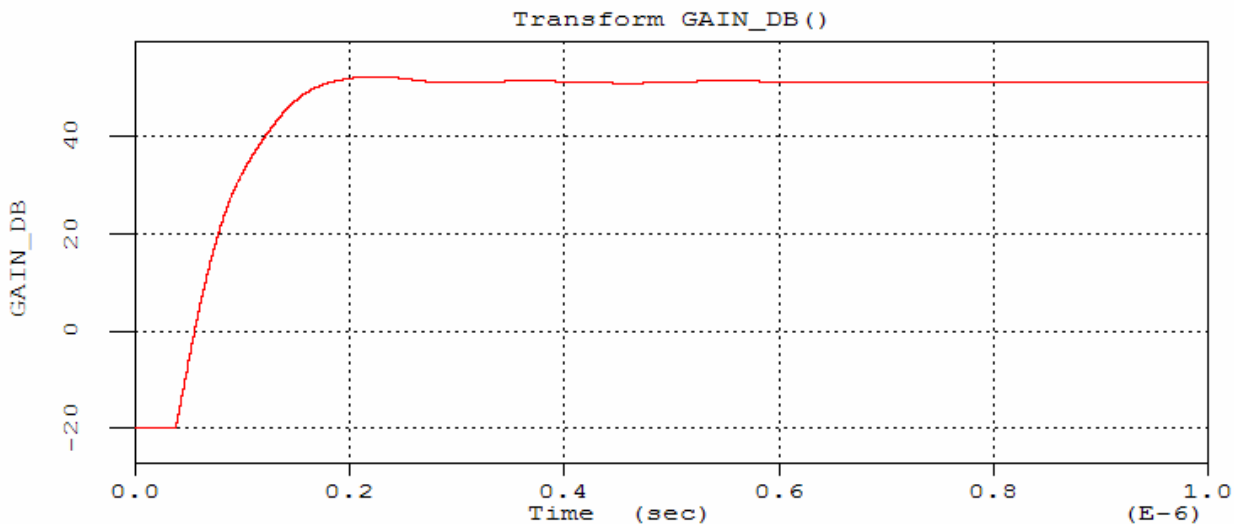
This figure is the gap voltage in cavity 1. It is examined for amplitude, frequency and FFT. The same information is available for the other cavities as well.



The following figure is the power in the output load of cavity 7. From this and the input power we can evaluate the gain.



The next figure is the gain. The end value of the gain is automatically extracted and written to the results file.



Finally, look at the results file with Mugman or a text editor. We see that the gain is 51.35 dB.

```
Exploring Magic - [C:\MagicDeveloper\Build\SourceBFK0\BFKResults.txt]
File Edit Search Options Display Help
-----
Comment #Simulation Started: 06-09-2004 23:16:46# ;
Comment #Hot Test Simulation Completed: 06-10-2004 00:54:07# ;
-----
?
Num_Cavities = 7 ; ! Number of cavities used.

RF_Freq = 476.00000 MHz ;
In_Power = 4.1000 Watts ;
Bconfine = 0.0200 tesla;
Voltage = 81000. volt ;
Current = 25.200 Amp ;

Output_Power = 559.6 kiloWatt ;
output_Gain = 51.351 ;
```

At this point, one can start another hot test, and vary the input power or the drive frequency.

Appendix IV.

Determining R/Q, coupling coefficient, beam loading and stability (G. Scheitrum, A. Jensen)

Overview

The details of the determination of shunt impedance R/Q, coupling coefficient M, beam loading Q_b , and a method for determining stability for various cavity modes are presented in this Appendix. The Los Alamos SUPERFISH program group is used to illustrate the calculation of R/Q and M although any electromagnetic field code can be used. SUPERFISH is available and may be downloaded from Los Alamos at <http://laacg1.lanl.gov/laacg/services/psann.html>. The beam loaded Q that is needed for a cavity stability analysis is computed from a Wessel-Berg formulation using a Mathcad worksheet. The results of the Q_b calculation are then used to do a detailed stability analysis for the XC8 klystron output structure. The primary calculations and key equations are the same as those found in the Mathcad file for gain calculations (see Appendix I).

This document has six sections. The first section provides the analysis for a method used to measure R/Q using the perturbation of cavity fields using a dielectric rod. This method was used regularly before electromagnetic field simulation became commonplace. The second section illustrates the calculation of R/Q using SUPERFISH. The third section describes the calculations of R/Q for an extended interaction cavity. The fourth section shows how the coupling coefficient M can be obtained using the same SUPERFISH model. The fifth section of this document discusses the calculation of Q_b and the setup of the Mathcad file to determine the stability of individual cavity modes. The last section is a step by step analysis of the zero-mode in the XC8 output structure. This same approach may be applied to any output structure or mode by simply changing the input variables in the Mathcad worksheet. The SUPERFISH and Mathcad files which accompany these calculations can be found in the attached CD.

1. Measuring R/Q using a dielectric rod and Slater's perturbation method

Next to the coupling coefficient M , the cavity R/Q is the most important parameter to be determined in the design of a new klystron (see Ch. 4). Before computers became commonplace, cavity R/Qs were determined by constructing cold-test models of the cavities and performing perturbation measurements based on the well-known Slater perturbation formula⁴⁷ to calculate R/Q. This procedure may still be of interest to the reader since it provides considerable insight on the function of a klystron cavity and its gap. For that reason it will be described in this Appendix, along with a simulation-based R/Q calculation that does not require cold test.

R/Q is the ratio of the *shunt impedance* R of a cavity (defined as, $R = \frac{VV^*}{W} = \frac{|V|^2}{W}$, i.e. the ratio of the square of the voltage across the gap to the power lost in the resonator walls); and the *cavity Q* (defined as $Q = \frac{\omega U}{W}$, i.e. $2\pi f$ times the energy stored in the cavity divided by the power lost in the resonator walls).

Combining the two equations above, gives,

$$\frac{R}{Q} = \frac{|V|^2}{2\omega U} = \frac{\left(\int_{-\infty}^{\infty} |E_z| dz \right)^2}{2\omega U}$$

where the cavity is assumed to be gridless and the field E_z is assumed to extend beyond the actual gap.

Now, if a dielectric rod of radius b and a relative dielectric constant ϵ is inserted at the center of the cylindrical cavity, the Slater perturbation theorem is reduced to,

$$\frac{\omega - \omega_0}{\omega_0} = \frac{\Delta\omega}{\omega_0} = \frac{-\pi b^2 (\epsilon - \epsilon_0) \int_{-\infty}^{\infty} |E_z|^2 dz}{4 \left(\frac{\Delta\omega}{\omega_0} \right)}$$

Taking into account that the frequency of the cavity will be reduced by the dielectric insertion ($\Delta\omega < 0$), and the $\epsilon = \epsilon_r \epsilon_0$, and using the definition for R/Q above, we can write a formula for R/Q in terms of the frequency shift measured in the perturbation cold test,

$$\frac{R}{Q} = \frac{1}{\pi^2 b^2 \epsilon_0 (\epsilon_r - 1)} \frac{\left(\int_{-\infty}^{\infty} |E_z| dz \right)^2}{\int_{-\infty}^{\infty} |E_z|^2 dz} \frac{\Delta f}{f_0^2}$$

Using $\epsilon_0 = 8.85 \times 10^{-12}$ farad/meter, we have the following formula in MKS,

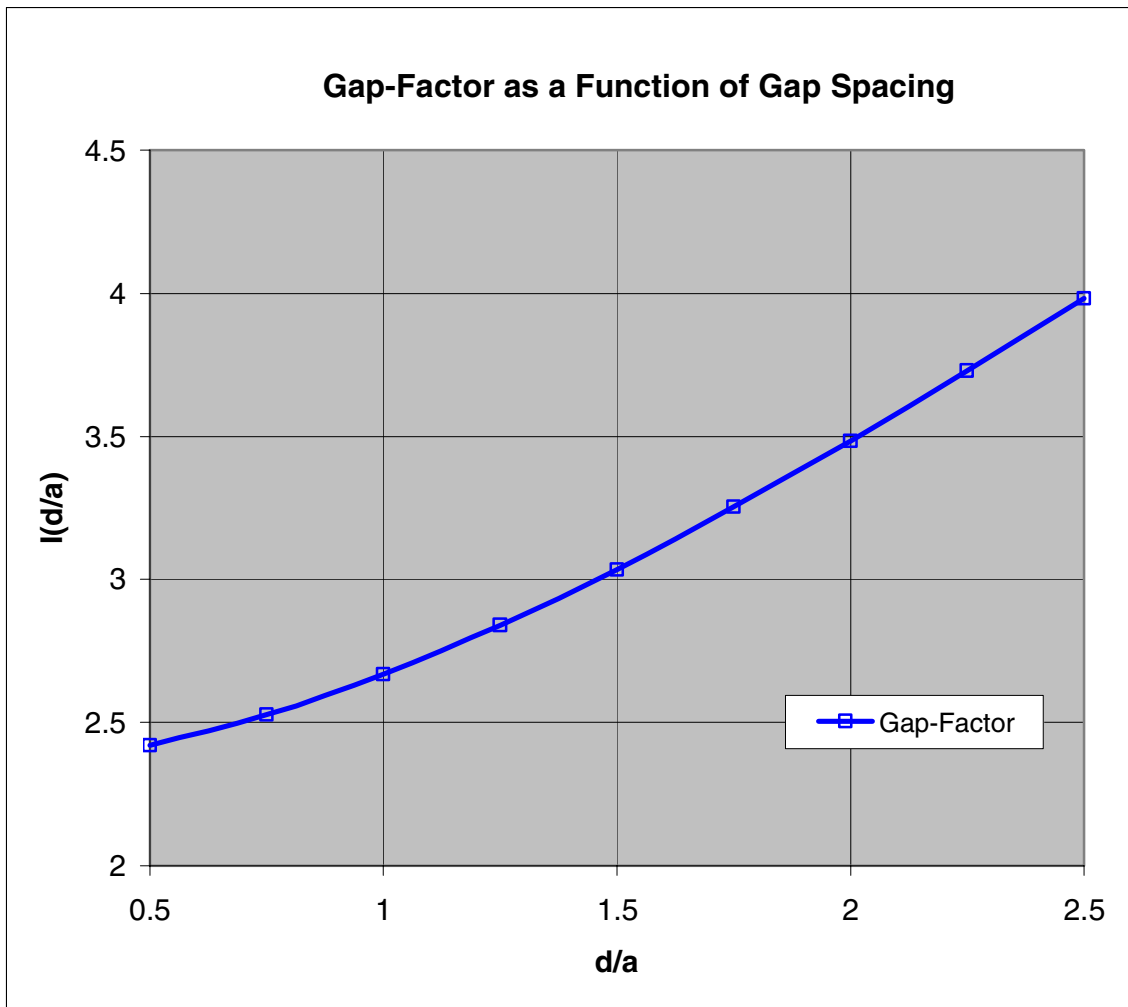
$$\frac{R}{Q} = \frac{(1.14 \times 10^{10}) a |\Delta f|}{b^2 (\epsilon_r - 1) f_0^2} I \left(\frac{d}{a} \right)$$

Where

$$I \left(\frac{d}{a} \right) = \frac{1}{a} \frac{\left(\int_{-\infty}^{\infty} |E_z| dz \right)^2}{\int_{-\infty}^{\infty} |E_z|^2 dz}$$

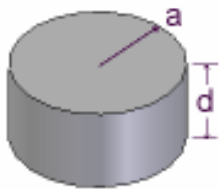
The quantity $I(d/a)$, where \underline{a} is the interior radius of the drift tube, and \underline{d} is the length of the gap, is plotted in the graph below, with the assumptions that the thickness of the drift tube is 1/5 of its radius \underline{a} and that the gap tips are blunt. Note that this procedure, which involves using an actual klystron cavity for cold test, together the graph that is based on the above assumptions,

is only approximate. The actual shape of the gap tips, as well as the thickness of the drift tube will influence the value of the R/Q calculated.



2. Determining R/Q for a resonant structure using computer simulation

The best example to use to become familiar with the process of calculating R/Q using a field simulation program is a pillbox cavity since its R/Q can be determined analytically. A pillbox cavity is a simple cylinder of radius “a” and length “d”.



For the TM_{010} mode in a pillbox cavity, the electric fields are all in the z direction and vary radially as the J_0 Bessel function.

$$E_z = E_0 J_0(kr)$$

The radial propagation constant k is defined by requiring that $E_z = 0$ at $r = a$ therefore $J_0(ka) = 0$ and $k = p_{01}/a$ where $p_{01} = 2.4048$ is the first zero of J_0 . Since the electric field is constant in z , the integral of $|E_z|dz$ is just $(E_0 * d)$. The stored energy is

$$U = \pi \epsilon d E_0^2 \frac{a^2}{2} J_1^2(ka)$$

Substituting into the equation for R/Q, the field magnitude drops out and the result is:

$$R/Q = \left(\frac{1}{c \pi \epsilon J_1^2(p_{01}) p_{01}} \right) \frac{d}{a} = 185 \frac{d}{a}$$

R/Q is a function of geometry but not frequency or wall losses in the cavity. A W-band cavity that is a scaled copy of an L-band cavity will have exactly the same R/Q.

For a pillbox cavity with a TM₀₁₀ mode at 10 GHz, $a = (p_{01} * c) / (2 * \pi * f) = 0.0115$ m. Setting $d = a$, the analytic calculation of R/Q gives a value of 185.

Now, let us calculate the R/Q for the same cavity using a computer simulation of its fields. This can be done with any electromagnetic simulation software that solves for cavity fields given the cavity geometry. This includes SUPERFISH, MAGIC, MAFFIA, HFSS, etc. SUPERFISH, written and maintained by Los Alamos National Laboratory, will calculate electromagnetic fields for 2D cylindrically symmetric structures but there are some pitfalls that must be avoided.

Caveat: SUPERFISH was written by accelerator physicists. They have a different definition of R/Q than the one used by tube engineers. In SUPERFISH, the postprocessor SFO will report a “Shunt Impedance” and an “r/Q”. Neither one is the R/Q used by tube engineers. The shunt impedance used in SUPERFISH is $(E_0^2 L) / P$, an impedance per unit length and $r/Q =$

$2(V_0 T)^2 / \omega U$, where T (called a transit time factor – more on this in a subsequent section) is equivalent to the klystron engineer’s coupling factor M. If everything in the simulation is set up correctly, so that SUPERFISH integrates the voltage along the correct path, the cavity center is at $z = 0$ and the correct beam velocity has been used, then the $R/Q = (r/Q) / (2T^2)$. The factor of 1/2 converts the peak voltage values to RMS values. If everything is not set up correctly, the voltage along the axis (or other desired path) can be calculated by the SF7 postprocessor and the internal integration routine in TABLPLOT. The stored energy is already reported in the SUPERFISH output file *.SFO where the * represents the filename assigned by the user to the input datafile. In the example below the input file would be PILL10.af and the corresponding output file would be PILL10.SFO.

[PILL10.af SUPERFISH input file listing](#)

```
10-GHz TM010 Short Pillbox Cavity
reg kprob=1, ; SUPERFISH problem
dx=.02, ; X mesh spacing
freq=10000., ; Starting frequency in MHz
xdri=1.,ydri=1.14741 $ ; Drive point location
$po x=0.0,y=0.0 $ ; Start of the boundary points
$po x=0.0,y=1.14741 $ ; r = 1.14741 cm
$po x=1.14741,y=1.14741 $ ; z = 1.14741 cm, r = 1.14741 cm
$po x=1.14741,y=0.0 $ ;
$po x=0.0,y=0.0 $ ; note closed structure has same
```

; entries for first and last point
; In SUPERFISH cylindrically symmetric problems $x = z$, $y = r$

To run AUTOFISH, double click on the "PILL10.af" filename. It will output several files. PILL10.T35, PILL10.SFO, OUTAUT.TXT, OUTFIS.TXT, etc. If the AUTOFISH program fails to complete, read the two input text files to find the error. Correct the error and rerun AUTOFISH.

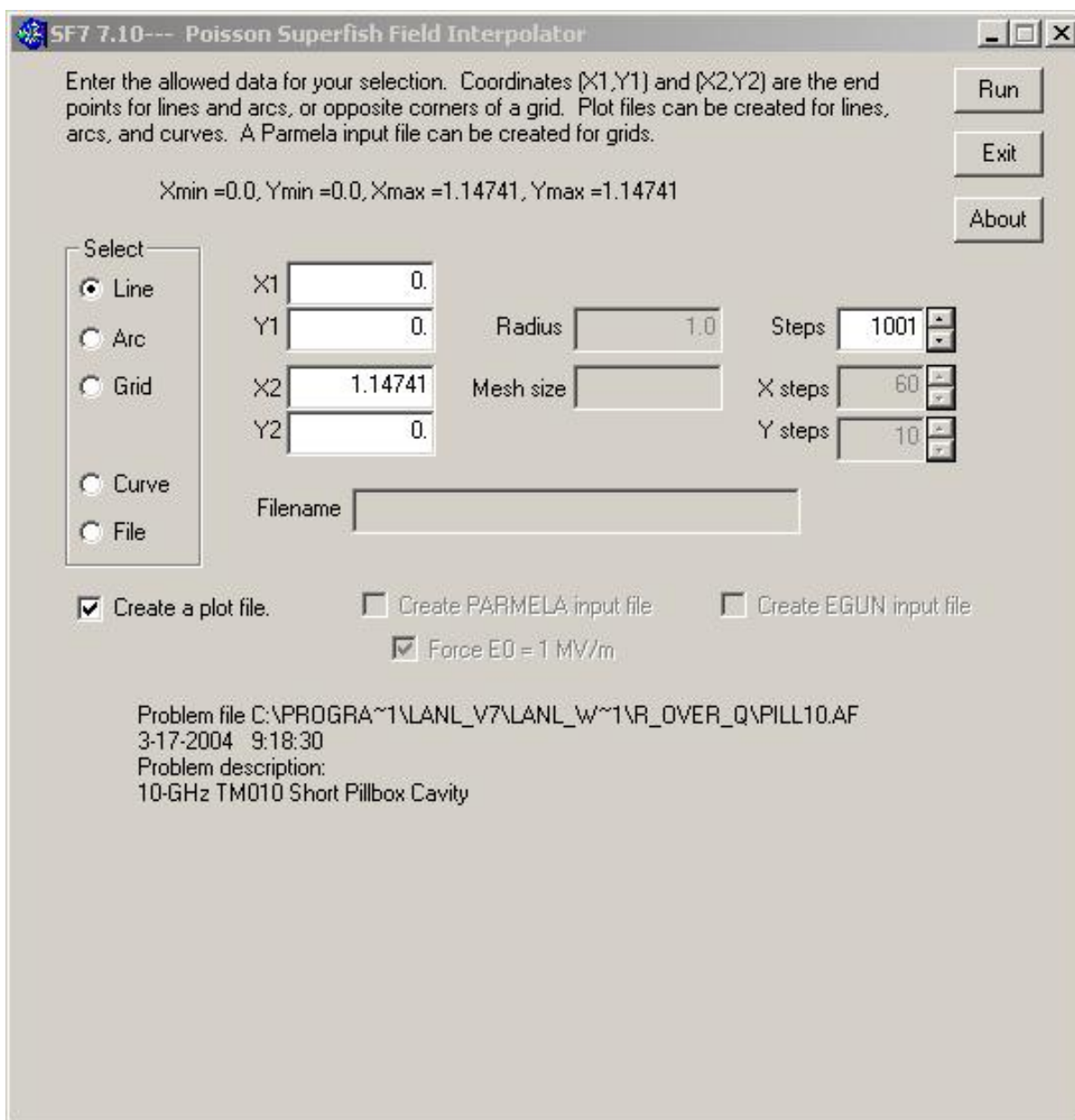
Last page of PILL10.SFO

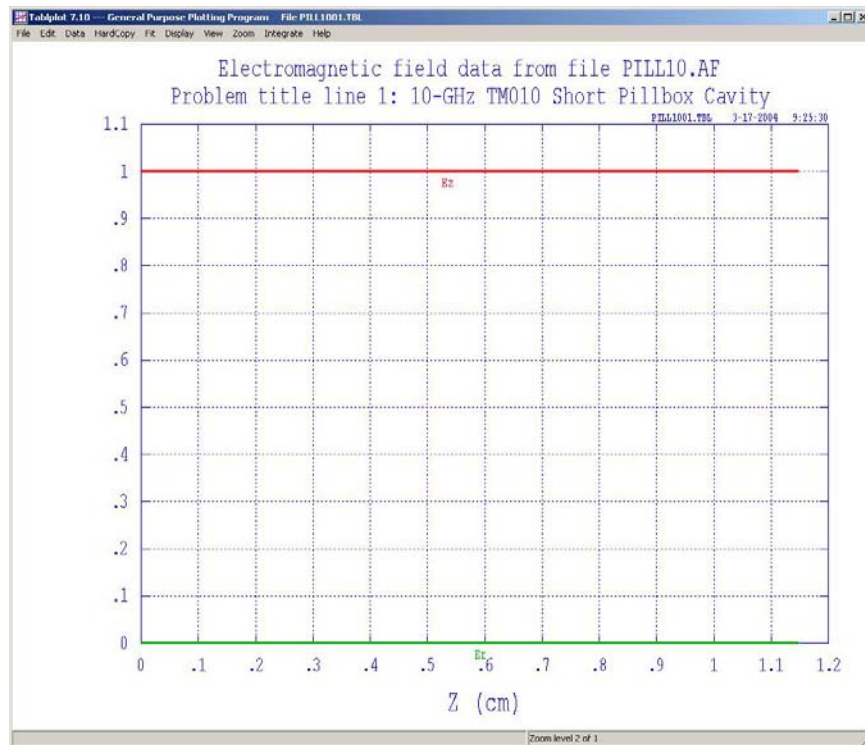
SUPERFISH output summary for problem description:
10-GHz TM010 Short Pillbox Cavity

All calculated values below refer to the mesh geometry only.
Field normalization (NORM = 0): EZERO = 1.00000 MV/m
Frequency = 10000.09011 MHz
Particle rest mass energy = 938.271998 MeV
Beta = 0.7654765 Kinetic energy = 519.886 MeV
Normalization factor for $E_0 = 1.000$ MV/m = 5187.058
Transit-time factor $\text{Abs}(T+iS) = 0.0000031$
Stored energy = 5.65182E-06 Joules
Using standard room-temperature copper.
Surface resistance = 26.08934 milliOhm
Normal-conductor resistivity = 1.72410 microOhm-cm
Operating temperature = 20.0000 C
Power dissipation = 20.4561 W
 $Q = 17360.0$ Shunt impedance = 560.912 MOhm/m
 $R_s * Q = 452.910$ Ohm $Z * T * T = 0.000$ MOhm/m
 $r/Q = 0.000$ Ohm Wake loss parameter = 0.00000 V/pC
Average magnetic field on the outer wall = 1376.86 A/m, 2.47293 W/cm²
Maximum H (at Z,R = 0.96624,1.14741) = 1376.85 A/m, 2.47291 W/cm²
Maximum E (at Z,R = 1.13735,1.14741) = 1.00356E-04 MV/m, 1.2215E-06 Kilp.
Ratio of peak fields $B_{\text{max}}/E_{\text{max}} = 17240.6426$ mT/(MV/m)
Peak-to-average ratio $E_{\text{max}}/E_0 = 0.0001$

After running SUPERFISH, the stored energy is available in the *.SFO file. The integrated electric field is obtained by running the postprocessor 'SF7'. This program is used to output the field data stored in binary in the *.T35 file. The data will be interpolated along the line, arc or rectangular area specified with equal spacing for a user defined number of steps. To execute the program, right click on PILL10.T35 and choose (Interpolate SF7).

The dialog box shown below is used to select the start and stop points for a line along the axis of the cavity. When run, it creates a TABLPLOT file named PILL1001.TBL which contains electric field data for E_z and E_r along the specified line. Since the electric field is constant along z the plot produced is just a straight line.





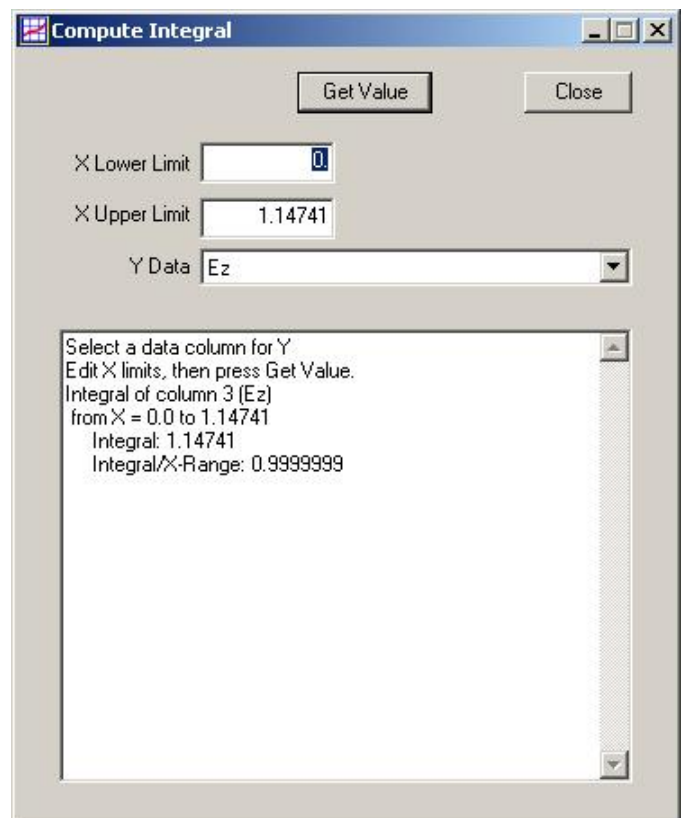
One of the drop-down menu choices from the TABLPLOT file is “Integrate”. Clicking on it opens the dialog box on the right. The dialog box lets you define the limits of integration and field value to be integrated (E_z , E_r , $|E|$, H). In this case the normalization done in SUPERFISH produced an E_0 value of 1 MV/m. Since the electric field is constant vs z , the integral is just $E_0 \cdot (z_2 - z_1)$

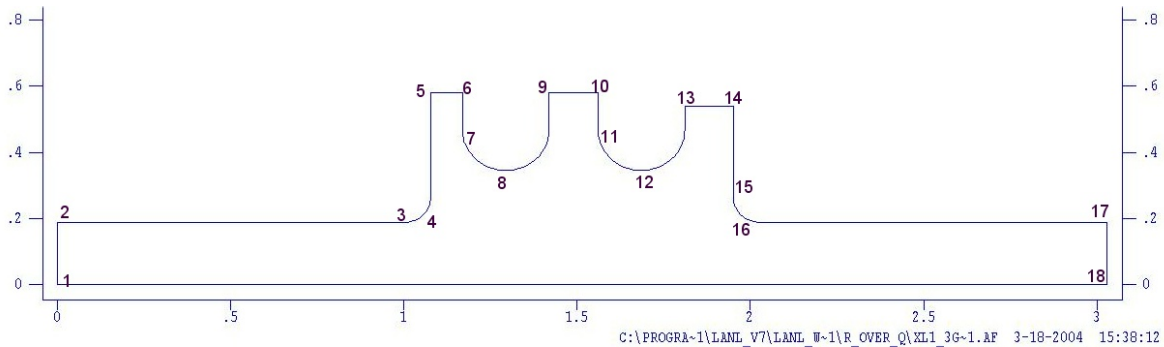
Integrated Voltage = 11.4741 kV
 Resonant frequency = 10 GHz
 Stored Energy $U = 5.65182E-06$ J
 $R/Q = V^2/2\omega U = 185.37 \Omega$

The calculated value of R/Q from the SUPERFISH simulation is 0.2% larger than the analytic value.

3. R/Q for an extended interaction cavity

A little more complex example is provided by the 3 gap output cavity from SLAC’s XL-1 klystron. The XL-1 was the first of a series of 11.424 GHz 50 MW klystrons for the NLC. It used a 3 gap standing wave cavity to reduce the electric field gradient in the output cavity. The numbers in the figure below correspond to the points defined in the input file for SUPERFISH.





The input file for SLAC's XL1 three cell standing wave output cavity is listed below. The numbers on the right are not part of the input file. They were added to make it easier to identify the features in the cavity geometry. The input file name is "XL-1_3gap.af".

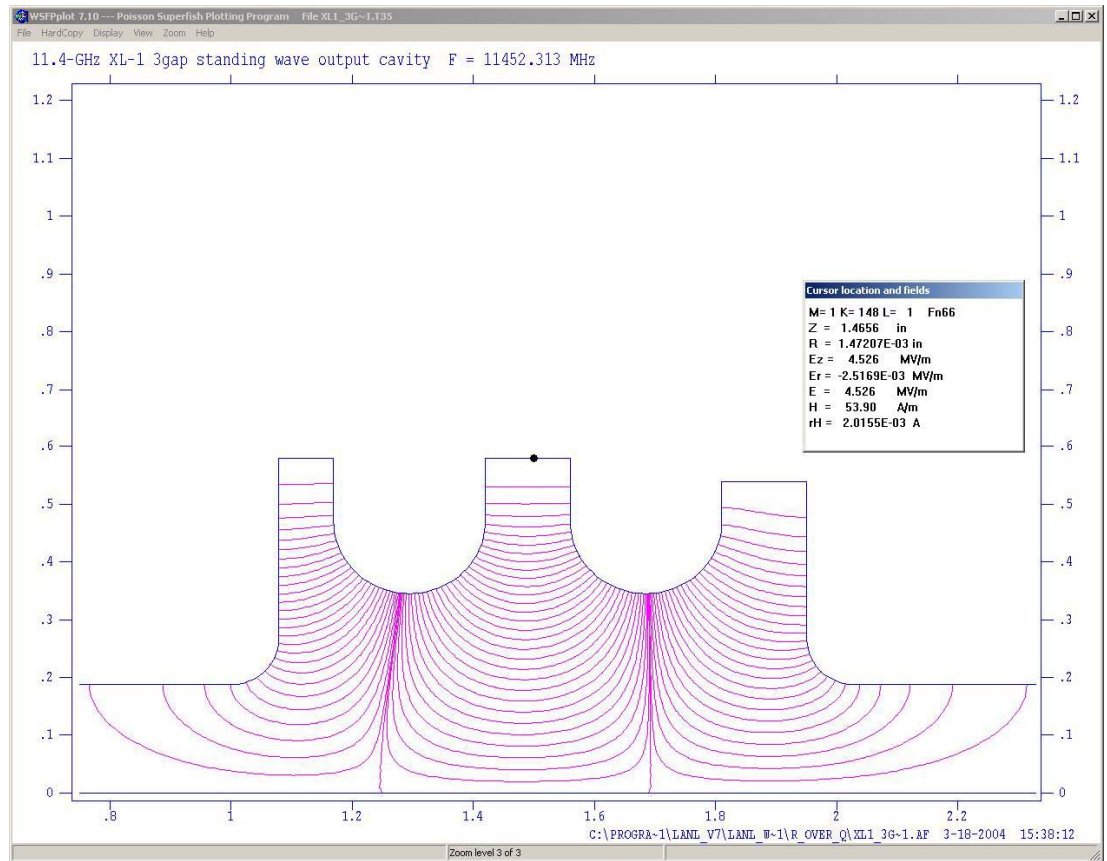
11.4-GHz XL-1 3gap standing wave output cavity

```

$reg kprob=1, ; SUPERFISH problem
dx=.010, ; X mesh spacing
freq=11424., ; Starting frequency in MHz
xdri=1.5,ydri=0.5792, ; Drive point location
conv=2.54 $ ; Dimensions are in inches
$po x=0.0,y=0.0 $ ; Start of the boundary points 1
$po x=0.0,y=0.1875 $ ; drift tube radius = 0.1875 in 2
$po x=1.0,y=0.1875 $ ; drift tube length = 1.0 in, r = 0.1875 in 3
$po nt=2,x0=1.0,y0=0.2661,r=0.0786,theta=360 $ ; radius of cavity edge 4
$po x=1.0786,y=0.5792 $ ; left cavity backwall radius = .5792 in 5
$po x=1.1693,y=0.5792 $ ; spacer width = .0907 in 6
$po x=1.1693,y=0.47 $ ; start of radius 7
$po nt=2,x0=1.2945,y0=0.47,r=0.1252,theta=360 $ ; 180° arc for disk aperture 8
$po x=1.4197,y=0.5792 $ ; center cavity backwall radius = .5792 in 9
$po x=1.56,y=0.5792 $ ; spacer width = .1403 in 10
$po x=1.56,y=0.47 $ ; start of radius 11
$po nt=2,x0=1.6852,y0=0.47,r=0.1252,theta=360 $ ; 180° arc for disk aperture 12
$po x=1.8104,y=0.5384 $ ; right cavity backwall radius = .5384 in 13
$po x=1.9507,y=0.5384 $ ; spacer width = .1403 in 14
$po x=1.9507,y=0.2661 $ 15
$po nt=2,x0=2.0293,y0=0.2661,r=0.0786,theta=270 $ 16
$po x=3.0293,y=0.1875 $ ; drift tube 17
$po x=3.0293,y=0.0 $ 18
$po x=0.0,y=0.0 $ ;

```

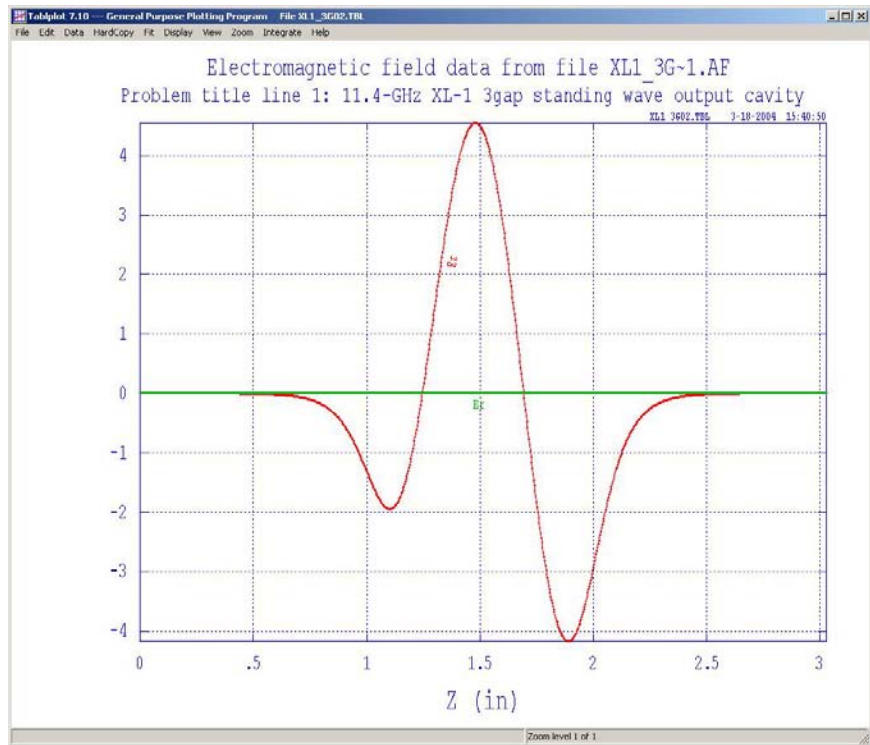
The plot on the right shows the electric field for the π -mode in the three-gap output cavity. Note that the field changes sign where the field lines intersect the axis. Below is the SFO summary for problem description:



11.4-GHz XL-1 3gap standing wave output cavity

All calculated values below refer to the mesh geometry only.
 Field normalization (NORM = 0): EZERO = 1.00000 MV/m
 Frequency = 11452.31327 MHz
 Particle rest mass energy = 938.271998 MeV
 Beta = 1.0000000
 Normalization factor for E0 = 1.000 MV/m = 94181.405
 Transit-time factor Abs(T+iS) = 0.6550239
 Stored energy = 0.0012806 Joules
 Using standard room-temperature copper.
 Surface resistance = 27.91950 milliOhm
 Normal-conductor resistivity = 1.72410 microOhm-cm
 Operating temperature = 20.0000 C
 Power dissipation = 20.0765 kW
 Q = 4589.74 Shunt impedance = 3.833 MOhm/m
 Rs*Q = 128.143 Ohm Z*T*T = 1.644 MOhm/m
 r/Q = 27.567 Ohm Wake loss parameter = 0.49591 V/pC
 Average magnetic field on the outer wall = 23025.5 A/m, 740.11 W/cm²
 Maximum H (at Z,R = 1.4197,0.5288) = 26129.9 A/m, 953.134 W/cm²
 Maximum E (at Z,R = 1.57952,0.402874) = 9.92618 MV/m, 0.113264 Kilp.
 Ratio of peak fields Bmax/Emax = 3.3080 mT/(MV/m)
 Peak-to-average ratio Emax/E0 = 9.9262

On the right is a plot of the axial electric field for the π -mode in the three-gap XL-1 output cavity. The integral of $|E_z|$ vs z is obtained by taking the absolute value of the E_z data in the TABLPLOT file and integrating over z . This can be done by hand or the TABLPLOT input file can be edited to change all the negative field values to positive and then integrated using TABLPLOT.



It is important to note that the integral has mixed units in the TABLPLOT dialog box.

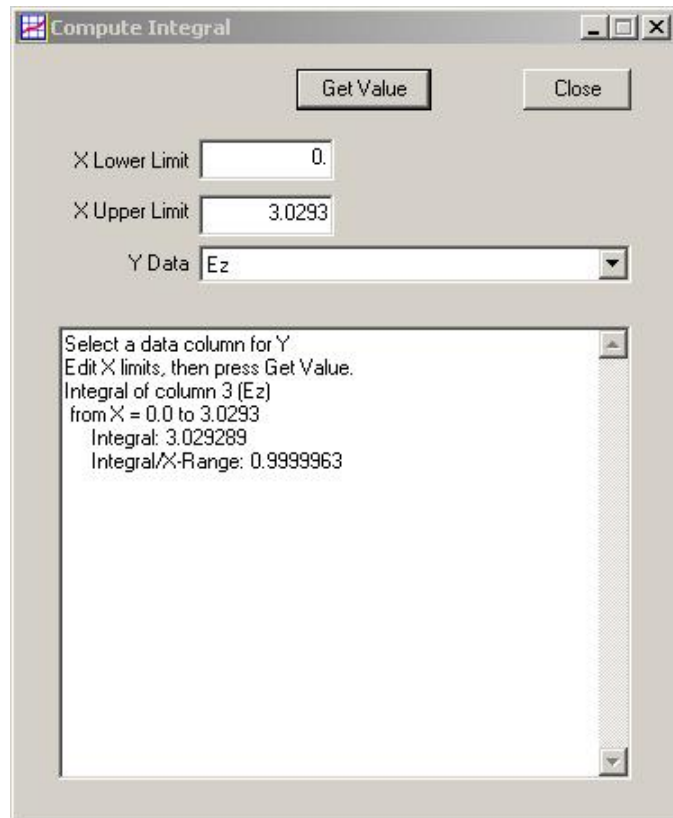
E_z is in MV/m but z is in inches. This will depend upon the units used for the input geometry file. Converting all units to MKS, $V = 3.0293 \text{ MV-in/m} * .0254 \text{ m/in} = 76.9 \text{ kV}$. The stored energy U from SFO is [0.0012806 J](#).

Then,

$$R/Q = V^2/2\omega U = 64.25 \Omega$$

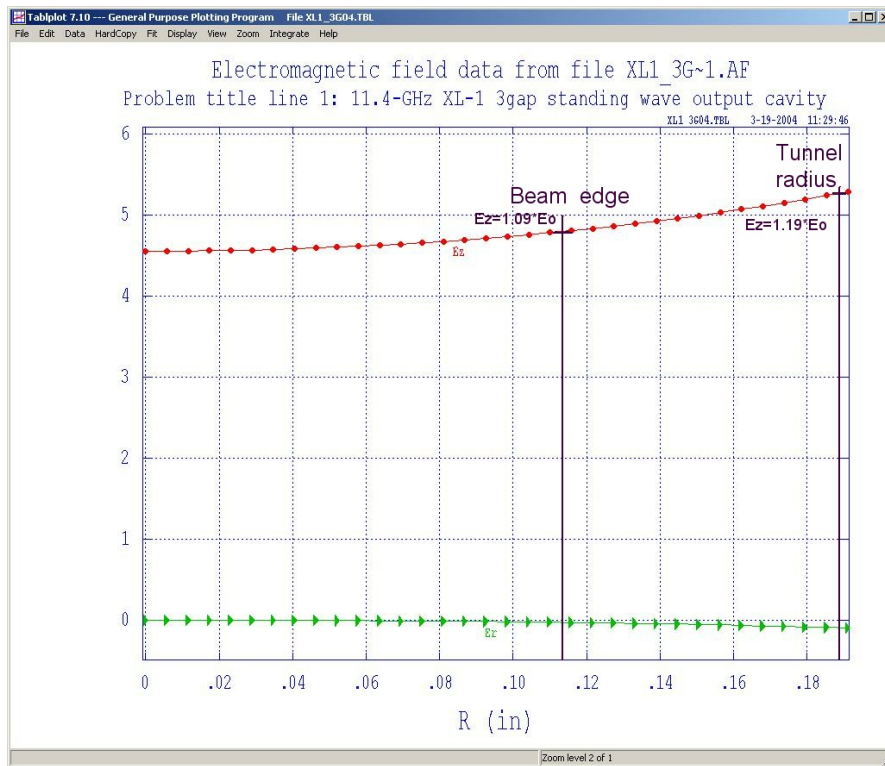
Since the voltage in the gap varies radially as $I_0(\gamma r)$, the effective shunt impedance depends on both filling factor and γa . If γa is 2 the electric field at the edge of the beam can be 40% higher than on axis. This is partially compensated by the reduced fringing of the cavity field into the drift region at a larger radius. See the plot of E_z vs z for $r = 0$ and $r = b$ at the end of this section.

For the XL-1, $\gamma a = .74$ a relatively small value. Calculating R/Q at beam edge and at $r = .707r_b$ (assume 60% fill factor) and using SF7 to obtain integrated voltage at each radius gives the following values of R/Q at different radii.

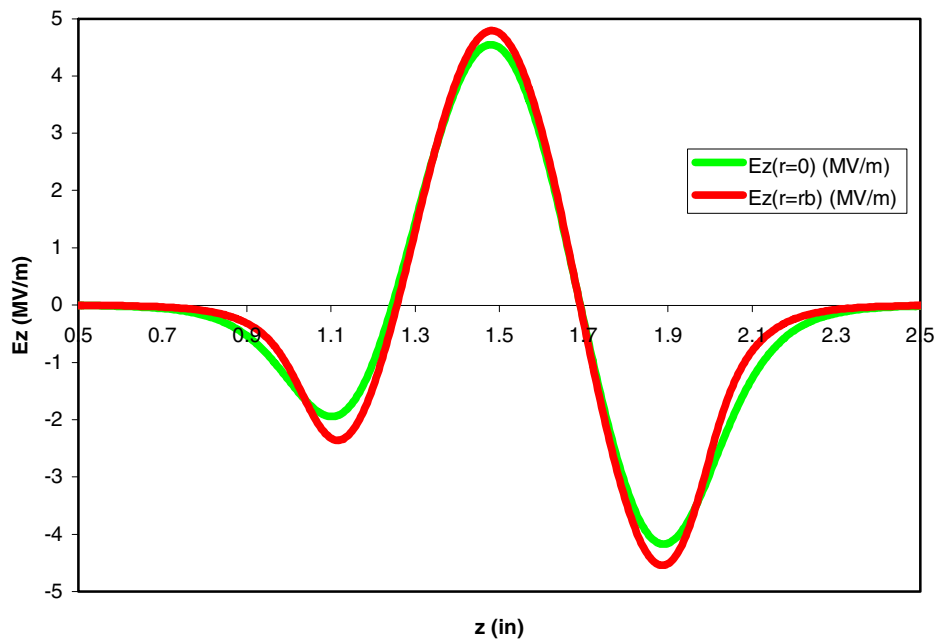


$$R/Q(r=0) = 64.25 \Omega, R/Q(r=.707r_b) = 64.62, R/Q(r=r_b) = 65.26 \Omega$$

For this small γ_a , the difference in integrated voltage from axis to beam edge is small and can be neglected.



Ez vs z for r=0 and r=rb



4. Determining the coupling factor M using SUPERFISH

The coupling factor M is a measure of the effective voltage seen by an electron transiting a resonant cavity compared to the peak voltage produced across the gap when the electric field is at its maximum value.

$$M(\beta_e) = \frac{\int_{-\infty}^{\infty} E_z e^{j\beta_e z} dz}{\int_{-\infty}^{\infty} E_z dz} = \frac{V_{eff}}{V_1}$$

This accounts for the fact that the electron has a finite transit time across the resonant cavity gap. In SUPERFISH the “transit time factor – T” is the microwave tube engineer’s coupling coefficient M except that the integration limits are defined by the ends of the simulation geometry. In order to get the coupling coefficient directly from SFO, the problem inputs must be set up correctly. First, the default particle in SUPERFISH is a proton with a rest mass energy of 938 MeV. The input parameter ‘RMASS’ must be set to the correct value for electrons, either -1 or .511. The minus sign indicates that the particle is identified from a table of particle-types shown below. A positive value of rest mass gives the particle’s rest mass energy in MeV.

Table X-20 from SUPERFISH Manual SFPOSTP.DOC

Particle	RMASS	Rest-mass energy (MeV)	Uncertainty (eV)
e [±]	-1	0.510998902	0.021
H ⁺	-2	938.271998	38
H ⁻	-3	939.2939815	~38
D ⁺	-4	1875.612762	75
D ⁻	-5	1876.634745	~75
³ He ²⁺	-6	2808.39132	110
⁴ He ²⁺	-7	3727.37904	150
μ [±]	-8	105.6583568	5.2

The beam velocity must be specified in order to determine β_e for the integration. SUPERFISH uses the variable name BETA= v/c to define beam velocity. DO NOT confuse this with β_e = w/v, which is the electronics propagation constant. In the example below, BETA is set to 0.5, which corresponds to a beam voltage of 80kV.

If the cavity geometry is not centered at z = 0, the variable ZCTR must be included in the input file to give the correct result from the transit time integral. For klystron cavities where the cavity fields extend into the drift tube, sufficient drift tube length must be modeled to allow the on axis fields to decay to <1% of the peak field.

The modified PILL10_M.af file used to calculate the coupling factor M for the pillbox cavity is listed below.

10-GHz TM010 Short Pillbox Cavity with modifications for calculating M

```
$reg kprob=1, ; SUPERFISH problem
BETA=.5 ; v/c normalized particle velocity
RMASS=-1, ; rest mass (particle-type - electron)
KMETHOD=1, ; use beta to compute wavenumber 'k'
ZCTR=0.5737 ; center of cavity
dx=.02, ; X mesh spacing
freq=10000., ; Starting frequency in MHz
xdri=1.,ydri=1.14741 $ ; Drive point location

$po x=0.0,y=0.0 $ ; Start of the boundary points
$po x=0.0,y=1.14741 $ ; r = 1.14741 cm
$po x=1.14741,y=1.14741 $ ; z = 1.14741 cm, r = 1.14741 cm
$po x=1.14741,y=0.0 $ ;
$po x=0.0,y=0.0 $ ; note closed structure has same
; entries for first and last point

; In SUPERFISH cylindrically symmetric problems
; x= z, y= r
```

The last page of the SFO output file for this case is listed below.

```
SUPERFISH output summary for problem description:
10-GHz TM010 Short Pillbox Cavity
Problem file: C:\LANL\MYFILES\R_OVER_Q\PILL10.AF 8-13-2004 9:04:16
-----
--
All calculated values below refer to the mesh geometry only.
Field normalization (NORM = 0): EZERO = 1.00000 MV/m
Frequency = 10000.09011 MHz
Particle rest mass energy = 0.510999 MeV
Beta = 0.5000000 Kinetic energy = 0.079 MeV
Normalization factor for E0 = 1.000 MV/m = 5187.058
Transit-time factor Abs(T+iS) = 0.2793658 "Coupling coeff M"
Stored energy = 5.65182E-06 Joules calculated in
Using standard room-temperature copper. SUPERFISH
Surface resistance = 26.08934 milliOhm
Normal-conductor resistivity = 1.72410 microOhm-cm
Operating temperature = 20.0000 C
Power dissipation = 20.4561 W
Q = 17360.0 Shunt impedance = 560.912 MOhm/m
Rs*Q = 452.910 Ohm Z*T*T = 43.777 MOhm/m
r/Q = 28.934 Ohm Wake loss parameter = 0.45450 V/pC
Average magnetic field on the outer wall = 1376.86 A/m, 2.47293 W/cm^2
Maximum H (at Z,R = 0.96624,1.14741) = 1376.85 A/m, 2.47291 W/cm^2
Maximum E (at Z,R = 1.13735,1.14741) = 1.00356E-04 MV/m, 1.2215E-06 Kilp.
Ratio of peak fields Bmax/Emax = 17240.6426 mT/(MV/m)
Peak-to-average ratio Emax/E0 = 0.0001
```

The results of the coupling coefficient calculation can be checked by using the transit time factor and r/Q to calculate R/Q . From the previous section:

$$R/Q = \frac{r/Q}{2T^2} = \frac{28.934}{2(0.27936)^2} = 185.4$$

which gives the same result as the original R/Q calculation.

So, using SUPERFISH and resetting the default values for BETA and RMASS, the ‘on-axis’ value of the coupling coefficient M can be read from the value listed in the SFO output as “Transit-time factor.”

For coupling coefficients that are off the beam axis, the fields required for the integrations can be obtained from the postprocessor SF7 and then integrated to find the value at any desired radius.

5. Calculation of beam loaded Q and cavity stability using Mathcad

To begin using the stability file in Mathcad, several variables must be supplied on page 5 of the Mathcad worksheet. They are listed below for reference,

- V_0 - DC beam voltage (V)
- I_0 - DC beam current (V)
- f_0 - Operating frequency (GHz)
- a - Tunnel radius (m)
- b - Beam radius (m)

The above variables are typical cavity parameters and may be entered as in the Mathcad small signal gain worksheet in Appendix I.

To run the Mathcad file, a cavity or output structure must first be simulated in SUPERFISH to obtain the field distributions at $r=a$ and on the axis. The process for importing this data into Mathcad is discussed in detail on the 5th page of the Mathcad file and in the next section of this file. The process must be repeated for every mode (since only one mode or frequency can be examined at a time and each mode is associated with a single input file from SUPERFISH).

The following variables must also be entered,

- conv - Units/cm (from SUPERFISH AF input file)
- symmetry - 0 for even symmetry and 1 otherwise
- npoints - Plot resolution (# of points on the abscissa)
- U - Cavity stored energy (from SUPERFISH SFO output file)

“conv” is the unit conversion factor used in the SUPERFISH input file (*.af). If “conv” was not used in SUPERFISH it is set to 1. The variable “symmetry” is set to 0 if only half of the cavity is simulated (since the cavity may be symmetric about its center), otherwise it is set to 1.

The final variable, U (stored energy), is used as an input to calculate the R/Q of the cavity. After simulating the cavity in SUPERFISH, the value for the stored energy can be found in the *.sfo file associated with the original input file. Once U has been found, it is necessary to run SF7 (as described in the next section) to evaluate the field distribution on axis and at $r=a$. Next, the names of the files generated by SF7 must be entered on page 5 of the Mathcad worksheet and the files themselves must be relocated to the same directory as the Mathcad worksheet. At this point Mathcad is ready to simulate the output structure.

The remainder of the Mathcad file is used for displaying the results. On page 5, the yellow highlighted areas display the key results of the simulation. Page 6 presents a plot for the field distribution (for fields at both $r=a$ and on axis) versus distance and a plot of the beam

loaded Q versus voltage. These results may then be updated by changing the variables on page 5 and recalculating the simulation.

XC8 Output Structure in the 0-Mode (Tutorial)

The Mathcad stability file may be used to evaluate the beam loaded Q, Qb, for any output structure and mode. In this section, the Mathcad stability file will be used to evaluate the output structure for the XC8 klystron, in the zero-mode. The same approach may then be used for the remaining three modes or other structures, as desired.

To begin, open the Mathcad file by double clicking the file labeled “XC8 Stability.mcd,” which is located in the CD. Once the document has been opened, scroll down to the 5th page. The first half of the page should be the same as Figure AIV-1.

Results

`sf_file_r_equals_a` \equiv READPRN("0.txt") "0.txt" is the input file associated with the 0 mode for the XC8 klystron at r=a. "0axis.txt" is the input file associated with the 0 mode on axis.

`sf_file_axis` \equiv READPRN("0axis.txt")

To create an equivalent files for other output structures .

- (1) Run Superfish using the chosen geometry.
- (2) Superfish will create a *.T35 file.
- (3) Open the created *.T35 file in the program, SF7.
- (4) Enter the data prompted for (this data should be associated with the field at r=0 for R/Q calculations and r=a for all other calculations).
- (5) A *.TBL file will be created (you will need to create one for both the on axis field and the field at r=a).
- (6) Open the *.TBL file and delete everything except for the data found in the main set of columns.
- (7) Save the edited *.TBL files under other names.
- (8) Place the files in the same directory as this one.
- (9) Enter the files' name inside of the READPRN functions above.

For further details read Appendix IV.

Reminder: Update the input file, R/Q, f0, U, etc. for every new mode or cavity.

<code>V0</code> \equiv 450000	Beam Voltage (V)	<code>conv</code> \equiv 2.54	Units Per cm (From Superfish *.AF file)
<code>Io</code> \equiv 517	Beam Current (A)		
<code>f0</code> \equiv 8.462	Mode Frequency (GHz)	<code>symmetry</code> \equiv 1	0 - even symmetry 1 - no symmetry
<code>a</code> \equiv 0.004762	Tunnel Radius (m)		
<code>b</code> \equiv 0.002857	Beam Radius (m)	<code>npoints</code> \equiv 150	Plotting Resolution
<code>U</code> \equiv 1.61070 $\cdot 10^{-4}$	Stored Energy (From Superfish *.SFO file)		

Input Variables on Page 5 of XC8 Stability.mcd

A step by step process for simulating the zero-mode is studied next.

The XC8.af file, in Appendix IV, is an input file for the program, SUPERFISH. All the files that are about to be generated have already been simulated and are located in the appendix. However, the process for generating each file is discussed next.

- ▶ Open XC8.af in a word editor such as Notepad.
- ▶ In the first section of the file is a variable labeled “freq.” SUPERFISH will search for the closest mode to this frequency. Since the zero-mode is close to 8000MHz, replace 14000, after the variable “freq”, with 8000.
- ▶ Save the file and close it.
- ▶ Double click the file to simulate it in SUPERFISH (this generates the solution file “XC8.T35”).
- ▶ Run the Program SF7 by right clicking on the “XC8.T35” file and selecting “Interpolate (SF7)”.
- ▶ A dialog window for the SF7 program should now be displayed. This program will find the field along a given line. In this case the field along the axis is required, so Y2 is changed to from 0.6523 to 0. Press run.
- ▶ After pressing run the field is tabulated in the XC801.TBL file, which has been renamed 0axis.tbl in the appendix.
- ▶ Open XC801.TBL in notepad. The file contents should be similar to that shown below, with the, “...”, replaced by several lines of text and or data. Delete the highlighted regions shown below and save the file as 0axis.txt and close it.

```

...
Ez
Er
E
H
EndLabels

Data
:
: Z R Ez Er |E| H
: (in) (in) (MV/m) (MV/m) (MV/m) (A/m)
0.000000 0.000000 3.534599E-05 0.000000E+00 3.534599E-05 0.000000E+00
0.032000 0.000000 3.802072E-05 0.000000E+00 3.802072E-05 0.000000E+00
0.064000 0.000000 4.633658E-05 0.000000E+00 4.633658E-05 0.000000E+00
0.096000 0.000000 6.155754E-05 0.000000E+00 6.155754E-05 0.000000E+00
...
EndData
EndFile

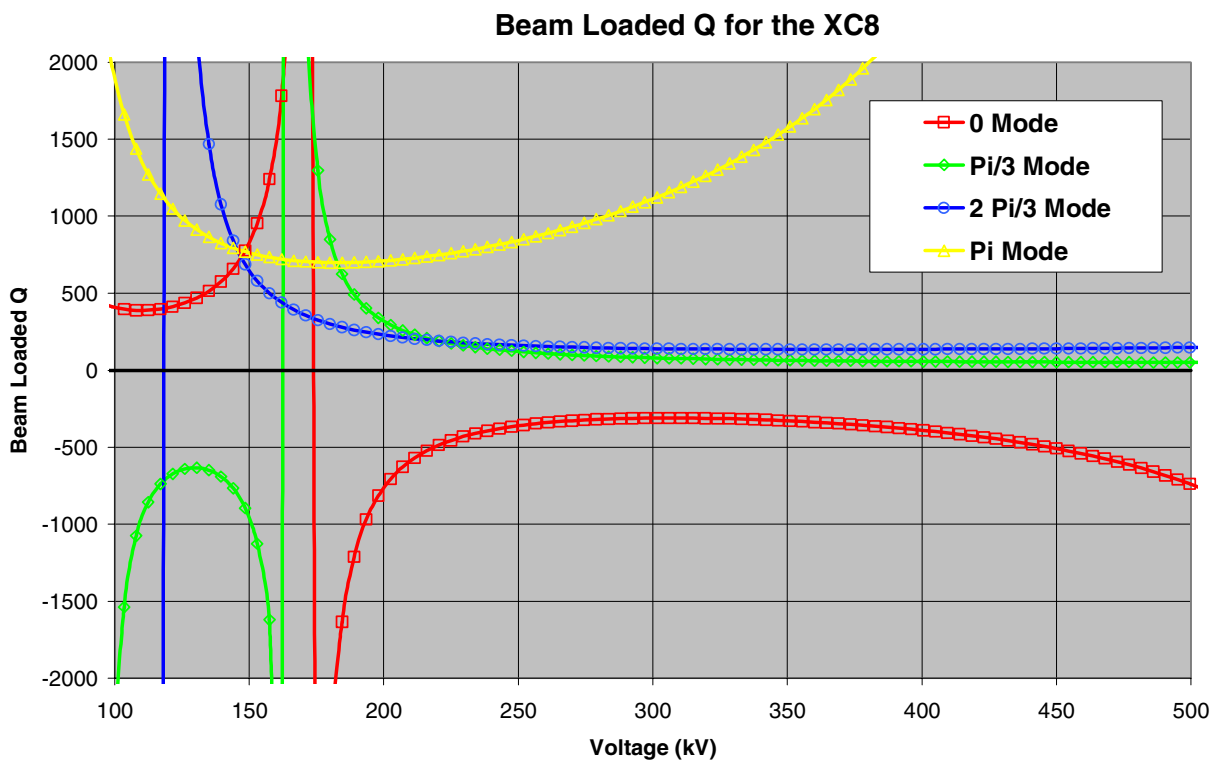
```

- ▶ Right click on the XC8.T35 file and select “Interpolate (SF7).” Now instead of finding the field on axis, the field is now interpolated at the drift tube radius. This is done by changing Y1 to 0.1785 and Y2 to 0.1785. Press Run.
- ▶ As in the method of finding the R/Q, open the generated TBL file and delete the text above and below the data. This file is saved as 0.txt in the Appendix.
- ▶ Right click on the XC8.T35 file and select “Postprocess (SFO).”
- ▶ Open the file XC8.SFO or the file in the appendix 0mode.SFO. Scroll to the bottom of the file and find the line labeled Stored energy,

Stored energy = 1.61070E-04 Joules

- ▶ Enter the value for stored energy, $1.61070E-04$ Joules, into the Mathcad variable U (highlighted in green on page 5). Close the SFO file.
- ▶ In the blue highlighted region, enter 0axis.txt as the input file after the variable sf_file_axis and 0.txt after sf_file_r_equals_a. At this point make sure that these two files are located in the same directory as the Mathcad worksheet.
- ▶ Double click on the T35 file to verify that the frequency, f_0 , in Mathcad is correct.
- ▶ Verify that the rest of the highlighted green variables on page 5 of the Mathcad worksheet match your desired input parameters.
- ▶ Click somewhere in the 6th page of Mathcad and run the simulation by pressing the equals button or the F9 key.
- ▶ A plot of the beam loaded Q vs. voltage should be displayed on the 6th page.

This concludes the tutorial for finding the beam loaded Q using Mathcad and SUPERFISH. The same approach may be used to calculate the beam loaded Q for the other three modes, the results are shown below in Figure IV-2.



Beam Loaded Q for the XC8

6. Listing of Mathcad worksheet for stability analysis

Define Constants:

$c \equiv 2.99792510^8$	Speed of Light
$m_e \equiv 9.109 \cdot 10^{-31}$	Electron Charge
$e \equiv 1.602 \cdot 10^{-19}$	Electron Rest Mass
$\epsilon_0 \equiv 8.854187810^{-12}$	Permittivity of Free Space

Sweep Parameters:

$K_o := \frac{I_o}{V_o^{1.5}}$	Perveance	$K_o = 1.7127 \times 10^{-6}$
$num_points := npoints + \text{mod}(npoints, 2)$	Make npoints an Even Number	
$o := 0.5 \cdot num_points$	Index Where the Voltage Array, V, is V_o	
$i := 0.. num_points$	Plotting Resolution	
$V_i := V_o + i \cdot \frac{1.99 V_o}{num_points} - \frac{1.99 V_o}{2}$	Assign Voltages Symmetrically About V_o	
$I_i := (V_i)^{1.5} \cdot K_o$	Assign Currents Associated With Each Voltage to Produce Constant Perveance	

Initialize Variables:

$\eta := \frac{e}{m_e}$	Electron Charge to Mass Ratio	$\eta = 1.7587 \times 10^{11}$
$J_o := \frac{I}{\pi \cdot b^2}$	Beam Current Density (A/m^2)	$J_{o_o} = 2.0161 \times 10^7$
$J_{beam} := \frac{J_o}{100^2}$	Beam Current Density (A/cm^2)	$J_{beam_o} = 2.0161 \times 10^3$
$K := K_o \cdot 10^6$	Microperveance	$K = 1.7127$
$V_d := .0304 V \cdot K \cdot \left(\frac{1}{4} + \ln \left(\frac{a}{b} \right) \right)$	Potential Beam Depression (@ $r = 0.707 * b$)	$V_{d_o} = 1.7827 \times 10^4$

$V_{od} := V - V_d$	Depressed Beam Potential	$V_{od_0} = 4.3217 \times 10^5$
$G_o := \frac{I_o}{V_{od}}$	(Depressed) Beam Admittance	$G_{o_0} = 1.1963 \times 10^{-3}$
$\sigma := 1 + \frac{V_{od}}{511000}$	Relativistic Mass Factor	$\sigma_0 = 1.8457$
$v_{on} := \left[\frac{1}{\sigma} \cdot \sqrt{(\sigma^2 - 1)} \right]$	v/c for a Relativistic Particle with Potential Depression	$v_{on_0} = 0.8405$
$\beta_e := \frac{2 \cdot \pi \cdot f_0 \cdot 10^9}{v_{on} \cdot c}$	Electron propagation Constant	$\beta_{e_0} = 211.002$
$\gamma := \left(\beta_e \cdot \sqrt{1 - v_{on}^2} \right)$	Radial Propagation Constant	$\gamma_0 = 114.3184$

----- PLASMA REDUCTION FACTORS -----

Calculation of the Plasma Reduction Factor, R, for the Pencil Beam Geometry, Using the Method of Branch and Mihran.

$$\begin{aligned} \gamma_a &:= \gamma \cdot a & \gamma_{a_0} &= 0.5444 \\ \gamma_b &:= \gamma \cdot b & \gamma_{b_0} &= 0.3266 \end{aligned}$$

Plasma Frequency

$$\omega_p := \left[\sqrt{\eta \cdot \frac{J_o}{\epsilon_0 \cdot v_{on} \cdot c} \cdot \left(\frac{1}{\sigma^{1.5}} \right)} \right] \quad \omega_{p_0} = 1.5898 \times 10^{10}$$

Calculate the Approximate Reduction Factor, R:

$$R := \sqrt{1 - 2 \cdot I_1(\gamma_b) \cdot K_1(\gamma_b) - 2 \cdot \frac{K_0(\gamma_a)}{I_0(\gamma_a)} \cdot I_1(\gamma_b)^2}$$

$R_0 = 0.197$

Reduced Plasma Frequency and Propagation Constant

$$\begin{aligned} \omega_q &:= (\omega_p \cdot R) & \beta_{q_0} &:= \frac{\omega_{q_0}}{v_{on} \cdot c} \end{aligned}$$

----- FILE DATA -----

Read in data (on axis) from the SUPERFISH file listed on pg. 5 of this worksheet.

$z_axis := sf_file_axis^{(0)}$ z (location on the z-axis)
 $r_axis := sf_file_axis^{(1)}$ r (radial location) - Unused
 $Ez_axis := sf_file_axis^{(2)}$ Ez Field Component
 $Er_axis := sf_file_axis^{(3)}$ Er Field Component - Unused
 $Emag_axis := sf_file_axis^{(4)}$ Magnitude of the Electric Field - Unused
 $H_axis := sf_file_axis^{(5)}$ H Field Component - Unused
 $N_axis := length(z_axis) - 1$ Length of the Above Arrays

Read in data (at r=a) from the SUPERFISH file listed on pg. 5 of this worksheet.

$z := sf_file_r_equals_a^{(0)}$ z (location on the z-axis)
 $r := sf_file_r_equals_a^{(1)}$ r (radial location) - Unused
 $Ez := sf_file_r_equals_a^{(2)}$ Ez Field Component
 $Er := sf_file_r_equals_a^{(3)}$ Er Field Component - Unused
 $Emag := sf_file_r_equals_a^{(4)}$ Magnitude of the Electric Field - Unused
 $H := sf_file_r_equals_a^{(5)}$ H Field Component - Unused
 $N := length(z) - 1$ Length of the Above Arrays

----- R/Q Calculation -----

This section calculates R/Q from the included SUPERFISH file on pg. 5 of this worksheet. Note: R/Q must be calculated on axis. Also, Ez is assumed to be in MV/m. The stored energy, U, is entered manually by the user. It is determined by SUPERFISH and displayed in the *.SFO output file.

$$V_{axis} := \sum_{n=0}^{N_{axis}-1} \left[\left| \left(\frac{Ez_axis_{n+1} + Ez_axis_n}{2} \right) \cdot (z_axis_{n+1} - z_axis_n) \cdot \frac{conv}{100} \right| \right]$$

$$\omega_0 := 2 \cdot \pi \cdot f_0 \cdot 10^9$$

$$RQ := \frac{(V_{axis} \cdot 10^6)^2}{2 \cdot \omega_0 \cdot U} \quad RQ = 385.7182$$

----- Coupling Coefficient Calculation -----

Coupling Coefficient at the Beam Edge

$$\text{CosTerm}(n, \beta) := \cos \left[\frac{\beta \cdot 0.5(z_{n+1} + z_n) \cdot \text{conv}}{100} \right] \cdot [(z_{n+1} - z_n) \cdot \text{conv}]$$

$$\text{SinTerm}(n, \beta) := \text{symmetry} \cdot i \cdot \sin \left[\frac{\beta \cdot [0.5(z_{n+1} + z_n)] \cdot \text{conv}}{100} \right] \cdot [(z_{n+1} - z_n) \cdot \text{conv}]$$

$$\text{Ma}(\beta) := \frac{\left| \sum_{n=0}^{N-1} \left[\left(\frac{Ez_{n+1} + Ez_n}{2} \right) \cdot (\text{CosTerm}(n, \beta) + \text{SinTerm}(n, \beta)) \right] \right|}{\sum_{n=0}^{N-1} \left[\left| \left(\frac{Ez_{n+1} + Ez_n}{2} \right) \cdot (z_{n+1} - z_n) \cdot \text{conv} \right| \right]}$$

Coupling Coefficient Averaged Over the Beam Radius

$$M(\beta) := \text{Ma}(\beta) \cdot \sqrt{\frac{I0(\beta \cdot b)^2 - I1(\beta \cdot b)^2}{I0(\beta \cdot a)^2}}$$

----- Qb Calculations -----

Gb/Go Calculated Using SUPERFISH and the M+ M- Approach (from WesselBerg).

$$M_Min := \overrightarrow{M(\beta_e - \beta_q)}$$

$$M_Plus := \overrightarrow{M(\beta_e + \beta_q)}$$

$$Gb_Go := \overrightarrow{\left[\frac{\beta_e}{8 \cdot \beta_q} \cdot (|M_Min|^2 - |M_Plus|^2) \cdot \frac{2}{\sigma \cdot (\sigma + 1)} \right]}$$

$$Qb := \frac{1}{Gb_Go \cdot \frac{I}{Vod} \cdot RQ}$$

Input Data and Results

Results

`sf_file_r_equals_a ≡ READPRN "0.txt")`

"0.txt" is the input file associated with the 0 mode for the XC8 klystron at r=a. "0axis.txt" Is the input file associated with the 0 mode on axis.

`sf_file_axis ≡ READPRN "0axis.txt")`

To create an equivalent files for other output structures:

- (1) Run SUPERFISH using the chosen geometry.
- (2) SUPERFISH will create a *.T35 file.
- (3) Open the created *.T35 file in the program, SF7.
- (4) Enter the data prompted for (this data should be associated with the field at r=0 for R/Q calculations and r=a for all other calculations).
- (5) A *.TBL file will be created (you will need to create one for both the on axis field and the field at r=a).
- (6) Open the *.TBL file and delete everything except for the data found in the main set of columns.
- (7) Save the edited *.TBL files under other names.
- (8) Place the files in the same directory as this one.
- (9) Enter the files' name inside of the READPRN functions above.

For further details read Appendix IV.

Reminder: Update the input file, f0, U, etc. for every new mode or cavity.

<code>Vo ≡ 450000</code>	Beam Voltage (V)	<code>conv ≡ 2.54</code>	Units Per cm (From SUPERFISH *.AF file)
<code>Io ≡ 517</code>	Beam Current (A)		
<code>f0 ≡ 8.462</code>	Mode Frequency (GHz)	<code>symmetry ≡ 1</code>	0 - even symmetry 1 - no symmetry
<code>a ≡ 0.00476</code>	Tunnel Radius (m)		
<code>b ≡ 0.00285</code>	Beam Radius (m)	<code>npoints ≡ 150</code>	Plotting Resolution
<code>U ≡ 1.6107010⁻⁴</code>	Stored Energy (From SUPERFISH *.SFO file)		

The following are variables evaluated at the operating frequency, current, and voltage.

$$\beta_{e_0} = 211.002$$

Propagation Constant

$$G_b/G_o = -4.2583 \times 10^{-3}$$

G_b/G_o from SUPERFISH Using M+ M-

$$M_a(\beta_{e_0}) = 0.0632$$

Coupling Coefficient @ r=a from SUPERFISH

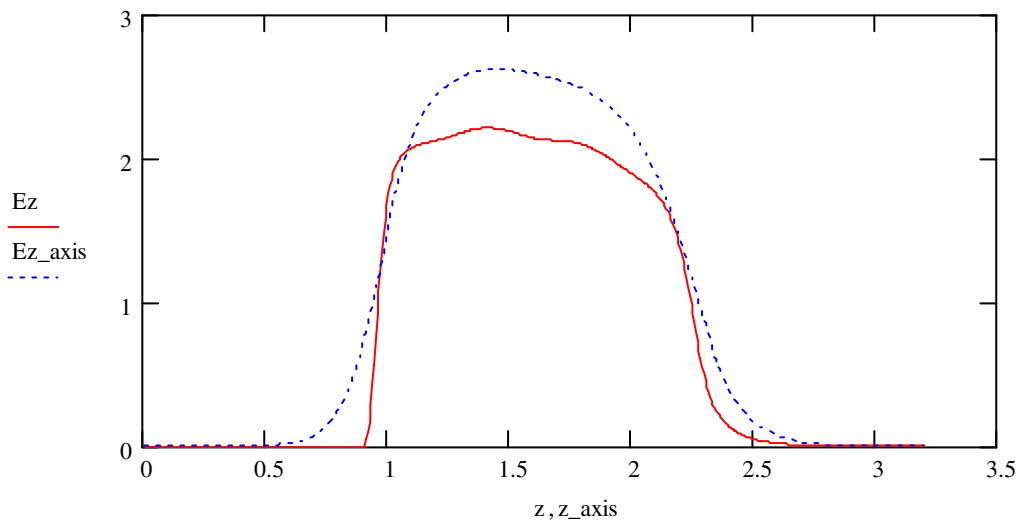
$$M(\beta_{e_0}) = 0.0521$$

Coupling Coefficient (Averaged) from SUPERFISH

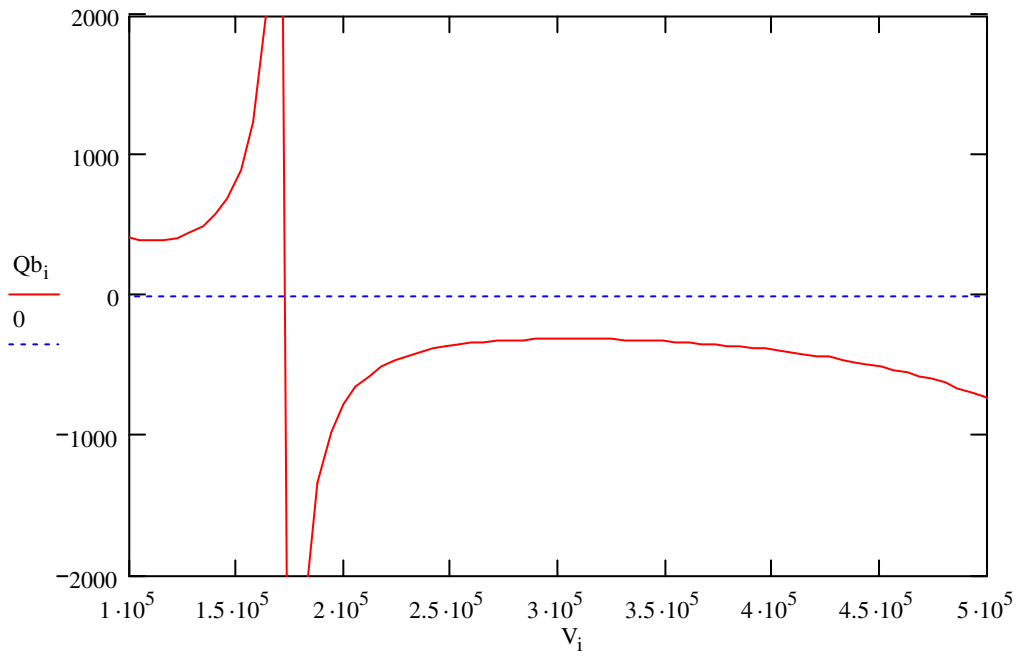
$$RQ = 385.7182$$

R/Q from SUPERFISH (Use the Field on Axis)

Plots & Figures



Ez Field Distributions vs. Distance



Qb vs. Voltage

Appendix V.

Relativistic Corrections

The principal formulae used for klystron design in the main text are non-relativistic. The corrections listed below are essential to the design of accelerator klystrons, with beam voltages well above 50 kV.

Quantity	Symbol	Multiply by:
Perveance	K	$1 - (3/28)(\sigma + 1)$
Brillouin field	B_b	$[2/(\sigma + 1)]^{1/4}$
Dc beam velocity	u_0	$\frac{1}{\sigma} \sqrt{(1 + \sigma)/2}$
Coupling coefficient	M	$2\sigma / [\sigma(\sigma + 1)]$
Beam loading conductance	G_b/G_0	$4/(\sigma + 1)^2$
Plasma frequency	ω_p	$(1/\sigma)[2/(\sigma + 1)]^{1/4}$
Plasma propagation factor	β_p	$[2/(\sigma + 1)]^{3/4}$

Where,

$$\sigma = \sqrt{1 - \left(\frac{u_0}{c}\right)^2}$$

REFERENCES

-
- ¹ Sprehn, D., "Current Status of the Next Linear Collider X-Band Klystron Development Program," presented at EPAC 2004 in Lucerne, Switzerland, (July, 2004).
- ² Choroba, S., J. Hameister, S. Jarylkapov, "Performance of an S-Band Klystron at an Output Power of 200 MW," *Proceedings of the XIX International Linac Conference*, vol. 2, Pg. 917, (August, 1998).
- ³ Mann, J., D. Robinson, "X-Band CW Generator Development," RADC Report prepared for EIMAC Division of Varian, San Carlos, CA, (August, 1968).
- ⁴ Armstrong, E. "A Method of Receiving Short Continuous Waves" published in a disclosure to the US Signal Corps, (June 3, 1918).
- ⁵ Von Döring, H., "Der Heil'sche Generator, ein spezielles Klystron," published in German journal *Frequenz*, Pg. 138, (1987).
- ⁶ Heil, A. A., O. Heil, "Eine neue Methode zur Erzeugung kurzer, ungedämpfter, elektromagnetischer Wellen grober Intensität," *Zeitschrift Für Physik*, Verlag Von Julius Springer, Berlin, (1935).
- ⁷ Hansen, W. W., R. D. Richtmyer, "On Resonators Suitable for Klystron Oscillators," *Journal. Of Appl. Physics*, 10, Pg. 189-199, (1939).
- ⁸ Ginzton unpublished diaries
- ⁹ Ginzton, E. L., W. Hansen, W. Kennedy, "A Linear Electron Accelerator," *Review of Scientific Instr.* Vol.19, Pg. 48, (February, 1948).
- ¹⁰ Varian, D., Russell and Sigurd Varian, The Inventor and the Pilot, Pacific Books, Palo Alto, CA, (1983).
- ¹¹ Gewartowski, J. W., H. A. Watson, Principles of Electron Tubes, D. Van Nostrand Company, Inc, 1965.
- ¹² Sprehn, D., op.cit.
- ¹³ Ford, J., "Little Linacs Fight Cancer," Stanford Linear Accelerator Center, *Beam Line*, Vol. 23 No. 1, Spring, 1993.
- ¹⁴ Luebke, W., G. Caryotakis, "Development of a One Megawatt CW Klystron," *Microwave Journal*, (August 1966).
- ¹⁵ Chodorow, M., T. Wessel-Berg, "A High-Efficiency Klystron with Distributed Interaction," *IRE Trans. Of Electron Devices*, Pg. 44, (Jan. 1961).
- ¹⁶ Burke, D. L., "The NLC Technical Program," *Proceedings of the Symposium on Electron Linear Accelerators in Honor of Richard B. Neal's 80th Birthday*, SLAC-R-526 Neal97-006, (April 2001).
- ¹⁷ Sprehn, D., op.cit.
- ¹⁸ Fowkes, W. R., G. Caryotakis, E. Doyle, E. Jongewaard, C. Pearson, R. Phillips, J. Sackett, E. Wright, "1.2 MW Klystron for Asymmetric Storage Ring B Factory," *SLAC PUB 6778*, (March 1995).
- ¹⁹ Balkcum, A., E. Wright, H. Bohlen, M. Cattelino, L. Cox, M. Cusick, K. Eppley, S. Forrest, F. Friedlander, A. Staprans, L. Zitelli, "Operation of a 1.3 GHz, 10 MW Multiple Beam Klystron," *IVEC 2004*, Pg. 280, (April 2004).
- ²⁰ Lien, E. "High efficiency Klystron Amplifiers" European Microwave Conference MOGA (1970)
- ²¹ Webster, D. L., "Cathode-Ray Bunching," *J. Appl. Phys.* 10, Pg. 501, (1939)
- ²² Feenberg, E., "Notes on Velocity Modulation," *Sperry Gyroscope Lab. Report 5521-1043*, Sperry Gyroscope Co., Inc., Garden City, NY, (Sept. 25, 1945).
- ²³ Warnecke, R., and P. Guénard, Les Tubes Électroniques à Commande par Modulation de Vitesse, Paris: Gauthier Villars (1959).
- ²⁴ Fremlin, J. H., A. W. Gent, D.P.R. Petrie, P. J. Wallis and S. G. Tomlin, "Principles of Velocity Modulation," *IEEE Journal 93*, Part III A Pg. 875-917,(1946) .
- ²⁵ Branch, G. M. Jr., "Electron Beam Coupling in Interaction Gaps of Cylindrical Symmetry," *IRE Trans. On Elec. Dev.*, Pg. 193-206, (May, 1961).
- ²⁶ Feenberg, E., op.cit.
- ²⁷ Chodorow, M., C. Susskind, Fundamentals of Microwave Electronics, McGraw-Hill Book Company, New York, (1964)
- ²⁸ Zitelli, L. T., "Space-Charge Effects in Modulated Electron Beams," Ph.D. Dissertation, Stanford University, (March, 1950).
- ²⁹ Wessel-Berg, T., "A General Theory of Klystrons with Arbitrary, Extended Interaction Fields," Technical Report, Stanford Microwave Laboratory Report No. 376, (March, 1957).
- ³⁰ Hamilton, D. R., J. K. Knipp, J. B. Horner Kuper, Klystrons and Microwave Triodes, The Maple Press Company, York, PA, (1948)

-
- ³¹ Ramo, S., "The Electronic-Wave Theory of Velocity-Modulation Tubes," *Proceedings of the I.R.E.*, Pg. 757-763, (December, 1939)
- ³² Branch, G. M., T. G. Mihran, "Plasma Frequency Reduction Factors in Electron Beams," *IRE Trans. On Elec. Dev.* ED-2, Pg. 3, (1955).
- ³³ Wessel-Berg, T., "Space-Charge Wave Theory of Interaction Gaps and Multi-Cavity Klystrons with Extended Fields," *Norwegian Defence Research Report No. 32*, (1960).
- ³⁴ Bode, H., Network Analysis and Feedback Amplifier Design, D. Van Nostrand Co., (1945).
- ³⁵ Valley, G. E., H. Wallman, Vacuum Tube Amplifiers, McGraw-Hill Co. (1948).
- ³⁶ Bode, H., op.cit.
- ³⁷ Beck, A. H. W., Thermionic Valves their Theory and Design, Cambridge at the University Press, London, (1953).
- ³⁸ Webber, S. E., "Large Signal Bunching of Electron Beams by Standing-Wave and Traveling-Wave Systems," *IRE Trans on Electron Devices*, Pg. 365-372, (October, 1959).
- ³⁹ Rowe, J. E., "Nonlinear Electron-Wave Interaction Phenomena," New York Academic Press, (1965)
- ⁴⁰ Yonezawa, H., O. Yukio, "A One-Dimensional Disk Model Simulation for Klystron Design," SLAC-TN-84-5, (May 1984).
- ⁴¹ Bode, H., op.cit.
- ⁴² Luebke, W. G. Caryotakis, op.cit..
- ⁴³ Chodorow, M., T. Wessel-Berg, op.cit.
- ⁴⁴ Symons, R.S and Begum, S.R. "Extended Interaction Output Circuit Using Modified Disk-Loaded Waveguide. U.S. Patent 5,469,022. Nov. 21, 1995
- ⁴⁵ Besov, Y. "Multiple Beam Klystrons," High Energy Density Microwaves, Pajaro Dunes, CA, AIP Conference Proceedings 474, Pg. 91-105, (October, 1998)
- ⁴⁶ В. Я. Иванов, Методы автоматизированного проектирования приборов электронной оптики, Академия Наук СССР, Сибирское Отделение, Институт Математики, Новосибирск 1986.
http://www.slac.stanford.edu/~ivanov/code_poisson3/poisson3.pdf
- ⁴⁷ Slater, J. C., Microwave Electronics, Van Nostrand, Princeton, NJ, 1950, p 81